



**HAL**  
open science

# Experimental evaluation and modeling of a nonlinear absorber for vibration attenuation : design, identification, and analysis

Déborah Lavazec

► **To cite this version:**

Déborah Lavazec. Experimental evaluation and modeling of a nonlinear absorber for vibration attenuation : design, identification, and analysis. Materials. Université Paris-Est, 2017. English. NNT : 2017PESC1217 . tel-01739616

**HAL Id: tel-01739616**

**<https://pastel.hal.science/tel-01739616>**

Submitted on 21 Mar 2018

**HAL** is a multi-disciplinary open access archive for the deposit and dissemination of scientific research documents, whether they are published or not. The documents may come from teaching and research institutions in France or abroad, or from public or private research centers.

L'archive ouverte pluridisciplinaire **HAL**, est destinée au dépôt et à la diffusion de documents scientifiques de niveau recherche, publiés ou non, émanant des établissements d'enseignement et de recherche français ou étrangers, des laboratoires publics ou privés.



## Thèse de Doctorat

Spécialité : Mécanique

---

**Experimental evaluation and modeling  
of a nonlinear absorber for vibration attenuation.  
Design, identification, and analysis.**

Évaluation expérimentale et modélisation  
d'un absorbeur non-linéaire pour l'atténuation des vibrations.  
Conception, identification et analyse.

---

présentée par

**Déborah Lavazec**

le 21 décembre 2017

afin d'obtenir le grade de

**Docteur de l'Université Paris-Est**

### **Jury**

M. Jean-François Deü	Rapporteur
M. Fabrice Thouverez	Rapporteur
M. Didier Clouteau	Président du jury
M. Gwendal Cumunel	Examineur
M. Denis Duhamel	Co-directeur de thèse
M. Christian Soize	Co-directeur de thèse



# Acknowledgments

Ce travail a bénéficié d'une aide de l'état gérée par l'ANR au titre du programme des Investissements d'Avenir ANR-11-LABX-002-01. Il a été réalisé conjointement au sein du laboratoire Navier (UMR 8205) à l'École des Ponts ParisTech et au laboratoire MSME (UMR 8208) à l'Université Paris-Est Marne-la-Vallée.

Je tiens à remercier les professeurs Jean-François Deü et Fabrice Thouverez pour m'avoir fait l'honneur d'accepter de rapporter ma thèse. Je remercie également le professeur Didier Clouteau pour avoir accepté d'examiner ce travail et de présider le jury de thèse.

Mes remerciements vont à présent à mes deux directeurs de thèse, le professeur Denis Duhamel et le professeur Christian Soize, pour avoir accepté d'encadrer mon travail lors de ces trois dernières années, ainsi que pour leur expertise et leur rigueur.

Je tiens également à remercier mon encadrant Gwendal Cumunel, pour sa présence continue au cours de cette thèse, et tout particulièrement pour sa grande aide apportée sur les montages expérimentaux et sur les mesures expérimentales.

Je remercie également les membres, permanents et non-permanents, des laboratoires Navier et MSME pour leur gentillesse et leur sympathie.

Enfin, je tiens à remercier ma famille et mes amis pour leur présence et leur soutien.

## **Évaluation expérimentale et modélisation d'un absorbeur non-linéaire pour l'atténuation des vibrations. Conception, identification et analyse.**

Thèse préparée au laboratoire Navier<sup>(1)</sup> et au laboratoire Modélisation et Simulation Multi-Echelle<sup>(2)</sup> :

(1) Laboratoire Navier, Université Paris-Est, ENPC/IFSTTAR/CNRS, 6 et 8 Avenue Blaise Pascal, Cité Descartes, Champs-sur-Marne, 77455 Marne La Vallée Cedex 2, France

(2) Laboratoire Modélisation et Simulation Multi Echelle, Université Paris-Est, MSME, UMR 8208 CNRS, 5 bd Descartes, 77454 Marne-la-Vallée, France

### **Résumé.**

En raison de leurs grandes longueurs d'onde, les vibrations mécaniques en basses fréquences ne peuvent être facilement réduites dans les structures par l'utilisation de matériaux dissipatifs. Malgré ces difficultés, l'atténuation des vibrations en basses fréquences reste un enjeu important. Pour résoudre ce problème, différents axes de recherche ont été étudiés et ont été mis en application pour stocker et dissiper l'énergie vibratoire comme l'utilisation d'oscillateurs linéaires, composés d'une masse, d'un ressort et d'un amortisseur. Leur fréquence de résonance doit coïncider avec la fréquence de résonance de la structure que l'on veut atténuer. L'utilisation d'absorbeurs se comportant comme des oscillateurs ayant un comportement non linéaire est une alternative intéressante. En effet, grâce à un étalement fréquentiel de la réponse de l'oscillateur, celui-ci permet d'atténuer les vibrations de la structure sur une plus large bande de fréquence que ceux ayant un comportement linéaire, sans avoir de dédoublement de la résonance de la réponse en deux pics. Les travaux présentés ici se placent dans le cadre de la réduction vibratoire, à l'échelle macroscopique, en basses fréquences, pour lesquelles les premiers modes structuraux sont excités. Un absorbeur non linéaire a été conçu, réalisé et analysé expérimentalement, modélisé et identifié expérimentalement pour mettre en évidence le phénomène d'élargissement de la bande de fréquence de la réponse. Les effets de cet absorbeur sur le comportement dynamique d'une poutre console ont ensuite été numériquement étudiés, à partir d'un modèle de poutre couplée à des absorbeurs non linéaires. Un modèle réduit et son solveur stochastique ont été développés dans ce cadre. Les résultats ont exposé le fait que l'absorbeur non linéaire permet une atténuation de la réponse de la poutre, sans le dédoublement de la résonance.

**Mots clés :** Absorbeur non linéaire, Atténuation des vibrations, Conception, Expériences, Modélisation, Identification expérimentale, Réduction du bruit

## **Experimental evaluation and modeling of a nonlinear absorber for vibration attenuation. Design, identification, and analysis.**

### **Abstract.**

Due to their long wavelengths, mechanical vibrations at low frequencies cannot easily be reduced in structures by using dissipative materials. Despite these difficulties, the attenuation of vibration at low frequencies remains an important concern. To solve this problem, several ways of research have been explored and have been applied to vibration energy pumping such as linear oscillators, composed of a mass, a spring, and a damper. Their resonance frequency must coincide with the resonant frequency of the structure that has to be attenuated. The absorbers that are oscillators with a nonlinear behavior constitute an interesting alternative. The response of the nonlinear oscillator allows for obtaining an attenuation of vibration over a broader frequency band than the response of linear oscillator, without splitting the resonance that has to be attenuated into two resonances. The work presented here is in the frame of the vibratory reduction, on a macro-scale, at low frequencies, for which the first structural modes are excited. A nonlinear absorber has been designed, experimentally realized and analyzed, modeled and experimentally identified to highlight the phenomenon of broadening the frequency band of the response. The effects of this absorber on the dynamic behavior of a cantilever beam have been numerically studied, using a model of the beam coupled to nonlinear absorbers. A reduced-model and its stochastic solver have also been developed. The results obtained show that the nonlinear absorber allows for obtaining an attenuation on the beam response, without splitting of the resonance that has to be attenuated.

**Keywords:** Nonlinear absorber, Vibration attenuation, Design, Experiments, Modeling, Experimental identification, Noise reduction



# Contents

<b>Acknowledgments</b>	<b>3</b>
<b>Résumé de la thèse</b>	<b>11</b>
<b>Notations</b>	<b>13</b>
<b>1 Introduction and objectives</b>	<b>15</b>
1.1 Context and objectives . . . . .	15
1.2 Reduction of vibration by direct dissipation at middle and high frequencies . . . . .	16
1.2.1 Direct dissipation of vibration . . . . .	16
1.2.2 Reduction of vibration and noise at middle and high frequencies . . . . .	17
1.3 Reduction of vibration at low frequencies by linear absorbers . . . . .	18
1.3.1 Attenuation of vibration at low frequencies by a linear absorber corresponding to a one-DOF linear oscillator . . . . .	18
1.3.2 Attenuation of noise and vibration at low frequencies by MDOF linear oscillators-based absorbers . . . . .	21
1.3.3 Attenuation of noise and vibration at low frequencies by linear continuous absorbers . . . . .	22
1.4 Attenuation of noise and vibration at low frequencies by nonlinear absorbers . . . . .	24
1.5 Scientific approach & outline of the thesis . . . . .	27
<b>2 Nonlinear model of the absorber and stochastic solver</b>	<b>29</b>
2.1 Introduction . . . . .	29
2.2 Model of the nonlinear oscillator . . . . .	30
2.3 Stochastic solver and signal processing . . . . .	32
2.3.1 Stochastic solver . . . . .	32
2.3.2 Time and frequency sampling . . . . .	33
2.3.3 Generation of independent realizations of Gaussian stationary stochastic process $F_s$ . . . . .	33
2.3.4 Störmer-Verlet integration scheme . . . . .	34
2.3.5 Signal processing . . . . .	36
2.4 Validation of the stochastic solver with a linear oscillator . . . . .	37
2.5 Conclusion . . . . .	40

<b>3</b>	<b>Experimental design, measurements, and model identification of the absorber</b>	<b>41</b>
3.1	Introduction . . . . .	41
3.2	Experimental design . . . . .	41
3.3	Experimental measurements . . . . .	44
3.3.1	Manufacturing of the test absorber . . . . .	44
3.3.2	Description of the experimental procedure . . . . .	44
3.3.3	Experimental results . . . . .	47
3.4	Experimental identification of the model . . . . .	47
3.5	Conclusion . . . . .	53
<b>4</b>	<b>Construction of a model of a beam with absorbers</b>	<b>55</b>
4.1	Introduction . . . . .	55
4.2	One-dimensional model of the beam . . . . .	56
4.3	Reduced Model . . . . .	57
4.4	Expression of powers related to the mechanical system . . . . .	60
4.5	Stochastic solver and signal processing . . . . .	63
4.5.1	Stochastic solver . . . . .	63
4.5.2	Generation of independent realizations of Gaussian stationary stochastic process $g^{\text{exp}}$ . . . . .	64
4.5.3	Störmer-Verlet integration scheme . . . . .	64
4.5.4	Signal processing . . . . .	67
4.6	Conclusion . . . . .	67
<b>5</b>	<b>Numerical simulation of absorber effects on the dynamical behavior of an elastic beam</b>	<b>69</b>
5.1	Introduction . . . . .	69
5.2	Parameterization of the damped elastic beam . . . . .	70
5.3	Eigenmodes of the beam . . . . .	71
5.4	Definition of the configurations . . . . .	71
5.5	Construction of the reduced-order model and frequency band of the analysis . . . . .	72
5.6	Signal processing . . . . .	72
5.7	Quantities of interest . . . . .	72
5.8	Numerical analysis of the effects of a linear absorber . . . . .	74
5.9	Numerical results and analysis for the beam coupled with a non-linear absorber . . . . .	75
5.10	Conclusion . . . . .	78
<b>6</b>	<b>Conclusions and Perspectives</b>	<b>81</b>
6.1	Summary . . . . .	81
6.2	Perspectives . . . . .	82
6.3	Scientific production . . . . .	83
	<b>Appendices</b>	<b>85</b>

<i>CONTENTS</i>	9
<b>Appendix A Qualitative effects of stiffness, damping, and shape on the nonlinear behavior of an absorber</b>	<b>85</b>
A.1 Qualitative effects of stiffness and damping on the power density of a nonlinear oscillator . . . . .	85
A.2 Qualitative effects of the shape of the absorber on its nonlinear behavior . . . . .	87
<b>Appendix B Parametric study on the dimension of the beams that compose the absorber</b>	<b>89</b>
<b>Bibliography</b>	<b>93</b>



# Résumé de la thèse

Des recherches sur la réduction des vibrations et du bruit induit sont en cours depuis très longtemps. Des méthodes de réduction sont connues, contrôlées et appliquées dans le domaine des hautes et moyennes fréquences, entre autres par l'utilisation de systèmes passifs tels que les matériaux poroélastiques dissipatifs intégrés dans des éléments structuraux, et par des systèmes semi-actifs et actifs. Cependant, pour les matériaux poroélastiques, cette réduction est plus difficile à obtenir dans le domaine des basses fréquences, pour lequel les longueurs d'onde ont une dimension caractéristique supérieure à celle des pores des matériaux dissipatifs, rendant ces derniers moins efficaces.

Malgré ces difficultés, l'atténuation des vibrations en basses fréquences reste un enjeu important. Pour résoudre ce problème, différents axes de recherche ont été explorés et ont été mis en application pour stocker et dissiper l'énergie vibratoire. La technologie la plus connue est basée sur l'utilisation d'absorbeurs à masse accordée. Ces derniers se comportent comme des oscillateurs linéaires composés d'une masse, d'un ressort et d'un amortisseur. Ils sont fixés à la structure pour laquelle on souhaite atténuer les vibrations à une certaine fréquence, et sont conçus de manière à ce que leur fréquence de résonance soit la fréquence gênante de la structure. Les principaux inconvénients de ces dispositifs sont leur capacité à n'atténuer les vibrations qu'autour d'une étroite bande de fréquences centrée sur leur fréquence de résonance.

Pour palier ces difficultés, l'utilisation d'absorbeurs ayant un comportement non linéaire est une alternative intéressante. En effet, grâce à un étalement fréquentiel de la réponse de l'oscillateur, celui-ci permet d'atténuer les vibrations de la structure sur une plus large bande de fréquence qu'un absorbeur ayant un comportement linéaire. Les travaux réalisés dans cette thèse ont été développés dans ce cadre. Il est cependant à noter que seuls les systèmes purement mécaniques ont été abordés, mais que de nombreux travaux ont été effectués ces dernières années sur la réduction des vibrations à l'aide de systèmes semi-actifs électro-mécaniques basés sur l'utilisation de patchs piézoélectriques, et aussi à l'aide de systèmes de contrôle actif.

Les travaux présentés ici se placent dans le cadre de la réduction vibratoire dans des éléments structuraux, à l'échelle macroscopique, en basses fréquences, pour lesquelles les premiers modes de vibration sont excités. L'objectif final de ce travail est de réduire les vibrations d'éléments structuraux sur une large bande

basse fréquence à l'aide d'absorbeurs ayant un comportement non linéaire. Pour cela, la première étape a été de concevoir et d'analyser l'efficacité d'un absorbeur constitué d'une poutre console avec une masse concentrée à son extrémité libre. Cet absorbeur est conçu pour avoir un comportement dynamique non linéaire induit par les effets géométriques en déplacement finis de la masse. Cet absorbeur a été conçu pour stocker et dissiper l'énergie mécanique sur une large bande de fréquences autour de sa fréquence de résonance, à l'inverse d'une bande de fréquences étroite pour un absorbeur ayant un comportement linéaire.

Une modélisation mécanique a été développée pour cet oscillateur non linéaire et une méthode numérique de résolution des équations a été implémentée. Une conception de l'absorbeur a été faite en prenant en compte des contraintes existantes sur les paramètres de conception. Plusieurs conceptions ont été analysées et la conception retenue correspond à celle évoquée précédemment (poutre console avec une masse concentrée placée à son extrémité libre). La réalisation expérimentale de l'absorbeur retenu a été menée puis a été expérimentée. Les données expérimentales obtenues ont permis d'identifier les paramètres du modèle mécanique et ont permis de mettre en évidence l'atténuation espérée sur une large bande de fréquences pour cet absorbeur non linéaire.

Une fois l'absorbeur non linéaire conçu, construit, analysé expérimentalement, modélisé et identifié, la seconde étape de la recherche a été abordée. Elle a consisté à analyser, par simulations numériques, l'atténuation de la réponse vibratoire d'une poutre élastique dissipative induite par la présence de l'absorbeur non linéaire, excitée par une force stochastique stationnaire sur une bande de fréquences donnée. Pour cela, une modélisation complète du problème aux limites de la poutre couplée à des absorbeurs non linéaires a été développée. Un modèle réduit des équations non linéaires a été construit et un solveur stochastique associé a été implémenté.

Cette modélisation a permis de réaliser des simulations numériques afin de mettre en évidence les effets d'un absorbeur non linéaire sur le comportement vibratoire d'une poutre élastique. L'absorbeur non linéaire considéré est celui conçu, construit, analysé expérimentalement, modélisé et identifié. Deux configurations de poutre ont été étudiées. La première poutre est conçue de sorte que sa troisième fréquence de résonance coïncide avec celle de l'absorbeur, et la seconde poutre de sorte que sa fréquence fondamentale coïncide avec celle de l'absorbeur. D'autres simulations, en particulier avec des absorbeurs ayant un comportement linéaire, ont été réalisées dans le but de mieux comprendre les apports des absorbeurs non linéaires par rapport aux absorbeurs linéaires. Il a été observé que la présence d'un absorbeur non linéaire sur la poutre permet une atténuation d'un gain de plus de 2, sans le phénomène de séparation de la résonance que l'on cherche à atténuer en deux résonances séparées. L'introduction de plusieurs absorbeurs non linéaires permettrait d'obtenir une grande atténuation proportionnelle au nombre d'absorbeurs dont la localisation sur la structure serait optimisée.

# Notations

- $a, b$  correspond to constants in  $\mathbb{R}$ .
- $\mathbf{a}, \mathbf{b}$  refer to vectors with values in  $\mathbb{R}^n$ ,  $n \geq 1$ .
- $A, B$  random variables with values in  $\mathbb{R}$ .
- $\mathbf{A}, \mathbf{B}$  denote random vectors with values in  $\mathbb{R}^n$ ,  $n \geq 1$ .
- $[A], [B]$  refer to real matrices.
  
- $\cdot^{\text{exp}}$ : Experimental quantity.
  
- $\delta_{ij}$  is the Kronecker delta defined such that  $\delta_{ij} = 1$  if  $i = j$  and  $\delta_{ij} = 0$  if  $i \neq j$ .
- $E$  denotes the mathematical expectation.
- $\bar{z}$  is the conjugate of complex number  $z$ .
  
- $\mathbb{R}$  is the set of real numbers.
- $\mathbb{N}$  denotes the set of positive integers.
- $\Omega \subset \mathbb{R}$  refers to a subset of  $\mathbb{R}$ .
- $\mathcal{C}_{ad}$  is a admissible set.
- $(\Theta, \mathcal{T}, \mathcal{P})$  is a probability space.
  
- ABS: Acrylonitrile Butadiene Styrene
- DOF(s): Degree(s) of Freedom. One-DOF: One Degree of Freedom. MDOF: Multiple Degrees of Freedom
- FFT: Fast Fourier Transform
- NES: Nonlinear Energy Sink.
- PSD: Power Spectral Density
- TMD: Tuned Mass Damper.



# Chapter 1

## Introduction and objectives

### 1.1 Context and objectives

The reduction of vibration and induced noise is, for a very long time, an important concern in the field of research for industrial applications. This reduction is relatively well mastered at medium and high frequencies by using either passive technologies such as poroelastic materials inserted in composite structural elements or semi-active or active control technologies based, for instance, on the use of piezoelectric patches, but remains less efficient for low frequencies. For instance, for poroelastic materials, their low efficiencies are mainly due to the long wavelengths that exist in the low frequency band with respect to the pores dimensions of the material.

However, reducing vibration at low frequencies is an important issue, since many nuisances are associated with, such as road traffic or certain industrial machines. To get around this problem at low frequencies, several ways have been explored in order to store and to dissipate the energy of vibration. These technologies are presented in a bibliographical summary in Sections 1.3 and 1.4. Methods and devices based for reducing vibration at low frequencies are presented. This state of the art is not exhaustive. Some references are given such as the review on structural control [1], the handbook of noise and vibration control [2], Chapter 2 in the handbook of micromechanics and nanomechanics presenting micromechanics of elastic metamaterials, and a review of existing models for dynamic problems of metamaterials [3]. In Section 1.2, a list of techniques devoted to directly attenuate vibration is given in Section 1.2.1 and a short review of attenuation at mid and high frequencies is presented in Section 1.2.2.

In this list of existing technologies for absorbers, there are technologies based on the use of mechanical oscillators. This type of technology has extensively been studied in the literature, especially the Tuned Mass Dampers (noted TMD in the following). Their principle is to attach an oscillator to a main structure. This oscillator is tuned to the resonance frequency of the structure that it is desired to attenuate, enabling it to capture its vibrational energy. At the dynamical equilibrium for an harmonic response, the mechanical energy is transmitted from the structure to the absorber, is stored and dissipated by it. The disad-

vantage of these linear absorbers is an attenuation that is effective on a narrow frequency band around the eigenfrequency of the absorber and the apparition of an additional resonance due to the presence of the absorber. Details are provided in Section 1.3.1 for the one-DOF linear oscillators, in Section 1.3.2 for the multi-DOF (MDOF) linear oscillators, and in Section 1.3.3 for the continuous linear systems.

In order to overcome the difficulties of linear absorbers, it is advantageous to use nonlinear absorbers. In 1952, Roberson [4] has presented the equations of a nonlinear dynamic vibration absorber and highlighted the fact that an auxiliary body with nonlinear dynamical behavior offers significant advantages over a linear absorber. More recently, some works have been performed for analyzing vibration of nonlinear oscillators in a stochastic framework, such as in [5, 6, 7, 8] in which it is demonstrated the role plays by the nonlinearities in the transfer of the vibratory energy over a broad frequency band. Concerning the energy pumping by distributed nonlinear mechanical oscillators in order to attenuate vibration for mechanical systems at low frequencies, many works have been published and a review can be found in Section 1.4. The present work is devoted to passive purely mechanical systems for reducing the vibrations. Nevertheless, it should be noted that numerous works have been performed since many years for reducing vibration by using electro-mechanical systems such as the systems based on the use of shunted piezoelectric patches (see for instance [9, 10, 11]) and active controls for which a considerable number of papers have been published since three decades (see for instance as an illustration, [12, 13, 14, 15]).

This thesis is developed in the framework of the reduction of vibration in structural elements at macro-scale for the low-frequency band in which the first modes of vibration are excited. The final objective of this work is to reduce vibration on a broad low-frequency band by using nonlinear absorbers. For that, the first step of this work has been to design and to analyze the efficiency of a nonlinear absorber, which is made up of a cantilever beam with a point mass at its end. This absorber behaves as a nonlinear oscillator due to nonlinear geometrical effects induced by finite displacements of the point mass. This nonlinear absorber is designed so that the energy pumping is effective on a broad frequency band around its resonance frequency instead of a narrow frequency band as for a linear oscillator. Once the nonlinear absorber has been designed, manufactured, and experimentally tested, its efficiency has been highlighted by putting it on a main structure in order to analyze the vibration attenuation induced by the presence of the absorber at low frequencies.

## **1.2 Reduction of vibration by direct dissipation at middle and high frequencies**

### **1.2.1 Direct dissipation of vibration**

First, the simplest method for attenuating vibration is to introduce dissipation carried out by damping systems. The technologies based on passive damping systems are inexpensive, easy to design, and are well known systems. About the

direct dissipation of vibration, the main mechanical systems are the following.

- *Absorbers by friction.* In this case, the dissipation is obtained by friction between two solid surfaces. In this framework of dynamic analysis tool, we can refer, for instance, the dynamic Lagrangian frequency-time method for the vibration of dry-friction-damped systems developed by Nacivet *et al* [16].
- *Viscoelastic materials.* Their mechanism is based on their dissipative constitutive equations. This is the case, for instance, of a layer of polymer that is sandwiched between two metallic panels. Such a composite allows for attenuating the vibrations without changing the mechanical resistance. They are effective at mid and high frequencies.
- *Viscous damping absorbers.* They allow vibration dissipation due to the action of a piston forced by a fluid. This technology can be passive, semi-active or active.

### 1.2.2 Reduction of vibration and noise at middle and high frequencies

Techniques to reduce vibration and noise at middle and high frequencies have been extensively explored and are particularly effective. Since the work of this thesis focuses on vibration attenuation in low frequencies, only a brief review of existing methods is presented in this section. For more details, see for instance [17].

Porous materials are used to dissipate noise and vibration at middle and high frequencies. The characteristic size of their pores must be of the same order of magnitude as the wavelengths of the waves to be dissipated. When the wave comes into contact with the pore, some of its energy is transmitted, but another is refracted. Generally, a porous material constitutes a layer in a soundproofing wall. Two illustrations of using of a porous material are presented in Figure 1.1. In the first one, a porous layer is fixed to an impervious rigid wall and in the second one, there is a gap of air between the porous layer and the rigid wall. For each case, the absorption coefficient at oblique incident is shown in Figure 1.2. It can be seen that the porous material is very effective for absorbing waves at middle and high frequencies, but, at low frequencies (i.e lower than 400 Hz), it is not really effective.

## 1.3 Reduction of vibration at low frequencies by linear absorbers

### 1.3.1 Attenuation of vibration at low frequencies by a linear absorber corresponding to a one-DOF linear oscillator

This section focuses on the attenuation of vibration at low frequencies by a linear absorber corresponding to a one-DOF linear oscillator (simple oscillator).

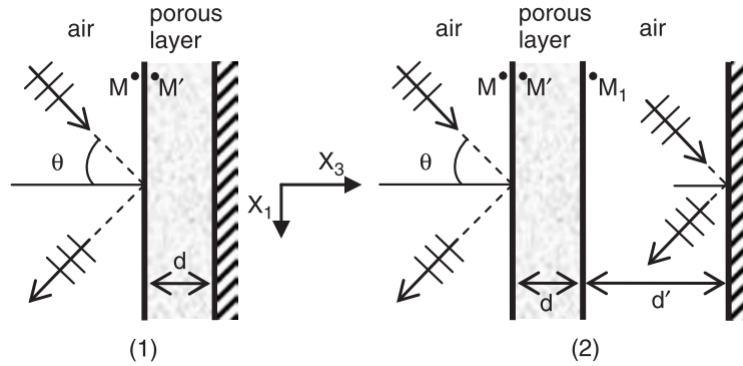


Figure 1.1: (1) A porous layer of thickness  $d$  is fixed to an impervious rigid wall. (2) There is a gap of air of thickness  $d'$  between the porous layer and the rigid wall. In both cases, the front face of the porous material is in contact with air. Taken from [17].

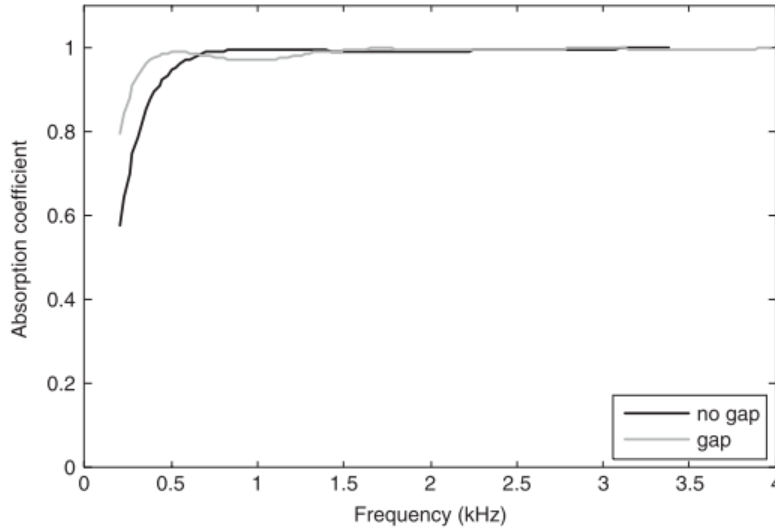


Figure 1.2: The absorption coefficient at oblique incident for both configurations of Figure 1.1. Taken from [17].

Among the first papers devoted to the energy pumping by simple oscillators, the work by Frahm [18] in 1911 can be cited, in which the author proposes to add an auxiliary body to a structure in order to attenuate the vibration due to periodic impacts. The resonance vibration of the main body are attenuated by the resonance of the absorber.

In nearer years, for vibratory energy, tuned-mass dampers (TMDs) have been studied. The principle is to add an oscillator (generally a mass-spring-damper system) to a main structure that exhibits an annoying resonance. The eigenfrequency of the damped oscillator is then adjusted for attenuating the resonance

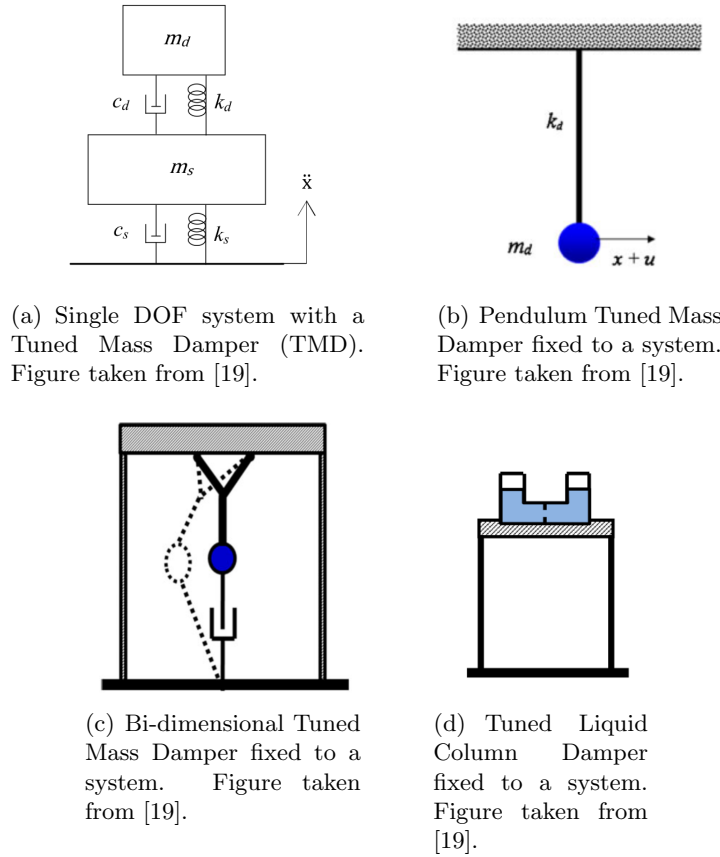


Figure 1.3: Schemes of four categories of TMDs.

amplitude. With that, the peak is split into two peaks of low amplitudes. A review made by Gutierrez Soto *et al* [19] presents a representative study on tuned-mass dampers. TMDs can be divided in four categories: conventional TMDs, pendulum TMDs (notes PTMDs), bi-directional TMDs (noted BTMDs), and tuned liquid column dampers (noted TLCDs). A scheme of a single DOF system with a conventional TMD is illustrated in Figure 1.3(a). The constant  $m_d$  is the TMD mass,  $k_d$ , and  $c_d$  are the stiffness and damping coefficients. The constant  $m_s$  is the system mass,  $k_s$ , and  $c_s$  are the stiffness and damping coefficients. PTMDs are constituted of a mass at the end of a cable attached to the system that is desired to damp (see Figure 1.3(b)). They are principally used for earthquakes: when the building is subjected to an earthquake, the PTMD creates a force in the opposite direction of the floor movement. BTMDs are a combination of two cables forming a Y-shape connecting to the mass at the middle, and a friction damper connected to the mass from the bottom (see Figure 1.3(c)). A TLCd is a type of TMD where the single mass is replaced with liquid, usually water. The sloshing of the water counterbalances the effects of external vibration (see Figure 1.3(d)).

The principal disadvantage of TMDs is their large dependence to their resonance

frequency. A change or an error of the calibration of the TMD or of the estimation of the frequency of excitation can substantially reduce the efficiency of the TMD and possibly occasion damages on the primary structure. A solution to this problem is to add not a single TMD to the structure, but multiple TMDs having resonant frequencies close to one another (see Section 1.3.2). Moreover, the efficiency of the TMD is closely related to the correct calibration in relation to the resonance frequency of the system that it is desired to damp. Unfortunately, due to the damage and aging that structures can undergo, TMDs can no longer be properly calibrated with time passing.

In the field of acoustics, the equivalent of TMD is the Helmholtz resonator. It is a container of gas (usually air) with an open hole (usually a neck). This system has a resonance frequency that depends on the volume of the container, the opening area, the neck length, and the velocity of sound such that

$$\text{Resonance frequency} = \frac{\text{Velocity of sound}}{2\pi} \sqrt{\frac{\text{Opening area}}{\text{Container volume} \times \text{Neck length}}}.$$

There is a mechanical-acoustical analogy between a Helmholtz resonator to attenuate sound and a mass-spring-damper oscillator to attenuate vibration. A complete definition of Helmholtz resonators and their operations can be found in [20]. It has been demonstrated that the shapes of the container volume and of the neck have no effects on the efficiency of the Helmholtz resonator (see [21]). Moreover, with self-tuned Helmholtz resonators, De Bedout *et al* in 1997 [22] have experimentally observed an attenuation up to 30 *dB*.

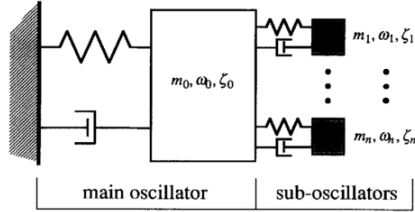
Some works have been made with a combination of TMDs and Helmholtz resonators to dissipate noise and vibration with a unique system, for instance [23, 24] in which this vibration and noise attenuation is applied into payload fairings.

In summary, TMDs and Helmholtz resonators can significantly attenuate sound and vibration at low frequencies but it is needed to have several number of them in order to attenuate over a broad frequency band. There are also semi-active and active attenuation systems for which an introduction can be found in [25, 26], they have the capability to adapt their resonant frequency using an external energy input but they have the disadvantage of needing an external power source to operate, which in some cases may have the opposite effect of adding energy to the system which need to be damped.

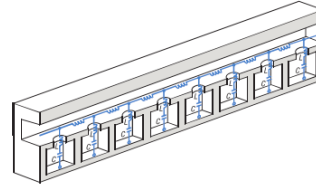
### 1.3.2 Attenuation of noise and vibration at low frequencies by MDOF linear oscillators-based absorbers

This section presents the attenuation of noise and vibration at low frequencies by MDOF (multiple degrees of freedom) linear oscillators-based absorbers. These absorbers can be assimilated to metamaterials. A metamaterial is generally a composite for which these mechanical properties do not exist at the natural state. For instance, there are materials with both negative permittivity

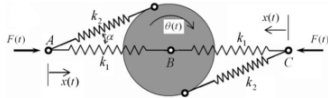
and negative permeability in optics with, for instance, the work of Veselago in 1968 [27] and the work of Smith *et al* in 2000 [28], they prove the existence of a frequency band in which both permeability and permittivity are negative.



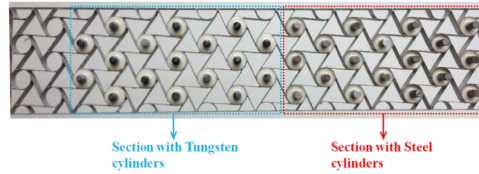
(a) System configuration of MDOF linear oscillators-based absorber. Figure taken from [29].



(b) Illustration of periodical daisy-chained Helmholtz resonators. Figure taken from [30].



(c) 1D representative mass-spring model of a chiral microstructure having simultaneously negative effective mass density and bulk modulus at certain frequencies. Figure taken from [31].



(d) Experimental realization of chiral material with resonators made of tungsten cylinders and steel cylinders. Figure taken from [32].

Figure 1.4: Illustrations of MDOF linear oscillators-based absorbers.

The numerical study of Xu and Igusa in 1992 [29], in which they have studied a configuration with multiple TMDs with equal stiffnesses and with equally spaced resonant frequencies (a scheme of the system configuration can be seen in Figure 1.4(a)), shows that when the number of TMDs becomes large, the obtained attenuation is equivalent to a single viscous damping, which is added to the damping of the main structure. A parallel work for noise attenuation is done in [30] with experimental validation of an array of Helmholtz resonators (see Figure 1.4(b)). These materials are defined such that having an effective dynamic modulus with negative values near the resonance frequency. This notion of negative values is also explained in [31], in which an elastic metamaterial which exhibits simultaneously negative effective mass density and bulk modulus is presented. The double-negative properties are achieved through a chiral microstructure that is capable of producing simultaneous translational and rotational resonances. A 1D representative model of this structure is presented in Figure 1.4(c).

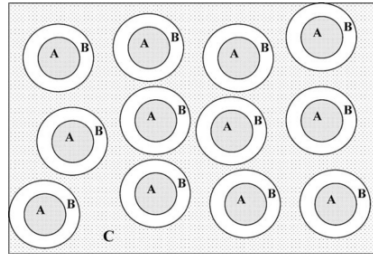
Since TMDs are only effective on a narrow frequency band, using multiple TMDs according on different frequencies can allow to pump energy over a

broader frequency band. This method is illustrated, for instance, in [33], in which is studied, analytically and experimentally, the dynamic behavior of a sandwich structure containing spring-mass resonators. It has been found that this system is capable of efficiently blocking waves at certain frequency range near the resonances. In 2012, Bandivadekar *et al* [34] have worked on the mass distribution of multiple TMDs in order to optimize vibration control of structures. Effects of damping have also been investigated. They have concluded that a higher mass, where the response is high, and a low damping are the best setting for absorbers. On the optimization of MDOF absorbers, we can also cite [35], in which an array of mass-spring resonators fixed to a thin plate is used for sound transmission loss at low frequencies. In [36], another study is done on an absorber composed of multiple mass-spring systems, with each system connected in serie to another one, not in parallel. In 2014, Zhu *et al* [32] present a chiral elastic metamaterial beam with multiple resonators for broadband vibration suppression (see Figure 1.4(d)). An experimental validation is added to the theoretical development. The attenuation of vibration is particularly efficient over 400 *Hz*. We can cite the work of Pai *et al*[37] as a parallel study for noise attenuation.

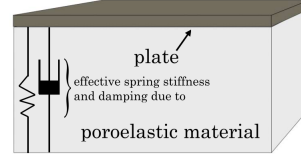
### 1.3.3 Attenuation of noise and vibration at low frequencies by linear continuous absorbers

This section presents the attenuation of noise and vibration at low frequencies by linear continuous absorbers. As MDOF linear oscillators-based absorbers introduced in Section 1.3.2, these systems can be assimilated to metamaterials.

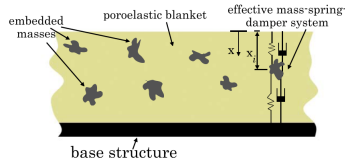
In 2003, Sheng *et al* [38] have designed a composite material constituted of inclusions of lead particles embedded in a rubber layer; the matrix is made of epoxy (see Figure 1.5(a)). This material has been able to attenuate local sonic resonances between 350 *Hz* and 2000 *Hz*. These results have been validated with an experimental realization. In [41], in 2007, a difference is made between the static volume-averaged mass density and the dynamic one which take into account the relative motion between the components of the metamaterial. With their definition, it is possible to expose a negative dynamic mass density locally. The same year, Ding *et al* [42] highlight a metamaterial with simultaneously negative bulk modulus and mass density. This metamaterial is a zinc blende structure consisting of one face-centered cubic array of bubble-contained-water spheres and another relatively shifted face-centered cubic array of rubber-coated-gold spheres in epoxy matrix. The negative bulk modulus and mass density are simultaneously derived from the coexistent monopolar resonances from the embedded bubble-contained-water spheres and dipolar resonances from the embedded rubber-coated-gold spheres. The Poisson ratio of the metamaterial also turns negative near the resonance frequency. In [43] is presented an experimental realization and a theoretical realization of a membrane-type acoustic metamaterial with negative dynamic mass, capable of sound attenuation in the [100 – 1000] *Hz* regime. In 2009, Lee *et al* [44] propose a 1D acoustic metamaterial with negative effective density using an array of thin elastic membranes.



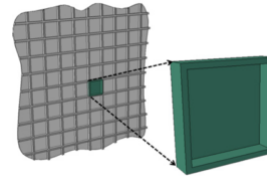
(a) Schematic structure of the composite material. “A” denotes a lead solid particle; “B” denotes a silicone rubber layer; and “C” denotes the matrix material of epoxy. Figure taken from [38].



(b) Effective distributed vibration absorber resulting from the interaction between a continuous top mass and a poroelastic material. Figure taken from [39].



(c) Scheme of poroelastic material with embedded masses, the “HG blanket” (heterogeneous blanket). Figure taken from [39].



(d) Cellular panel with its unit cell. Figure taken from [40].

Figure 1.5: Illustrations of linear continuous absorbers.

With this configuration, they have been able to obtain, numerically and experimentally, a complete acoustic cloaking between  $0\text{ Hz}$  and  $735\text{ Hz}$ . The same year, Fuller *et al* [39] present the efficiency of two configurations to attenuate vibrations at low frequencies: a continuous vibration absorber which utilizes a poroelastic material as the spring layer and an acoustic foam material as the continuous top mass (see scheme Figure 1.5(b)) and a poroelastic material into which a number of masses have been embedded (see scheme Figure 1.5(c)). These masses interact with the elasticity of the poroelastic material in order to form an array of spring-mass-dampers. Zhou *et al* [45] propose an unified analytic model for the effective mass density, effective bulk modulus, and effective shear modulus for elastic metamaterials composed of coated spheres embedded in a host matrix. An experimental realization of thin membrane-type acoustic metamaterials capable of a total reflection at certain frequencies can be found in [46], with an attenuation between  $50\text{ Hz}$  and  $1,000\text{ Hz}$ . Varanasi *et al* have proposed, in 2013, an efficient metamaterial to attenuate sound at low frequencies. This material is a panel constituted of an array of cellular unit structures, as it is illustrated in Figure 1.5(d). In 2016, Wang *et al* [47] have also developed a membrane-constrained acoustic metamaterial for low frequency sound insulation. We can also cite the study done on the design and the optimization of acoustic network resonators for tire/road noise reduction in [48].

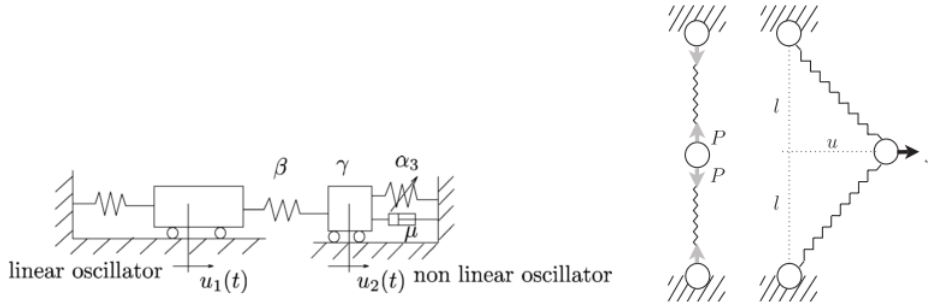
## 1.4 Attenuation of noise and vibration at low frequencies by nonlinear absorbers

This section focuses on the attenuation of noise and vibration at low frequencies by nonlinear oscillators-based absorbers. It is not possible to reference all research on the subject here, but a review can be found in [49].

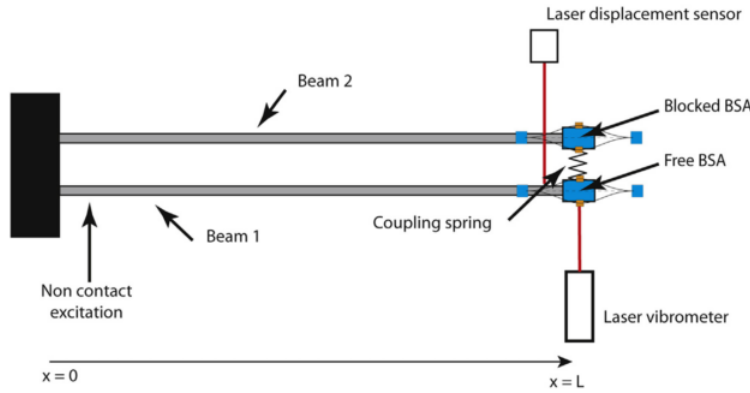
Equations of a dynamic vibration absorber with nonlinear dynamical behavior fixed to an auxiliary body, presented in 1952 by Roberson [4], highlighted the fact that a nonlinear dynamical behavior offers significant advantages over a linear absorber. We can cite some works, in which is analyzed vibration of nonlinear oscillators in a stochastic framework in order to demonstrate that nonlinearities are useful in the transfer of the vibratory energy over a broad frequency band, such as in [5, 6, 7, 8].

Concerning the energy pumping by one-DOF mechanical oscillator with nonlinear stiffness and linear damping in order to attenuate vibration and noise for discrete systems, many works have been published such as [50, 51], in which is presented numerical evidence of irreversible energy pumping by nonlinear mechanical oscillators. As the linear oscillators-based absorbers presented previously, nonlinear ones are designed to be added to a main structure to absorb its undesirable noise and vibration. We can see an illustration of this in Figure 1.6(a), taken from [52]. A variate of this configuration exists, in which the nonlinear spring and its associated damper are placed between two masses and in which the mass of the nonlinear absorber is free of constraint. In this article is also presented an experimental realization of a thin viscoelastic membrane for which the nonlinear behavior is obtained by large amplitudes of oscillation and which is capable of pumping sound energy. Other articles about using a thin viscoelastic membrane, with large displacements, for noise attenuation can be cited [53, 54]. In [55], the absorber is composed of two springs connected by a mass. The nonlinear behavior of this system is obtained by springs working off their axis, as illustrated in Figure 1.6(b). This configuration is theoretically and experimentally validated for the attenuation of the main structure vibration at low frequencies. Alexander *et al* [56] have also used springs off their axis to model a nonlinear absorber. Nili Ahmadabadi *et al* [57], in 2014, present a combination of a nonlinear oscillator-based absorber (with nonlinear stiffness and linear damping) with a piezoelectric device. Another configuration is proposed by Mattei *et al* [58] to attenuate vibration at low frequencies. The nonlinear absorber is made of a 3D-printed support on which is clamped a buckled thin small beam with a small mass fixed at its center having two equilibrium positions (see Figure 1.6(c)).

Concerning the attenuation of noise and vibration by MDOF oscillator-based absorbers with nonlinear stiffness and linear damping, many works have been published and some of them are cited here. In 1986, Soize [62, 63] has introduced a novel model of the vibration damping due to the vibrations of mechanical



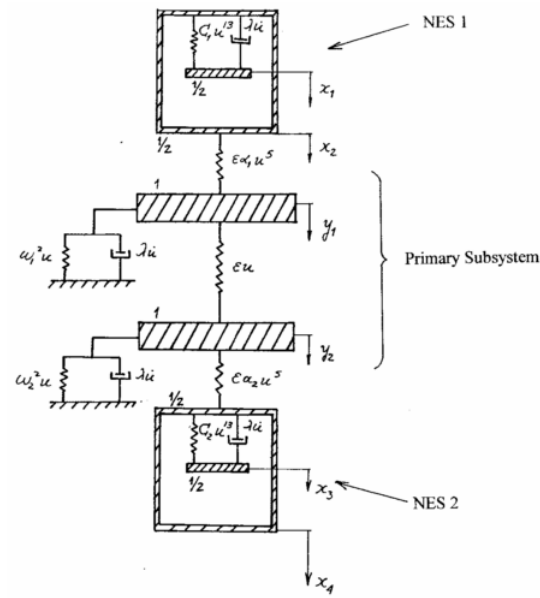
(a) A simple two DOF vibrating system for illustrating the pumping phenomenon. Figure taken from [52].  
 (b) Design of two linear springs working off their axis. Figure taken from [55].



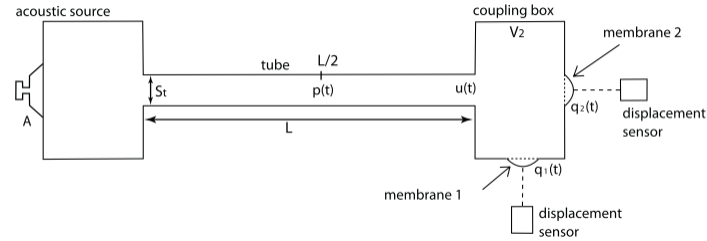
(c) Sketch of the experiment proposed by [58].

Figure 1.6: Illustrations of one-DOF nonlinear absorbers.

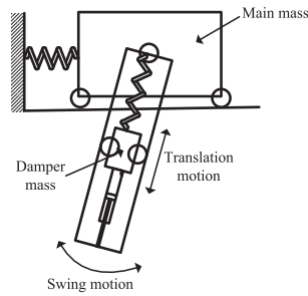
subsystems constituting the internal structural complexity. As an extension of the work done in [50, 51], [59] proposes to add a couple of nonlinear absorbers to a primary system in order to achieve robust energy pumping (a scheme can be seen in Figure 1.7(a)). The same configuration is studied in [64], in which one can see that the nonlinear absorbers can absorb a significant portion of the input energy in an irreversible way: the energy remains localized instead of spreading back into the primary system. Bellet *et al* [60] propose a generalization of [52, 53, 54] by using several nonlinear membrane absorbers for noise attenuation. A scheme of this experimental setup can be seen in Figure 1.7(b). We can also cite the paper from Viet *et al* [61], in which horizontal vibrations are reduced by a nonlinear single-mass two-frequency pendulum absorber (its scheme can be seen in Figure 1.7(c)). This configuration contains one mass moving along a bar while the bar can rotate around the point attached with the controlled structure. The two natural frequencies exist because of the two motions: swing and translation. Lamarque *et al* [65] propose an analytical and numerical study on the dynamical behavior of a nonlinear mechanical system with two DOFs during free and forced excitations.



(a) A linear main system with two nonlinear absorbers attached. Figure taken from [59].



(b) Scheme of the experimental setup with two membrane absorbers. Figure taken from [60].



(c) Concept of single-mass two-frequency pendulum absorber. Figure taken from [61].

Figure 1.7: Illustrations of MDOF nonlinear absorbers.

## 1.5 Scientific approach & outline of the thesis

The work performed in this thesis takes place in the framework of the reduction of vibration in structural elements at macro-scale at low frequencies for which the first structural modes are excited. The goal of this work is to design and test a absorber with nonlinear properties able to attenuate vibration at low frequencies over a broad frequency band.

For that, the first step of this work is to design and to analyze the efficiency of a nonlinear absorber, which is made up of a cantilever beam with a point mass at its end. This absorber behaves as a nonlinear oscillator due to nonlinear geometrical effects induced by the finite displacements of the point mass. The absorber is designed so that the energy pumping is effective on a broad frequency band around its resonance instead of a narrow frequency band as for a linear oscillator. The objective of this step is:

1. to design the nonlinear absorber in terms of shape, dimensions, and materials, in order that the vibratory energy is pumped on a broad frequency band around its first resonance,
2. to experimentally manufacture this system with a 3D-printing system,
3. to validate these dynamical properties with experiments,
4. to develop a mechanical model to predict the responses for stationary stochastic excitation,
5. and to perform the identification of the mechanical model with the experiments.

Once the nonlinear absorber is designed, modeled, and identified, the second step consists in analyzing its effect on the frequency response of a structural element in the low-frequency band. This step consists in analyzing by numerical simulations the effects of this nonlinear absorber on the dynamic behavior of a cantilever beam.

Given the adopted approach explained here, the thesis is organized as follows.

Chapter 2 is devoted to the construction of the mechanical model representative of the absorber with nonlinear behavior that has the capability to absorb energy. The related stochastic solver is also introduced.

Chapter 3 is devoted to the experimental realization of the absorber. First, the experimental design is performed in order to obtain an effective attenuation in the frequency band of analysis. The experimental measurements and the identification of the mechanical model are also presented.

Chapter 4 deals with the construction of the mechanical model representative of a beam coupled to nonlinear absorbers. The related stochastic solver is also introduced.

Chapter 5 is devoted to the numerical realizations of the beam with nonlinear absorbers based on the mechanical model developed in Chapter 4, in order to study the effects of the nonlinear absorber on the vibration response of the beam.

## Chapter 2

# Nonlinear model of the absorber and stochastic solver

### 2.1 Introduction

To facilitate the experimental steps and to know which parameters to use, it is interesting to carry out a numerical modeling reproducing the experiment. The modeling remains an approximation of the real system, and can not take all the parameters into account, due to the complexity of the system and the limitation of the computational resources. In this thesis, the focus is on noise and vibration absorption of a structure by an absorber over a broad frequency band at low frequencies. For this reason, the modeling of the absorber must especially take into account its nonlinear dynamic behavior, since, as seen in Chapter 1, nonlinearity allows absorption over a broader frequency band than linear behavior.

Among the various existing nonlinearities, it has been chosen that the nonlinear dynamic behavior of the absorber is due to large displacements. A one-DOF nonlinear oscillator is proposed to model the nonlinear dynamical behavior of the absorber. Even if a model with several DOFs would have provided more information, it remains interesting, in a first approach, to consider a rather simple model. As a matter of fact, the designed absorber (detailed in Chapter 3) has a preferred direction of excitation, therefore, its modeling by a one-DOF system remains an interesting approach to be studied.

The one-DOF nonlinear model is composed of a mass-spring-damper system with a nonlinear spring and a nonlinear damper, subjected to a stochastic excitation of its base (see the scheme displayed in Figure 2.1). The construction of the nonlinear forces associated to the spring and the damper is based on the linear viscoelasticity theory in large displacements, which is a nonlinear model.

In this chapter, the model of the nonlinear absorber is introduced in Section 2.2. Section 2.3 is devoted to the writing of the stochastic solver and to signal processing. Section 2.3.1 presents the stochastic solver based on the Monte Carlo method [66], then, in Section 2.3.2 is introduced the time and frequency

sampling of the solver. After that, Section 2.3.3 deals with the generation of independent realizations of Gaussian stationary stochastic process, which is applied to the base excitation. The stochastic solver is solved based on the Störmer-Verlet integration scheme [67, 68], which is detailed in Section 2.3.4. In addition, Section 2.3.5 displays the signal processing used. Finally, Section 2.4 gives a validation of the solver with a linear oscillator (for which the spring and the damper are linear).

## 2.2 Model of the nonlinear oscillator

A one-DOF nonlinear oscillator is proposed to model the nonlinear dynamical behavior of the absorber. As illustrated in Figure 2.1, the chosen one-DOF nonlinear model is made of a mass-spring-damper system with a nonlinear spring and a nonlinear damper. This oscillator is subjected to a stochastic excitation of its base. We introduce a parameterized family of one-DOF nonlinear oscillators, for which the proposed algebraic model is inspired/coherent with the linear viscoelasticity theory in finite displacements (nonlinear model) without memory [69, 70]. In addition, we want the stochastic response of the one-DOF nonlinear oscillator submitted to a centered stochastic excitation to be a centered stochastic process. This constraint will be taken into account in the construction of the nonlinear damping force and of the nonlinear stiffness force, deduced from the viscoelasticity theory in finite displacements.

Let  $X_{\text{imp}}(t)$  be the displacement imposed at the support in the absolute frame and  $X_s(t)$  be the relative displacement of the point mass with respect to the support. Let  $\{\ddot{X}_{\text{imp}}(t), t \in \mathbb{R}\}$  be the acceleration imposed to the support, which

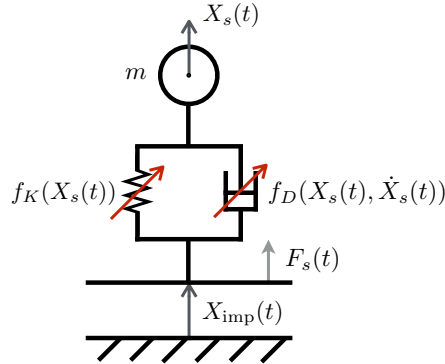


Figure 2.1: 1D simplified model.

is assumed to be a Gaussian stationary second-order centered stochastic process, defined on the probability space  $(\Theta, \mathcal{T}, \mathcal{P})$ , for which the power spectral density function is denoted by  $S_{\ddot{X}_{\text{imp}}}(\omega)$ . We are interested in finding the non-Gaussian stationary second-order centered stochastic process  $\{X_s(t), t \in \mathbb{R}\}$  that satisfies, for all  $t$  in  $\mathbb{R}$ , the following stochastic nonlinear equation

$$m(\ddot{X}_s(t) + \ddot{X}_{\text{imp}}(t)) + f_D(X_s(t), \dot{X}_s(t)) + f_K(X_s(t)) = 0 ,$$

which is rewritten as

$$m\ddot{X}_s(t) + f_D(X_s(t), \dot{X}_s(t)) + f_K(X_s(t)) = F_s(t) , \quad (2.1)$$

in which the applied stochastic force  $F_s(t)$  is written as

$$F_s(t) = -m \ddot{X}_{\text{imp}}(t) , \quad (2.2)$$

and where the nonlinear damping force  $f_D$  and the nonlinear stiffness force  $f_K$  are written as

$$f_D(X_s(t), \dot{X}_s(t)) = (c_1 + c_2|X_s(t)|)\dot{X}_s(t) , \quad (2.3)$$

$$f_K(X_s(t)) = k_1 X_s(t) + k_3 (X_s(t))^3 . \quad (2.4)$$

The absolute displacement  $X_a$  of the mass is such that

$$X_a(t) = X_s(t) + X_{\text{imp}}(t) . \quad (2.5)$$

In these equations,  $m$  is the participant mass of the absorber, associated with the one-DOF oscillator,  $c_1$  and  $c_2$  are the two parameters describing the nonlinear damping force, and  $k_1$  and  $k_3$  are the two parameters related to the nonlinear stiffness force. It should be noted that the algebraic expression of the nonlinear terms coming from the viscoelasticity theory without memory in finite displacements, should induce, for the nonlinear stiffness force, linear, quadratic, and cubic terms, corresponding to the nonlinear geometrical effect, and for the nonlinear damping force, a linear function of the velocity with a nonlinear coefficient of the displacement. Due to the constraint that we have introduced (centered response for a centered excitation), the quadratic term in the stiffness force must vanish and the nonlinear coefficient of the displacement in the damping force must be an even function of the displacement.

As we are interested in quantifying the vibratory energy absorbed by the oscillator, we introduced the mean input power  $\Pi_{\text{in}}$  and the mean power dissipated  $\Pi_{\text{diss}}$ , which are such that

$$\Pi_{\text{in}} = E\{F_s(t) \dot{X}_s(t)\} , \quad \Pi_{\text{diss}} = E\{f_D(X_s(t), \dot{X}_s(t)) \dot{X}_s(t)\} , \quad (2.6)$$

in which  $E$  is the mathematical expectation.

Since the stochastic processes  $F_s$  and  $\dot{X}_s$  are stationary, these two quantities are independent of time and can be rewritten

$$\Pi_{\text{in}} = \int_{\mathbb{R}} \pi_{\text{in}}(\omega) d\omega \quad , \quad \Pi_{\text{diss}} = \int_{\mathbb{R}} \pi_{\text{diss}}(\omega) d\omega ,$$

in which the density  $\pi_{\text{in}}(\omega)$  and  $\pi_{\text{diss}}(\omega)$  are such that

$$\pi_{\text{in}}(\omega) = S_{F_s \dot{X}_s}(\omega) \quad , \quad \pi_{\text{diss}}(\omega) = S_{f_D \dot{X}_s}(\omega) . \quad (2.7)$$

In Eq. (2.7),  $S_{F_s \dot{X}_s}$  is the cross-spectral density function of the stationary stochastic processes  $\{F_s(t), t \in \mathbb{R}\}$  and  $\{\dot{X}_s(t), t \in \mathbb{R}\}$ , and  $S_{f_D \dot{X}_s}(\omega)$  is the

cross-spectral density function of the stationary stochastic processes  $\{f_D(X_s(t), \dot{X}_s(t)), t \in \mathbb{R}\}$  and  $\{\dot{X}_s(t), t \in \mathbb{R}\}$ . It should be noted that  $\pi_{\text{diss}}(\omega)$  is equal to  $\pi_{\text{in}}(\omega)$  due to the power balance equation of the stochastic system. The frequency-dependent energy pumping is therefore characterized by  $\pi_{\text{in}}(\omega)$ . In order to qualify the efficiency of the energy pumping as a function of the intensity of the nonlinearity that will be characterized by the value of the dimensionless response amplitude defined in Chapter 3, we introduce the normalized quantity,

$$\pi_{\text{in, norm}}(\omega) = \frac{\pi_{\text{in}}(\omega)}{S_{F_s}(\omega)} . \quad (2.8)$$

In order to quantify the absorption generated by the absorber over a frequency band  $B$ , we introduced the value  $\text{ABS}_B$  by

$$\text{ABS}_B = \int_B \pi_{\text{in, norm}}(\omega) d\omega . \quad (2.9)$$

In order to experimentally identify the vector-valued parameter of the model, denoted by  $\mathbf{w} = (c_1, c_2, k_1, k_3)$ , which belongs to an admissible set  $\mathcal{C}_{\text{ad}}$ , we introduce the frequency dependent function  $\text{FRF}(\omega; \mathbf{w})^2$  by

$$\text{FRF}(\omega; \mathbf{w})^2 = \frac{|S_{\dot{X}_s F_s}(\omega)|^2}{|S_{F_s}(\omega)|^2} = |\pi_{\text{in, norm}}(\omega)|^2 , \quad (2.10)$$

in which the  $\mathbf{w}$ -dependence in the right-hand side of Eq. (2.10) has been removed.

It should be noted that if  $f_D(x, \dot{x}) = c_1 \dot{x}$  and  $f_K(x) = k_1 x$ , the model corresponds to the one of a linear oscillator and  $\text{FRF}^2$  represents the square of the modulus of the frequency response function of the associated linear filter for which  $F_s$  is the input and  $\dot{X}_s$  is the output.

## 2.3 Stochastic solver and signal processing

### 2.3.1 Stochastic solver

For constructing the stationary stochastic solution of the nonlinear differential equation defined by Eq. (2.1), the Monte Carlo method [66] is used. Let  $\{F_s(t; \theta_\ell), t \in \mathbb{R}\}$  be a realization of the stochastic process  $F_s$  for  $\theta_\ell$  in  $\Theta$ . We consider  $L$  independent realizations  $\theta_\ell = 1, \dots, L$  in  $\Theta$  constructed with the generator described in a next paragraph of this section. For each realization  $\theta_\ell$ , we would have then to solve the deterministic nonlinear differential equation associated with stochastic Eq. (2.1): calculate  $X(t; \theta_\ell)$  for all  $t$  in  $\mathbb{R}$  such that

$$m\ddot{X}(t; \theta_\ell) + f_D(X(t; \theta_\ell), \dot{X}(t; \theta_\ell)) + f_K(X(t; \theta_\ell)) = F_s(t; \theta_\ell) . \quad (2.11)$$

This deterministic Eq. (2.11) cannot be solved numerically for  $t$  belonging to an infinite interval. Consequently, this problem is replaced by the following approximate problem with initial conditions over a finite interval of length  $T$ : calculate

$X(t; \theta_\ell)$  for  $t$  belonging to the finite interval  $]0, T]$ , solution of Eq. (2.11) with the initial conditions at time  $t = 0$ ,

$$X(0; \theta_\ell) = 0 \quad , \quad \dot{X}(0; \theta_\ell) = 0 . \quad (2.12)$$

With such initial conditions, the transient part of the response would be 0 for a linear second-order dynamical system and it is assumed to be 0 or negligible for the family of the nonlinear second-order dynamical systems that are considered (we have effectively checked the validity of these hypotheses for the numerical application presented in the thesis). The part of the trajectory on  $[0, T]$  corresponds to the stationary response,  $X_s(t; \theta_\ell) \simeq X(t; \theta_\ell)$  for  $t$  in  $[0, T]$ . Time  $T$  that is related to the frequency resolution is defined in Section 2.3.2. The deterministic problem defined by Eq. (2.11) for  $t$  in  $]0, T]$ , with the initial conditions defined by Eq. (2.12) for  $t = 0$ , is solved by using the Störmer-Verlet scheme presented in Section 2.3.4.

### 2.3.2 Time and frequency sampling

For solving the nonlinear deterministic equation with initial conditions associated with a given realization  $\theta_\ell$ , we need to generate realizations of the Gaussian stationary stochastic process  $F_s$  on the time interval  $[0, T]$ . Consequently, the time and the frequency sampling are constructed with respect to this time interval. The signal processing requires a time sampling with a constant time step  $\Delta_t$  that is performed using the Shannon theorem for the stationary stochastic processes [71]. The sampling frequency is  $f_e = 2 f_{\max}$  where  $f_{\max}$  is the maximum frequency that exists in the frequency band of analysis and the time step is  $\Delta_t = 1/f_e$ . It is assumed that the frequency band of analysis is sufficiently broad in order that the power spectral density function  $\omega \mapsto S_{X_s}(\omega)$  has, approximately, the compact support  $2\pi[-f_{\max}, f_{\max}]$ . The corresponding time sampling is  $t_\alpha = \alpha \Delta_t$  with  $\alpha = 0, 1, \dots, N - 1$  in which the integer  $N$  is chosen in order that the time duration  $T = 8 s$ , with  $T = N \Delta_t$  yielding  $N = 16,384$ . The frequency resolution  $\Delta_f = 1/T = 0.125 \text{ Hz}$ . The corresponding sampling points in the frequency domain are  $f_\beta = -f_{\max} + (\beta + 1/2)\Delta_f$  for  $\beta = 0, 1, \dots, N - 1$ .

### 2.3.3 Generation of independent realizations of Gaussian stationary stochastic process $F_s$

The usual second-order spectral representation of the stationary stochastic processes is used [72, 73]. The power spectral density function  $S_{F_s}(\omega)$  of the Gaussian stationary second-order centered stochastic process  $F_s$  is such that  $S_{F_s}(\omega) = m^2 S_{\ddot{X}_{\text{imp}}}(\omega)$ , in which  $S_{\ddot{X}_{\text{imp}}}(\omega) = \omega^4 S_{X_{\text{imp}}}(\omega)$ . The autocorrelation function  $\tau \mapsto R_{\ddot{X}_{\text{imp}}}(\tau)$  of the stationary stochastic process  $\ddot{X}_{\text{imp}}$  is such that  $R_{\ddot{X}_{\text{imp}}}(\tau) = E\{\ddot{X}_{\text{imp}}(t + \tau)\ddot{X}_{\text{imp}}(t)\}$  and  $R_{\ddot{X}_{\text{imp}}}(\tau) = \int_R e^{i\omega\tau} S_{\ddot{X}_{\text{imp}}}(\omega) d\omega$ .

The generator of realizations of the Gaussian stationary second-order stochastic process  $\ddot{X}_{\text{imp}}$  is based on the usual spectral representation (see [74, 75]). Let  $\psi_{0,\ell}, \dots, \psi_{N-1,\ell}$  be  $N \times \ell$  mutually independent uniform random variables on  $[0, 1]$  and let  $\phi_{0,\ell}, \dots, \phi_{N-1,\ell}$  be  $N \times \ell$  mutually independent uniform random variables on  $[0, 2\pi]$ , which are independent of  $\psi_{0,\ell}, \dots, \psi_{N-1,\ell}$ . The spectral representation used is written, for all  $t$ , as

$$\ddot{X}_{\text{imp}}(t; \theta_\ell) \simeq \sqrt{2\Delta_\omega} \operatorname{Re} \left\{ \sum_{\beta=0}^{N-1} \sqrt{S_{\ddot{X}_{\text{imp}}}(\omega_\beta)} Z_{\beta,\ell} e^{-i\omega_\beta t} e^{-i\phi_{\beta,\ell}} \right\}, \quad (2.13)$$

with  $\Delta_\omega = 2\pi \Delta_f$ , where  $Z_{\beta,\ell} = \sqrt{-\log(\psi_{\beta,\ell})}$ , where  $\omega_\beta = 2\pi f_\beta$ , and where  $\operatorname{Re}$  denote the real part of complex numbers.

From Eq. (2.13), it can be deduced that, for all  $t$ , the realization  $\ddot{X}_{\text{imp}}(t; \theta_\ell)$  is written as

$$\ddot{X}_{\text{imp}}(t; \theta_\ell) \simeq \sqrt{2\Delta_\omega} \operatorname{Re} \left\{ \sum_{\beta=0}^{N-1} g_{\beta,\ell} e^{-i\omega_\beta t} \right\}, \quad (2.14)$$

in which  $g_{\beta,\ell} = \sqrt{S_{\ddot{X}_{\text{imp}}}(\omega_\beta)} Z_{\beta,\ell} e^{-i\phi_{\beta,\ell}}$ .

In practice, for each  $\ell$ , Eq. (2.14) is computed for  $t = t_\alpha$  with  $\alpha = 0, \dots, N-1$ . Consequently, the numerical calculation is done by using the FFT  $\{\hat{g}_{0,\ell}, \dots, \hat{g}_{N-1,\ell}\}$  of  $\{g_{0,\ell}, \dots, g_{N-1,\ell}\}$ , which is such that

$$\hat{g}_{\alpha,\ell} = \sum_{\beta=0}^{N-1} g_{\beta,\ell} \exp \{-2i\pi\alpha\beta/N\} \quad (2.15)$$

and which yields, for  $\alpha = 0, 1, \dots, N-1$ ,

$$\ddot{X}_{\text{imp}}(t_\alpha; \theta_\ell) = \sqrt{2\Delta_\omega} \operatorname{Re} \left\{ \exp \left\{ -i\pi\alpha \left( \frac{1-N}{N} \right) \right\} \hat{g}_{\alpha,\ell} \right\}. \quad (2.16)$$

### 2.3.4 Störmer-Verlet integration scheme

The Störmer-Verlet integration scheme is well suited for the resolution of dynamical Hamiltonian systems [67, 68] and stays very efficient for dissipative Hamiltonian systems, as proposed in [76]. Such a scheme preserves the mechanical energy during the numerical integration. Eq. (2.11) with initial conditions defined by Eq. (2.12) is then written as the following first-order differential equation, for  $t$  in  $]0, T]$ ,

$$\begin{cases} \dot{X}(t; \theta_\ell) = \frac{1}{m} Y(t; \theta_\ell), \\ \dot{Y}(t; \theta_\ell) = -f_D(X(t; \theta_\ell), \frac{Y(t; \theta_\ell)}{m}) - f_K(X(t; \theta_\ell)) + F_s(t; \theta_\ell). \end{cases} \quad (2.17)$$

We use the notations  $x_\ell^\alpha = X(t_\alpha; \theta_\ell)$  and  $y_\ell^\alpha = Y(t_\alpha; \theta_\ell)$ . The writing of an integration scheme is composed of two parts: (1) the initialization of the variables  $x_\ell^0 = y_\ell^0 = 0$ , (2) the calculation of the variables at the time  $t_{\alpha+1}$  when

they are known at time  $t_\alpha$ . The second part is obtained with the three steps as follows.

- The derivation of  $x_\ell$  at the time  $t_\alpha$  is written as  $\dot{x}_\ell^\alpha = \frac{x_\ell^{\alpha+1/2} - x_\ell^\alpha}{\Delta_t/2}$ . Since  $y_\ell^\alpha = m \dot{x}_\ell^\alpha$ ,  $x_\ell^{\alpha+1/2}$  is a function of  $x_\ell^\alpha$  and  $y_\ell^\alpha$  such that

$$x_\ell^{\alpha+1/2} = x_\ell^\alpha + \frac{\Delta_t}{2m} y_\ell^\alpha . \quad (2.18)$$

- The second equation in Eq. (2.17), written at time  $t_{\alpha+1/2}$ , yields

$$\dot{y}_\ell^{\alpha+1/2} = -f_D(x_\ell^{\alpha+1/2}, \frac{y_\ell^{\alpha+1/2}}{m}) - f_K(x_\ell^{\alpha+1/2}) + F_s(t_{\alpha+1/2}; \theta_\ell) . \quad (2.19)$$

Since  $y_\ell^{\alpha+1/2} = \frac{y_\ell^\alpha + y_\ell^{\alpha+1}}{2}$  and  $\dot{y}_\ell^{\alpha+1/2} = \frac{y_\ell^{\alpha+1} - y_\ell^\alpha}{\Delta_t}$ , the nonlinear damping force  $f_D$  is linearly dependent on  $y_\ell$ , and  $F_s(t_{\alpha+1/2}; \theta_\ell)$  is approximated by  $F_s(t_{\alpha+1}; \theta_\ell)$  because the excitation is only computed for  $t_\alpha = \alpha \Delta_t$  with  $\alpha = 0, 1, \dots, N-1$ , Eq. (2.19) can be rewritten

$$y_\ell^{\alpha+1} = y_\ell^\alpha + \Delta_t \left[ -\frac{1}{2} (f_D(x_\ell^{\alpha+1/2}, y_\ell^\alpha/m) + f_D(x_\ell^{\alpha+1/2}, y_\ell^{\alpha+1}/m)) - f_K(x_\ell^{\alpha+1/2}) + F_s(t_{\alpha+1}; \theta_\ell) \right] . \quad (2.20)$$

- The time derivative of  $x_\ell$  at time  $t_{\alpha+1}$  is written as  $\dot{x}_\ell^{\alpha+1} = \frac{x_\ell^{\alpha+1} - x_\ell^{\alpha+1/2}}{\Delta_t/2}$ . Since  $y_\ell^{\alpha+1} = m \dot{x}_\ell^{\alpha+1}$ ,  $x_\ell^{\alpha+1}$  is a function of  $x_\ell^{\alpha+1/2}$  and  $y_\ell^{\alpha+1}$  such that

$$x_\ell^{\alpha+1} = x_\ell^{\alpha+1/2} + \frac{\Delta_t}{2m} y_\ell^{\alpha+1} . \quad (2.21)$$

The Störmer-Verlet integration scheme for Eq. (2.17) is then written, for  $\alpha = 0, 1, \dots, N-1$ , as

$$\left\{ \begin{array}{l} x_\ell^{\alpha+1/2} = x_\ell^\alpha + \frac{\Delta_t}{2m} y_\ell^\alpha , \\ y_\ell^{\alpha+1} = y_\ell^\alpha + \Delta_t \left[ -\frac{1}{2} (f_D(x_\ell^{\alpha+1/2}, y_\ell^\alpha/m) + f_D(x_\ell^{\alpha+1/2}, y_\ell^{\alpha+1}/m)) - f_K(x_\ell^{\alpha+1/2}) + F_s(t_{\alpha+1}; \theta_\ell) \right] , \\ x_\ell^{\alpha+1} = x_\ell^{\alpha+1/2} + \frac{\Delta_t}{2m} y_\ell^{\alpha+1} , \end{array} \right. \quad (2.22)$$

in which  $F_s(t_{\alpha+1}; \theta_\ell) = -m \ddot{X}_{\text{imp}}(t_{\alpha+1}; \theta_\ell)$  and where  $x_\ell^0 = y_\ell^0 = 0$ .

It should be noted that there is a  $y_\ell^{\alpha+1}$ -dependence in the right-hand side of the second line of Eq. (2.22). It is possible to isolate all  $y_\ell^{\alpha+1}$ -dependence in the left-hand side of the equation. The integration scheme can then be rewritten, for  $\alpha = 0, 1, \dots, N - 1$ , as

$$\left\{ \begin{array}{l} x_\ell^{\alpha+1/2} = x_\ell^\alpha + \frac{\Delta_t}{2m} y_\ell^\alpha, \\ y_\ell^{\alpha+1} = \frac{1 - \frac{\Delta_t}{2m}(c_1 + c_2|x_\ell^{\alpha+1/2}|)}{1 + \frac{\Delta_t}{2m}(c_1 + c_2|x_\ell^{\alpha+1/2}|)} y_\ell^\alpha \\ \quad + \frac{\Delta_t}{1 + \frac{\Delta_t}{2m}(c_1 + c_2|x_\ell^{\alpha+1/2}|)} \left\{ -k_1 x_\ell^{\alpha+1/2} - k_3 (x_\ell^{\alpha+1/2})^3 + F_s(t_{\alpha+1}; \theta_\ell) \right\}, \\ x_\ell^{\alpha+1} = x_\ell^{\alpha+1/2} + \frac{\Delta_t}{2m} y_\ell^{\alpha+1}, \end{array} \right. \quad (2.23)$$

In case of a too strong nonlinearity or a too high amplitude of excitation, an oversampling can be required in order to preserve the precision and the stability of the scheme. Time step  $\Delta_t$  is splitted in  $n_s$  time steps noted  $\delta_t$  such that

$$\delta_t = \frac{\Delta_t}{n_s}. \quad (2.24)$$

The corresponding time sampling is  $t_\gamma = \gamma\delta_t$  with  $\gamma = 0, 1, \dots, n_s(N - 1)$ . With the notation introduced before  $x_\ell^\gamma = X(t_\gamma; \theta_\ell)$  and  $y_\ell^\gamma = Y(t_\gamma; \theta_\ell)$ , the Störmer-Verlet integration scheme defined by Eq. (2.22) can then be rewritten, for  $\gamma = 0, 1, \dots, n_s(N - 1)$ , as

$$\left\{ \begin{array}{l} x_\ell^{\gamma+1/2} = x_\ell^\gamma + \frac{\delta_t}{2m} y_\ell^\gamma, \\ y_\ell^{\gamma+1} = y_\ell^\gamma + \delta_t \left[ -\frac{1}{2}(f_D(x_\ell^{\gamma+1/2}, y_\ell^\gamma/m) + f_D(x_\ell^{\gamma+1/2}, y_\ell^{\gamma+1}/m)) \right. \\ \quad \left. - f_K(x_\ell^{\gamma+1/2}) + F_s(t_{\alpha+1}; \theta_\ell) \right], \\ x_\ell^{\gamma+1} = x_\ell^{\gamma+1/2} + \frac{\Delta_t}{2m} y_\ell^{\gamma+1}, \end{array} \right. \quad (2.25)$$

in which  $F_s(t_{\alpha+1}; \theta_\ell) = -m\ddot{X}_{\text{imp}}(t_{\alpha+1}; \theta_\ell)$  with  $t_\alpha = \alpha n_s \delta_t$  and where  $x_\ell^0 = y_\ell^0 = 0$ .

### 2.3.5 Signal processing

For estimating the power spectral density functions and the cross-spectral density functions defined in Eqs. (2.7) and (2.10), the periodogram method [71] with a rectangular time-window on  $]0, T]$  is used.

The power spectral density function of the stationary second-order centered stochastic process  $X$ , for which  $L$  realizations are known on time  $T$ , estimated, for  $\beta = 0, 1, \dots, N - 1$ , by

$$S_X(\omega_\beta) \simeq \frac{1}{2\pi} \frac{1}{L} \sum_{\ell=1}^L |\hat{x}^\ell(\beta)|^2, \quad (2.26)$$

in which

$$\hat{x}^\ell(\beta) = \sum_{\alpha=0}^{N-1} \Delta_t W_T(\alpha \Delta_t) x_\ell^\alpha e^{i\pi\alpha} e^{-2i\pi\alpha\beta/N}, \quad (2.27)$$

where the time-window is written as  $W_T(t) = \frac{1}{\sqrt{T}} \mathbb{1}_{[0,T]}(t)$ .

Similarly, the cross-spectral density function of the stationary second-order centered stochastic processes  $X$  and  $Y$  is estimated, for  $\beta = 0, 1, \dots, N - 1$ , by

$$S_{XY}(\omega_\beta) \simeq \frac{1}{2\pi} \frac{1}{L} \sum_{\ell=1}^L \hat{x}^\ell(\beta) \overline{\hat{y}^\ell(\beta)}, \quad (2.28)$$

in which

$$\hat{x}^\ell(\beta) = \sum_{\alpha=0}^{N-1} \Delta_t W_T(\alpha \Delta_t) x_\ell^\alpha e^{i\pi\alpha} e^{-2i\pi\alpha\beta/N}$$

and

$$\hat{y}^\ell(\beta) = \sum_{\alpha=0}^{N-1} \Delta_t W_T(\alpha \Delta_t) y_\ell^\alpha e^{i\pi\alpha} e^{-2i\pi\alpha\beta/N}.$$

## 2.4 Validation of the stochastic solver with a linear oscillator

A validation of the stochastic solver and the signal processing presented in Section 2.3 has been obtained through the case of a linear oscillator.

For a linear case, the vector-valued parameter of the model is written  $\mathbf{w} = (c_1, 0, k_1, 0)$ . For all  $t$  in  $\mathbb{R}$ , Eq. (2.1) can be rewritten as

$$m\ddot{X}_s(t) + c_1\dot{X}_s(t) + k_1X_s(t) = -m\ddot{X}_{\text{imp}}(t). \quad (2.29)$$

For such a linear oscillator, response  $X_s(t)$  to excitation  $F_s(t)$  can be obtained without a computational model, using the frequency response function  $\hat{h}(\omega)$  of the associated linear filter for which  $\omega \mapsto S_{X_{\text{imp}}}(\omega)$  is the power spectral density function of input  $X_{\text{imp}}$  and where  $\omega \mapsto S_{X_s}(\omega)$  is the power spectral density function of output  $X_s$ , such that,

$$S_{X_s}(\omega) = |\hat{h}(\omega)|^2 S_{X_{\text{imp}}}(\omega), \quad (2.30)$$

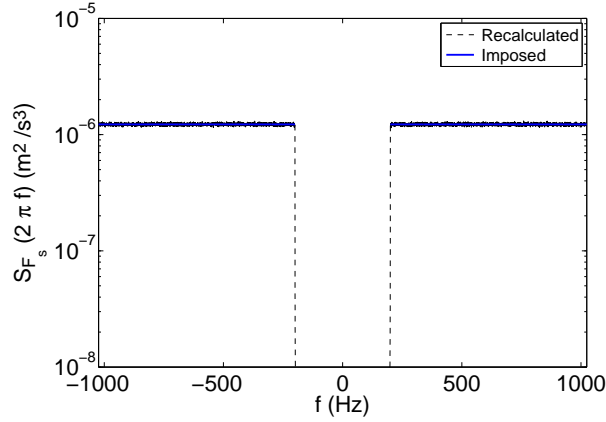


Figure 2.2: Imposed function  $\omega \mapsto S_{F_s^{\text{imp}}}(\omega)$  (blue solid line) and recalculated function  $\omega \mapsto S_{F_s^{\text{recl}}}(\omega)$  (black dashed line).

in which

$$|\hat{h}(\omega)|^2 = \frac{1}{\left(\frac{k_1}{m\omega^2} - 1\right)^2 + \left(\frac{c_1}{m\omega}\right)^2}. \quad (2.31)$$

Since the power spectral density function  $S_{X_s}(\omega)$  of  $X_s(t)$  is related to the power spectral density function  $S_{F_s}(\omega)$  of  $F_s(t)$  by the relation  $S_{X_s}(\omega) = \frac{1}{m^2\omega^4} S_{F_s}(\omega)$ .

Parameters used in the simulation are shown in Table 2.1. The power spectral density function  $S_{F_s}$  of the random excitation  $F_s$  is defined by

$$S_{F_s}(\omega) = \begin{cases} 0 & \text{if } \omega \in [-31.8, 31.8] \text{ rad/s} , \\ 1.225 \times 10^{-6} N^2 \times s & \text{if not.} \end{cases} \quad (2.32)$$

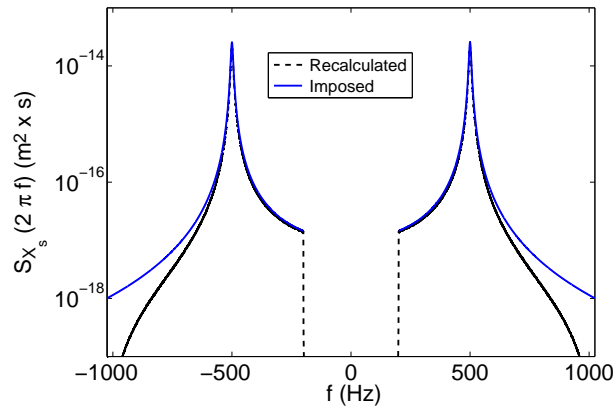
Parameter	Value
$m$	0.035 kg
$k_1$	$3.45 \times 10^5 N/m$
$c_1$	2.2 Ns/m
$L$	3,000
$T$	8 s
$f_{\text{max}}$	1,024 Hz
$n_s$	50

Table 2.1: Parameters used in the simulation of the linear oscillator.

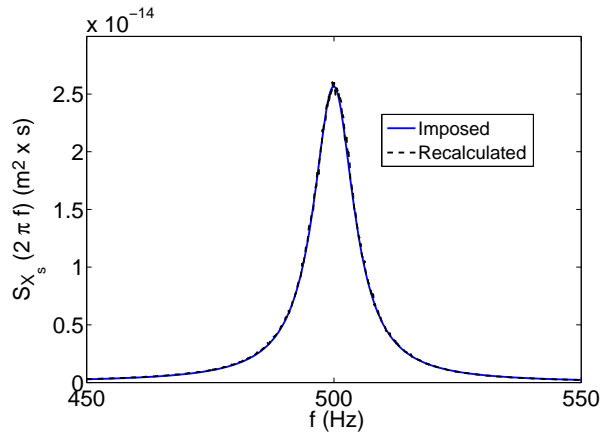
Figure 2.2 displays the imposed function  $\omega \mapsto S_{F_s^{\text{imp}}}(\omega)$  and the recalculated function  $\omega \mapsto S_{F_s^{\text{recl}}}(\omega)$ . Function  $S_{F_s^{\text{recl}}}(\omega)$  is obtained by using the periodogram method (see Section 2.3.5) on the independent realizations of process  $F_s^{\text{imp}}$  obtained by the generator presented in Section 2.3.3. The great agreement be-

tween  $S_{F_s^{\text{imp}}}(\omega)$  and  $S_{F_s^{\text{recal}}}(\omega)$  allows for the validation of the generator of realizations of Gaussian stationary second-order stochastic process, based on the usual spectral representation [74, 75] and the estimation of power spectral density functions using the periodogram method [71].

Figure 2.3 displays the power spectral density function  $\omega \mapsto S_{X_s^{\text{imp}}}(\omega)$  and the recalculated power spectral density function  $\omega \mapsto S_{X_s^{\text{recal}}}(\omega)$ . Function  $S_{X_s^{\text{imp}}}(\omega)$  is obtained using Eq. (2.30) and function  $S_{X_s^{\text{recal}}}(\omega)$  is calculated by means of the Störmer-Verlet integration scheme [67, 68] (see Section 2.3.1). Given the good agreement between the two functions, especially around the resonance, the use of the Störmer-Verlet integration scheme is validated.



(a)



(b)

Figure 2.3: Response function  $\omega \mapsto S_{X_s^{\text{imp}}}(\omega)$  (blue solid line) and recalculated function  $\omega \mapsto S_{X_s^{\text{recal}}}(\omega)$  (black dashed line) (a) with a logarithmic scale on  $[-f_{\text{max}}, f_{\text{max}}]$ ; (b) with a linear scale on  $[450 \text{ Hz}, 550 \text{ Hz}]$ .

## 2.5 Conclusion

In this chapter, a one-DOF model of the nonlinear absorber has been presented and the related stochastic solver has been developed. The model is constituted of a mass-spring-damper system with a nonlinear spring and a nonlinear damper, subjected to a stochastic excitation at its base. Some functions have been defined in order to identify parameters of the model with experiments in Chapter 3. The stochastic solver, which allows to calculate the displacement of the mass, is based on the Monte Carlo method. In addition, the time and frequency sampling are performed using the Shannon theorem and the generation of independent realizations of the excitation are achieved by using the usual second-order spectral representation of the stationary stochastic processes. The calculation of the response is then performed by the Störmer-Verlet integration scheme. As well, the power spectral density functions and the cross-spectral density functions are estimated by the periodogram method. A validation of the whole stochastic solver has been done on the case of a linear oscillator.

## Chapter 3

# Experimental design, measurements, and model identification of the absorber

### 3.1 Introduction

This chapter is devoted to the experimental realization of a nonlinear absorber to be used to reduce noise and vibration in a structure over a broad frequency band at low frequencies.

A mechanical model of the nonlinear absorber and the stochastic solver of its equation have been presented and validated in Chapter 2. The experimental design of the absorber whose response can be simulated with this nonlinear dynamical model is presented here. The experimental design, the manufacturing, and the measurements of the absorber are interesting for demonstrating the usefulness of the nonlinearity for the attenuation of noise and vibrations on a broad frequency band with realistic parameters in real conditions. In addition, the experimental data give the possibility to identify the parameters of the model and, consequently, to be able to predict the response of the absorber under other conditions than those presented here.

First, the experimental design of the absorber must be defined according to the model and some constraints. The design choice is presented in Section 3.2. Once the design is defined, the experimental campaign is presented in Section 3.3: Section 3.3.1 deals with the manufacturing of the test absorber and Section 3.3.2 provides a description of the experimental procedure. After that, the experimental results are displayed in Section 3.3.3. These results allow for identifying the model parameters, which is performed in Section 3.4.

### 3.2 Experimental design

*Defining the constraints for the design of the absorber and its consequences on the design.* The following constraints have been taken into account for defining the design.

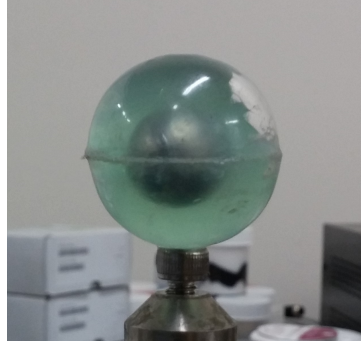
- The dimension of the absorber has been setted at about three centimeters in order to be representative of the scheduled technology for which such absorbers would be incorporate in a composite material at macroscale.
- The absorber must have a nonlinear dynamical behavior of the type presented in Chapter 2.
- The absorber must have the capability to exhibit a strong nonlinear geometrical effect with reasonable finite displacements to remain in the bulk whose geometry has previously been defined.
- The absorber must exhibit a relatively small damping in order to optimize the transmitted mechanical power to the nonlinear oscillator, thus to optimize the absorption.

A first numerical investigation has been performed for studying the qualitative effects of stiffness, damping, and shape on the nonlinear behavior of an absorber. The results, displayed in Appendix A, show that the energy transferred to the absorber is not affected for a softening or a hardening nonlinear stiffness. Moreover, the lower the damping of the absorber, the greater the bandwidth of the transferred energy. The first experimental system that we have worked on was made up of a point mass centered in a spherical plastic shell with an internal elastomer layer around the mass (see Figure 3.1(a)). The main advantage of this system was to have an isotropic absorption property no matter the direction of excitation. The elastomer had a hyperelastic behavior, however, after experimental tests, we have rejected this system because of the important damping due to the elastomer. After that, we studied a system inspired by the nonlinear energy sinks (NES) composed of a point mass linked to two prestressed traction springs clamped at their ends (see Figure 3.1(b)). In this configuration, the springs effectively had a nonlinear behavior when the point mass is excited in the transverse direction. However, too large displacements are needed to obtain a significant geometrical nonlinear effect that was not possible in our case. Then, we focused on two systems composed of a point mass attached to a beam. For the first one, the beam was bi-clamped and the point mass was located at its center. The second one was a cantilever beam with a point mass located at its free end. In these two cases, the excitation is transverse to the beam and the nonlinear behavior is obtained by the geometric nonlinearities of the beam submitted to finite displacements.

In this chapter, we have chosen to present only the absorber that has been designed with a cantilever beam and its point mass at its end. However, numerical computations and experimental measurements carried out on the absorber with a bi-clamped beam and its point mass at its center are shown in Appendix B.

*Design of the absorber.* To determine the length  $\ell$  of the beam, its bending stiffness  $EI$ , and the point mass  $m$ , we have used the equation of the first resonance frequency  $f_1$  of a cantilever beam with a point mass at its end:

$$f_1 = \frac{1}{2\pi} \sqrt{\frac{3EI}{m\ell^3}}, \quad (3.1)$$



(a) Tested absorber with an elastomer layer.



(b) Tested absorber with two springs.

Figure 3.1: Non-selected absorbers that have been tested: (a) absorber made up of a point mass centered in a spherical plastic shell with an internal elastomer layer around the mass; (b) absorber composed of a point mass linked to two prestressed traction springs glued at their ends.

for which it is assumed that the mass of the beam is negligible with respect to the point mass. The magnitudes of these parameters are shown in Table 3.1, in which  $f_1$ ,  $\ell$ , and  $E$  have been defined taken into account the experimental constraints for the manufacturing of the absorber and where  $I$  has arbitrarily been fixed in order to limit the number of design parameters.

Parameters	Magnitudes
$f_1$	$\leq 300 \text{ Hz}$
$\ell$	$\leq 0.03 \text{ m}$
$I$	$8.3 \times 10^{-14} \text{ m}^4$
$E$	$\{10^9, 250 \times 10^9\} \text{ Pa}$
$m$	$\geq 4.4033 \times 10^{-6} \text{ kg}$

Table 3.1: Magnitudes of the parameters for the design of the absorber.

*Material of the absorber.* The first idea for the material of the absorber was to use metallic parts (steel, aluminum) for the beam and the point mass. However, it was difficult to correctly embed the point mass to the beam and the beam to its support. That is why we have chosen to use a 3D-printing system and to print the beam, its support, and the point mass in a single piece, using a polymer material.

*Final design of the absorber with its support.* The absorber is attached to a rigid frame for which the CAO of the final design is shown in Figure 3.2(a). The point mass of the absorber is constituted of a cube, embedded at the free end of the beam. The other end of the beam is continuously connected to the frame. The beam length is  $0.026 \text{ m}$  and the width of its square section is around

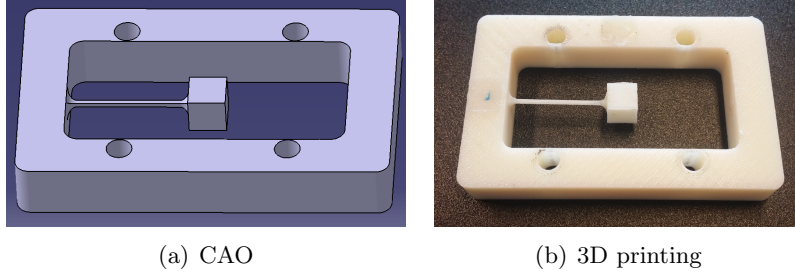


Figure 3.2: CAO and 3D printing of the test structure.

$0.001\text{ m}$ . The width of the cube is about  $0.008\text{ m}$ . The point mass  $m$  of the absorber is equal to the sum of the mass of the accelerometer attached to it for the measurements ( $0.4\text{ g}$ ), with the mass of the accelerometer cable ( $0.2\text{ g}$ ), and with the mass of the cube ( $0.55\text{ g}$ ), that is to say a total point mass of  $1.2\text{ g}$  (the mass of the beam is neglected as we have assumed). The mass density of ABS is  $1,780\text{ kg/m}^3$ . Some experimental traction tests have been carried out to identify the mechanical properties of ABS. The experiments give  $1.82 \times 10^9\text{ Pa}$  for the Young modulus and  $0.35$  for the Poisson coefficient. This absorber has been designed so that the first eigenfrequency of the frame is over  $1,000\text{ Hz}$  and the first eigenfrequency of the absorber around  $24\text{ Hz}$  (mode shapes of the first six modes can be seen in Figure 3.3 and the mode shape of the first eigenfrequency, that we are interested in, is displayed in Figure 3.3(c)), which shows that the frame can effectively be considered as rigid for analyzing the dynamical response of the absorber in the observed frequency band  $B_o$ , that is centered around the first eigenfrequency.

### 3.3 Experimental measurements

#### 3.3.1 Manufacturing of the test absorber

The absorber is manufactured using the 3D-printing system “Stratasys dimension elite”. The absorber and the rigid frame on which the absorber is attached, are printed in one piece in ABS (Acrylonitrile Butadiene Styrene) (see Figure 3.2(b)) that is a material commonly used for 3D printing with the fused deposition modeling technique.

#### 3.3.2 Description of the experimental procedure

We are interested in analyzing the stationary random response of the absorber in the frequency band of analysis  $B_a = [0, f_{\max}]$  with  $f_{\max} = 1,024\text{ Hz}$ , induced by the stationary random excitation generated by an imposed acceleration of the embedded end of the beam via the rigid frame (see Figure 3.4). This acceleration is equal to the acceleration that is imposed to the frame (that can be considered as rigid in the observed frequency band), on which a stationary random external force is applied (there is no elastic modes of the fixed frame in  $B_a$ , taking into account its junction/attachment to the shaker). The observed

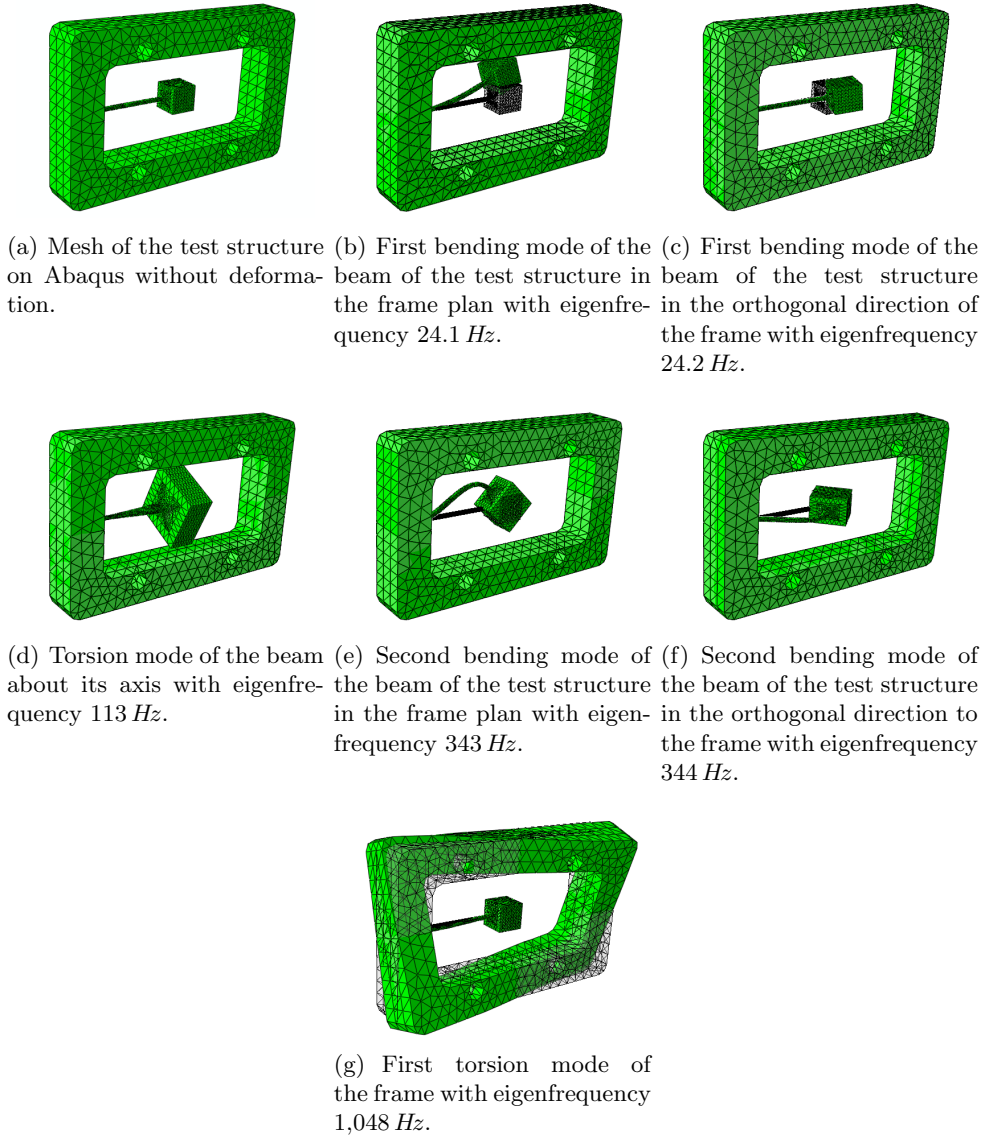


Figure 3.3: First modes of the test structure in the free-free conditions computed by the finite element method with Abaqus code.

frequency band is  $B_o = [21, 26] Hz \subset B_a$ , which contains a resonance for all the amplitudes that are considered for the excitation. A Gaussian stationary random excitation with a frequency bandwidth  $[5 - 800] Hz$  is applied, which is delivered by a shaker (Brüel & Kjaær 4808) with a power amplifier (Brüel & Kjaær 2719). The excitation signal,  $\ddot{X}_{\text{imp}}^{\text{exp}}$ , is measured by an accelerometer (Brüel & Kjaær 4507-B004) attached to the frame and the response of the absorber point mass  $\ddot{X}^{\text{exp}}$  by an accelerometer Endevco 2250A-10 attached to the point mass (see Figure 3.4). Using an accelerometer attached to the point mass for measuring its response is intrusive, however, in order to minimize the disturbances occurred by vibration of the cable, this cable have been glued to the

frame. The masses of the accelerometer and the cable have been also taking into account for the identification of the model. It should be noted that a monopoint velocimeter Polytech PDV-100 has been tested for measuring the response of the point mass without attached accelerometer, but the velocity of the point mass for high amplitudes of excitation was out of the measuring ranges of the device. We have then decided to perform all the measurements with the same experimental procedure, for consistency, with an accelerometer. The sensors data are acquired with National Instrument Hardware. A CompactDAQ module 9234 is used for the measurements of the two IEPE accelerometers and a module 9263 is used for the signal generation of the excitation. The modules are used with a 4-slot USB chassis 9174. The software used to process the measurements is SO Analyzer from m+p international. The useful bandwidth is set to  $1,024\text{ Hz}$  that leads us to a time sample rate of  $2,048\text{ Hz}$ . The block size is  $16,384$  points, which corresponds to an acquisition time of  $8\text{ s}$  for a measurement block and so the frequency step is equal to  $0.125\text{ Hz}$ . The overlap factor is chosen equal to  $66\%$ . The number of blocks that are processed is  $101$ , which corresponds to a total acquisition time of  $280\text{ s}$  for each excitation level. The  $H_1$  estimator with Hanning window is used to estimate the FRF functions. The experimental configuration can be viewed in Figure 3.4. Experimental responses have been measured for seven excitation levels. These cases are identified by the dimensionless response amplitude  $d/h$  in which  $h$  is the thickness of the beam ( $h = 0.001\text{ m}$ ) and  $d$  is defined as the statistical mean of the “peak-to-peak” deflection amplitudes relative to the frame obtained for each measurement block, such that, using Eq. (2.5),

$$d = \frac{1}{2} E \left\{ \max_t (X_s^{\text{exp}}(t)) - \min_t (X_s^{\text{exp}}(t)) \right\} \quad (3.2)$$

where  $X_s^{\text{exp}}(t) = X_a^{\text{exp}}(t) - X_{\text{imp}}^{\text{exp}}(t)$ .

For instance, if  $d/h = 1$ , the displacement of the absorber is of the order of magnitude of the thickness of the beam. Seven values of  $d/h$  are considered for the experiments and are, in percent,  $1.9$ ,  $11$ ,  $52.3$ ,  $82.4$ ,  $96.7$ ,  $131$ , and  $134$ .

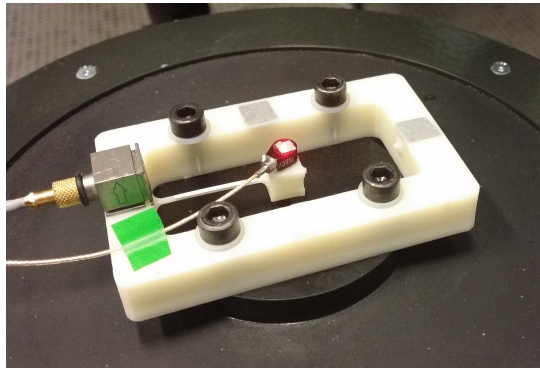


Figure 3.4: The experimental configuration.

### 3.3.3 Experimental results

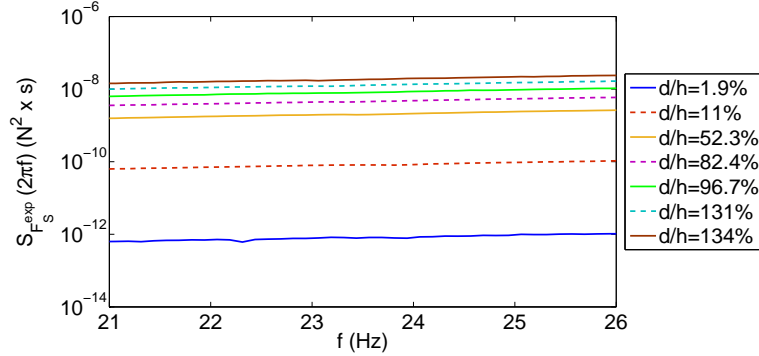


Figure 3.5: Experimental PSD functions  $S_{F_s}^{\text{exp}}$  of the excitation for the seven considered values of  $d/h$ .

The experimental power spectral density functions  $S_{F_x}^{\text{exp}}$  of the excitation are displayed in Figure 3.5 for seven considered values of  $d/h$ . Figure 3.6 depicts the square of the modulus  $\text{FRF}^{\text{exp}}(2\pi f)^2$  of the experimental frequency response function for each values of  $d/h$ . We focus on the response related to the eigenfrequency of the absorber corresponding to the first bending mode of the beam (its mode shape is shown in Figure 3.3(b)), which is the peak that we can see around 24 Hz in Figure 3.6(a). The other peaks are the response related to the eigenfrequencies that are greater.

For each measurement block, the displacement signals are obtained by numerical double integration of the acceleration signals. A high-pass filter is applied before each numerical integration. The experimental normalized input power density  $\pi_{\text{in, norm}}(2\pi f)$  is displayed in Figure 3.7 (which is the square root of  $\text{FRF}^{\text{exp}}(2\pi f)^2$  as noted in Eq. (2.10)).

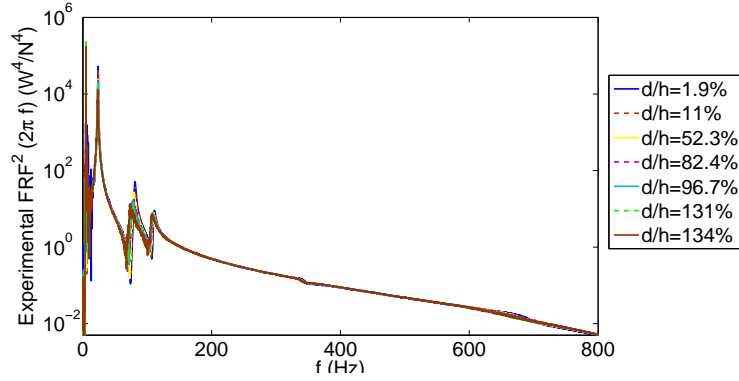
## 3.4 Experimental identification of the model

As explained in Chapter 2, for all the considered values of  $d/h$ , the experimental identification of the damping and stiffness parameters is performed by minimizing, over the observed frequency band  $B_o$ , the distance between the function  $\text{FRF}(\omega; \mathbf{w})^2$  (defined by Eq. (2.10)) computed with the model and its experimental counterpart  $\text{FRF}^{\text{exp}}(\omega)^2$  that is to say, by solving the following optimization problem,

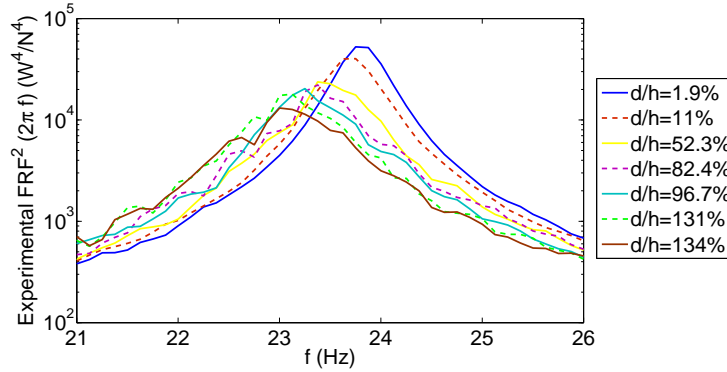
$$\mathbf{w}^{\text{opt}} = \arg \min_{\mathbf{w} \in \mathcal{C}_{\text{ad}}} J(\mathbf{w}) , \quad (3.3)$$

in which the objective function  $J(\mathbf{w})$  is written as

$$J(\mathbf{w}) = \int_{B_o} |\text{FRF}(\omega; \mathbf{w})^2 - \text{FRF}^{\text{exp}}(\omega)^2| d\omega . \quad (3.4)$$



(a)



(b)

Figure 3.6: Square of the modulus  $\text{FRF}^{\text{exp}}(2\pi f)^2$  of the experimental frequency response function for the seven values of  $d/h$  (a) on frequency band  $[0, 800]$  Hz, (b) on frequency band  $B_o$

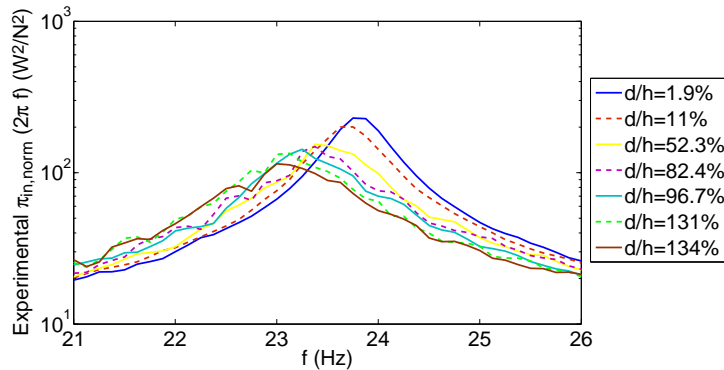


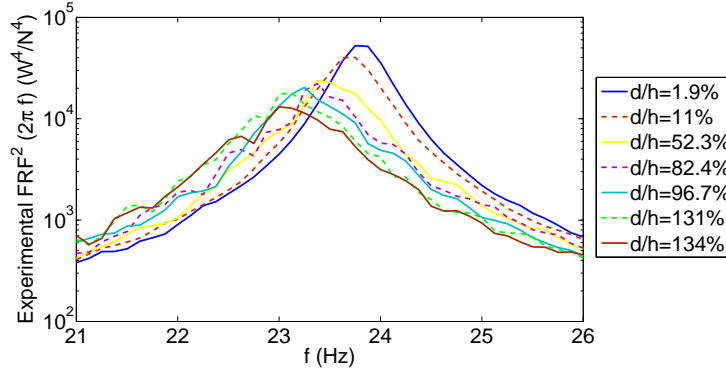
Figure 3.7: Experimental normalized input power density  $\pi_{\text{in, norm}}^{\text{exp}}(2\pi f)$  for the seven values of  $d/h$ .

Note that the right-hand side member of the above equation is the  $L^1$ -norm of the function  $\omega \mapsto \text{FRF}(\omega; \mathbf{w})^2 - \text{FRF}^{\text{exp}}(\omega)^2$ . The optimization problem has

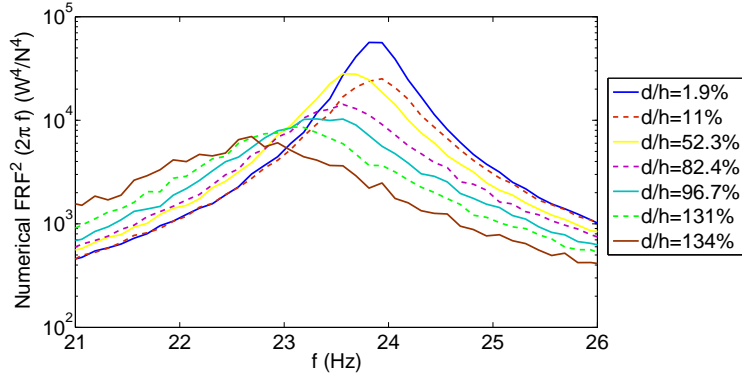
been solved by using a deterministic trial method. The optimal value  $\mathbf{w}^{\text{opt}} = (c_1^{\text{opt}}, c_2^{\text{opt}}, k_1^{\text{opt}}, k_3^{\text{opt}})$  obtained is

$$\begin{cases} c_1^{\text{opt}} = 0.0038 \text{ N s/m} , \\ c_2^{\text{opt}} = 10 \text{ N s/m}^2 , \\ k_1^{\text{opt}} = 26.8 \text{ N/m} , \\ k_3^{\text{opt}} = -4 \times 10^6 \text{ N/m}^3 . \end{cases} \quad (3.5)$$

During the identification process, we have noted that the damping effect is



(a)

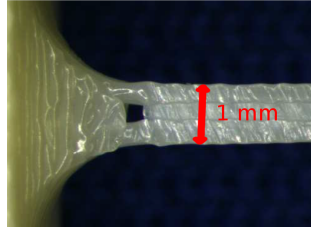


(b)

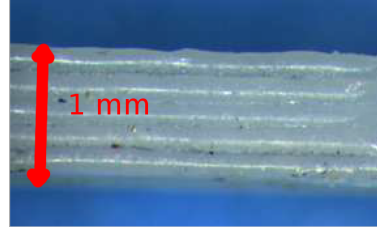
Figure 3.8: Experimental function  $\omega \mapsto \text{FRF}^{\text{exp}}(\omega)^2$  (Figure (a)) and optimized model function  $\omega \mapsto \text{FRF}(\omega; \mathbf{w}^{\text{opt}})^2$  (Figure (b)), for the seven values of  $d/h$ .

effectively nonlinear, that is coherent with the nonlinear dynamical model introduced in Section 2.2. This damping nonlinearity can also be explained by the fact that the beam of the 3D-printing absorber exhibits a stratified structure of layers with pores (miss of matter) generated by the 3D-printing process (Figure 3.9(c)). For high response amplitudes, the shear deformation induces small slides at the interface of the layers.

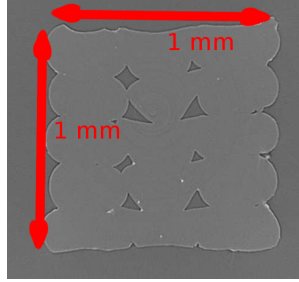
For each one of the seven values of  $d/h$ , Figure 3.8 displays the experimental function  $\omega \mapsto \text{FRF}^{\text{exp}}(\omega)^2$  and the optimized function  $\omega \mapsto \text{FRF}(\omega; \mathbf{w}^{\text{opt}})^2$  corre-



(a) Top view of the absorber beam.



(b) Side view of the absorber beam.



(c) View of a cross section of the absorber beam.

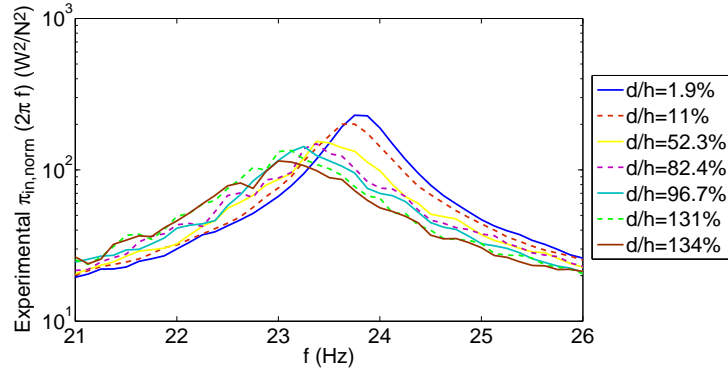
Figure 3.9: Several views of the 3D-printing beam of the absorber (obtained by microtomography).

sponding to the experimental identification of the model. The comparison of these two figures shows a reasonable agreement between the experiments and the identified model. These same results are displayed in Figure 3.12 with a graph for each value of  $d/h$  for another readability. The prevision could, perhaps, be improved by using a model with more than one degree of freedom.

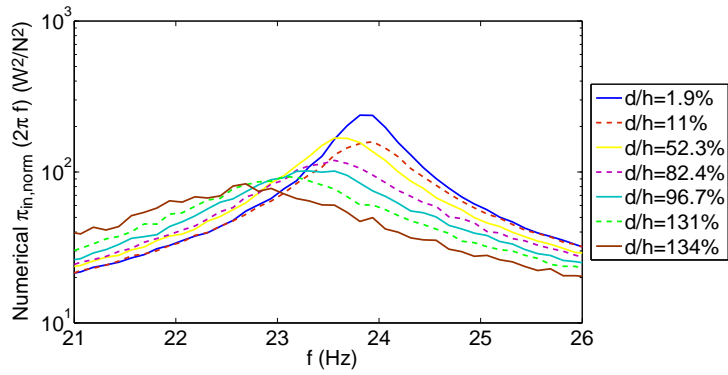
Figure 3.10 illustrates the experimental function  $\omega \mapsto \pi_{\text{in, norm}}^{\text{exp}}(\omega)$  and optimized model function  $\omega \mapsto \pi_{\text{in, norm}}(\omega; \mathbf{w}^{\text{opt}})$ , for the seven values of  $d/h$ . A reasonable agreement can also be seen between the prediction and the experiments.

Figure 3.11 displays, for each one of the seven values of  $d/h$ , the experimental absorption on  $B_o$ ,  $\text{ABS}_{B_o}^{\text{exp}}$  and optimized model absorption  $\text{ABS}_{B_o}(\mathbf{w}^{\text{opt}})$ . As is was previously explained for Figure 3.12, the identification is excellent for certain values of  $d/h$  ( $d/h = 11\%$  and  $d/h = 96.7\%$ ) and could be improved for some others ( $d/h = 1.9\%$  and  $d/h = 52.3\%$ ) by using a more sophisticated mechanical model.

Furthermore, the results presented in these figures confirm a strong effect of the nonlinearity that allows the pumping energy phenomenon to be efficient over a broader frequency band around the resonance frequency than for the linear case.



(a)



(b)

Figure 3.10: For the seven values of  $d/h$ , experimental function  $\omega \mapsto \pi_{in,norm}^{exp}(\omega)$  (Figure (a)) and optimized model function  $\omega \mapsto \pi_{in,norm}(\omega; \mathbf{w}^{opt})$  (Figure (b)).

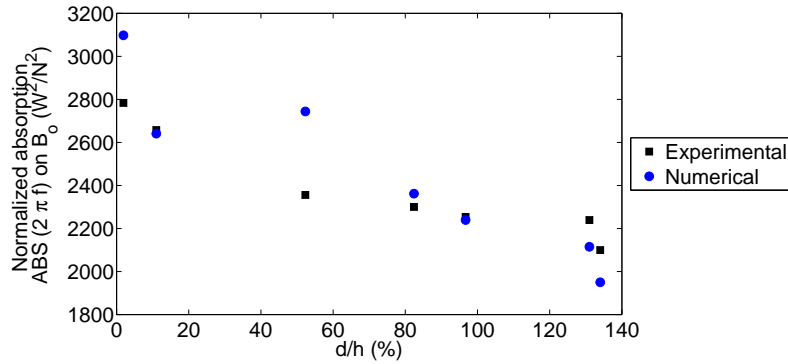


Figure 3.11: For the seven values of  $d/h$ , experimental absorption on  $B_o$ ,  $ABS_{B_o}^{exp}$ , (square symbol) and optimized model absorption,  $ABS_{B_o}(\mathbf{w}^{opt})$  (circle symbol).

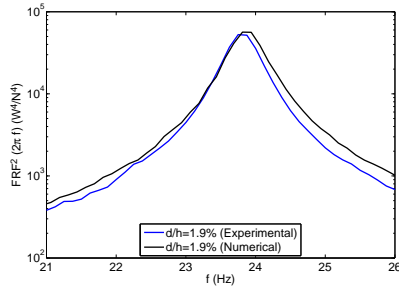
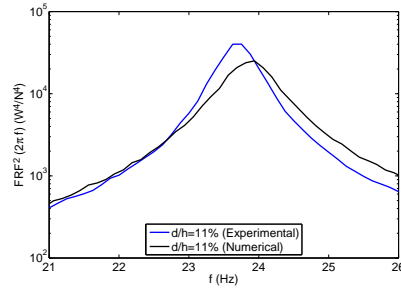
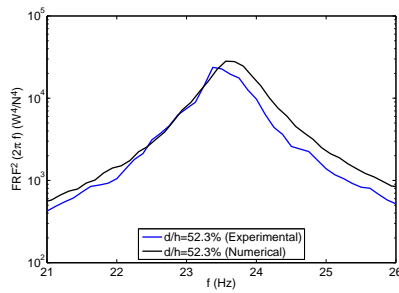
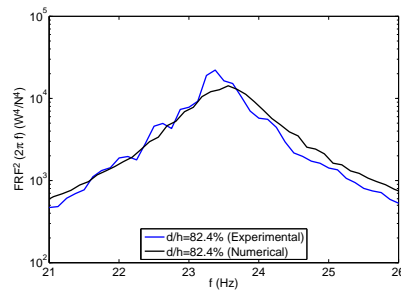
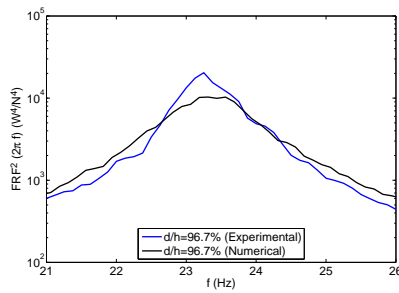
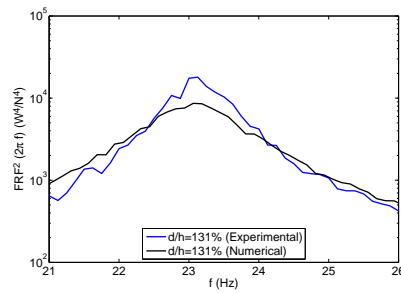
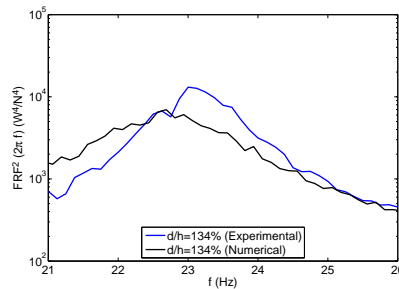
(a) For  $d/h = 1.9\%$ .(b) For  $d/h = 11\%$ .(c) For  $d/h = 52.3\%$ .(d) For  $d/h = 82.4\%$ .(e) For  $d/h = 96.7\%$ .(f) For  $d/h = 131\%$ .(g) For  $d/h = 134\%$ .

Figure 3.12: For the seven values of  $d/h$ , experimental function  $\omega \mapsto \text{FRF}^{\text{exp}}(\omega)^2$  (blue or grey lines) and optimized model function  $\omega \mapsto \text{FRF}(\omega; \mathbf{w}^{\text{opt}})^2$  (black lines).

### 3.5 Conclusion

In this chapter, an experimental absorber, with a nonlinear dynamical behavior, capable of reducing the noise and the vibration of a structure over a broad frequency band at low frequencies, has been designed based on the one-DOF nonlinear oscillator model, defined previously in Chapter 3. The absorber that is nonlinear at macroscale, has been manufactured with a 3D printing system. The dimension of this absorber could easily be reduced with the same technology, in order to be inserted in a macro-structural element. Experimental tests have been carried out on the sample and results have been displayed and discussed. The parameters of the nonlinear dynamical model of the absorber have been identified with experiments. Both the predictions given by the nonlinear dynamical model and the experiments confirm that the pumping energy phenomenon is more efficient over a broad frequency band around the resonance frequency than for a linear dynamical system.



## Chapter 4

# Construction of a model of a beam with absorbers

### 4.1 Introduction

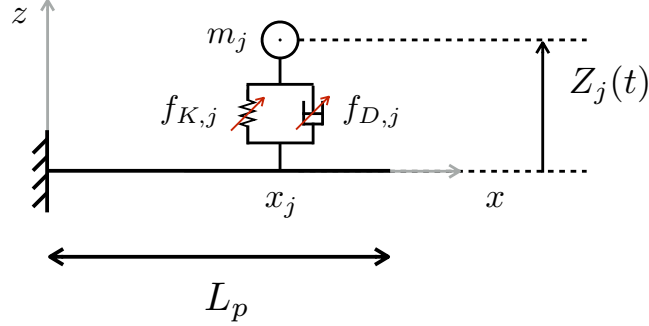
Chapter 2 has been devoted to the construction of a nonlinear model of an absorber capable of absorbing noise and vibration of an excitation over a broad frequency band at low frequencies. A stochastic solver of the model has also been described. Chapter 3 has displayed an experimental realization of this absorber and a validation of the model. Now that the nonlinear absorber is described, it is interesting to test it on a structure.

The chosen test structure is a beam, which has the advantage to be modeled by a one-dimensional model. The purpose of this chapter is thus to describe a one-dimensional model of an Euler-Bernoulli beam on which some nonlinear absorbers are set up.

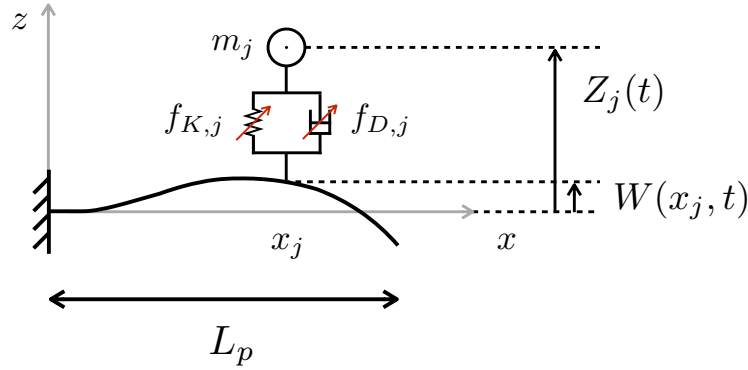
As presented in Chapter 2, the one-DOF nonlinear model of the absorber is composed of a mass-spring-damper system with a nonlinear spring and a nonlinear damper. The one-dimensional model of the beam represents a cantilever Euler-Bernoulli beam subjected to a stochastic excitation at its free end. A finite number of nonlinear absorbers is set up at different locations on the beam (see the scheme displayed in Figure 4.1).

In this chapter, the one-dimensional model of the beam with nonlinear absorbers is introduced in Section 4.2. A reduced model is described in Section 4.3. The expressions of different power spectral density functions used to interpret the results of the model are presented in Section 4.4. Section 4.5 is devoted to the writing of the stochastic solver and to signal processing. Section 4.5.1 presents the stochastic solver based on the Monte Carlo method [66]. After that, Section 4.5.2 exposes the generation of independent realizations of Gaussian stationary stochastic process that is the excitation imposed at the free end of the beam. The stochastic solver is based on the Störmer-Verlet integration scheme [67, 68], which is detailed in Section 4.5.3. The time and frequency sampling and the signal processing used are the same that those used in Chapter 2.

## 4.2 One-dimensional model of the beam



(a) Model with the beam fixed, at initial position.



(b) Model with the beam in motion.

Figure 4.1: Model of the beam with an absorber at two instants. The nonlinear damping force  $f_{D,j} \left( Z_j(t) - W(x_j, t), \dot{Z}_j(t) - \frac{\partial W}{\partial t}(x_j, t) \right)$  and the nonlinear stiffness force  $f_{K,j} \left( Z_j(t) - W(x_j, t) \right)$  are written in the figure without their dependencies in order to simplify the scheme.

A one-dimensional model composed with an Euler-Bernoulli beam with nonlinear absorbers is constructed (see the scheme displayed in Figure 4.1). The absorbers are nonlinear oscillators of the type described in Chapter 2. We focus on the bending of the cantilever beam, with a constant section and an exterior force  $g^{\text{ext}}(x, t)$  imposed at its free end. Let  $L_p$ ,  $S$ ,  $\rho$ ,  $c_p$ ,  $E$ , and  $I$  be respectively the length of the beam, its section, its density, its damping coefficient, its Young modulus, and its area moment of inertia. There are  $n$  nonlinear oscillators that are fixed on the beam, without eccentricity. Let  $m_j$  be the mass of the nonlinear oscillator  $j$  and  $\mathbf{w}_j = (c_{1,j}, c_{2,j}, k_{1,j}, k_{3,j})$  be the vector of parameters, in which  $c_{1,j}$  and  $c_{2,j}$  are two parameters describing the nonlinear damping force  $f_{D,j}$  for the nonlinear oscillator  $j$ , and  $k_{1,j}$  and  $k_{3,j}$  its two parameters describing the nonlinear stiffness force  $f_{K,j}$ , in accordance to the model of the nonlinear

oscillator presented in Section 2.2. The forces  $f_{D,j}$  and  $f_{K,j}$  are such that

$$\begin{aligned} f_{D,j} \left( Z_j(t) - W(x_j, t), \dot{Z}_j(t) - \frac{\partial W}{\partial t}(x_j, t) \right) &= (c_{1,j} + c_{2,j} |Z_j(t) - W(x_j, t)|) \\ &\quad \times \left( \dot{Z}_j(t) - \frac{\partial W}{\partial t}(x_j, t) \right) , \\ f_{K,j} (Z_j(t) - W(x_j, t)) &= k_{1,j} (Z_j(t) - W(x_j, t)) + k_{3,j} (Z_j(t) - W(x_j, t))^3 . \end{aligned} \quad (4.1)$$

For each nonlinear oscillator  $j = 1, \dots, n$ , we have the following equation

$$\begin{aligned} m_j \ddot{Z}_j(t) + f_{D,j} \left( Z_j(t) - W(x_j, t), \dot{Z}_j(t) - \frac{\partial W}{\partial t}(x_j, t) \right) \\ + f_{K,j} (Z_j(t) - W(x_j, t)) = 0 \end{aligned} \quad (4.2)$$

where  $x_j$  is the position of the nonlinear oscillator  $j$  on the beam,  $Z_j$  is the absolute displacement of the nonlinear oscillator  $j$ , and  $W(x_j, t)$  the absolute displacement of the beam at the point  $x_j \in [0, L_p]$ .

The equation of the Euler-Bernoulli beam with boundary conditions is such that

$$\left\{ \begin{array}{l} \rho S \frac{\partial^2 W(x, t)}{\partial t^2} + c_p \frac{\partial W(x, t)}{\partial t} + EI \frac{\partial^4 W(x, t)}{\partial x^4} = g^{\text{ext}}(x, t) + \sum_{j=1}^n F_j(t) \delta_0(x - x_j) , \\ W(0, t) = 0, \forall t , \\ \frac{\partial W}{\partial x}(0, t) = 0, \forall t , \\ EI \frac{\partial^2 W}{\partial x^2}(L_p, t) = 0, \forall t , \\ EI \frac{\partial^3 W}{\partial x^3}(L_p, t) = -F_s(t), \forall t . \end{array} \right. \quad (4.3)$$

where  $g^{\text{ext}}(x, t)$  represents the density of external forces applied to the beam, where  $F_s(t)$  is the  $z$ -component of the external force applied to the beam at  $x = L_p$ , and where  $F_j(t)$  is the force applied to the beam induced by the nonlinear oscillator  $j$ , which is written as

$$F_j(t) = f_{D,j} \left( Z_j(t) - W(x_j, t), \dot{Z}_j(t) - \frac{\partial W}{\partial t}(x_j, t) \right) + f_{K,j} (Z_j(t) - W(x_j, t)) . \quad (4.4)$$

### 4.3 Reduced Model

The reduced-order model is classically constructed by using the weak/variational formulation [77, 78] of the boundary value problem defined by Eq. (4.3). Let  $\langle v, w \rangle_{L^2}$  be the inner/scalar product in  $L^2([0, L_p])$  defined by

$$\langle v, w \rangle_{L^2} = \int_0^{L_p} \rho S v(x) w(x) dx . \quad (4.5)$$

Let  $\mathcal{C}_{ad}$  be the admissible set that is a subspace of  $L^2([0, L_p])$ , which are sufficiently differentiable functions, such that

$$\mathcal{C}_{ad} = \left\{ x \mapsto w(x) : ]0, L_p[ \rightarrow \mathbb{R}, \delta w(0) = 0, \frac{\partial \delta w}{\partial x}(0) = 0 \right\} . \quad (4.6)$$

We define the following bilinear forms on  $\mathcal{C}_{ad} \times \mathcal{C}_{ad}$  such that

$$\left\{ \begin{array}{l} \mathcal{M}(w, \delta w) = \int_0^{L_p} \rho S w(x) \delta w(x) dx = \langle w, \delta w \rangle_{L^2} , \\ \mathcal{C}(w, \delta w) = \int_0^{L_p} c_p w(x) \delta w(x) dx = \frac{c_p}{\rho S} \langle w, \delta w \rangle_{L^2} , \\ \mathcal{K}(w, \delta w) = \int_0^{L_p} EI \frac{\partial^2 w}{\partial x^2} \frac{\partial^2 \delta w}{\partial x^2} dx , \\ \mathcal{F}^{\text{ext}}(\delta w; t) = \int_0^{L_p} g^{\text{ext}}(x, t) \delta w(x) dx + F_s(t) \delta w(L_p) , \\ \mathcal{F}_j(\delta w; t) = \int_0^{L_p} F_j(t) \delta_0(x - x_j) \delta w(x) dx = F_j(t) \delta w(x_j) . \end{array} \right. \quad (4.7)$$

The weak formulation Eq. (4.3) is rewritten, for all  $\delta w \in \mathcal{C}_{ad}$ , as

$$\mathcal{M} \left( \frac{\partial^2 W(x, t)}{\partial t^2}, \delta w \right) + \mathcal{C} \left( \frac{\partial W(x, t)}{\partial t}, \delta w \right) + \mathcal{K} (W(x, t), \delta w) = \mathcal{F}^{\text{exp}}(\delta w, t) + \sum_{j=1}^n \mathcal{F}_j(\delta w; t) . \quad (4.8)$$

Let  $\mathbf{\Omega} = \{\Omega_1, \dots, \Omega_{N_m}\}$  and  $\boldsymbol{\varphi} = \{\varphi_1, \dots, \varphi_{N_m}\}$  be respectively the  $N_m$  eigenfrequencies and the associated eigenmodes of the beam not coupled with the oscillators. Let  $\lambda_\alpha = \Omega_\alpha^2$ , with  $0 < \dots < \lambda_{N_m}$ , be the eigenvalue such that

$$\mathcal{K}(\varphi_\alpha, \delta \varphi) = \lambda_\alpha \mathcal{M}(\varphi_\alpha, \delta \varphi) \quad , \quad \delta \varphi \in \mathcal{C}_{ad} . \quad (4.9)$$

The reduced-order model is obtained by projecting  $W(\cdot, t)$  on the subspace of  $\mathcal{C}_{ad}$  spanned by  $\{\varphi_1, \dots, \varphi_{N_m}\}$ ,

$$W(x, t) \simeq \sum_{\alpha=1}^{N_m} Q_\alpha(t) \varphi_\alpha(x) , \quad (4.10)$$

where  $\mathbf{Q}(t) = (Q_1(t), \dots, Q_{N_m}(t))$  is the vector of the generalized coordinates. The value of  $N_m$  has to be chosen for obtaining a good convergence.

We define the reduced mass, damping, and stiffness matrices such that

$$\begin{aligned} [M]_{\beta\alpha} &= \mathcal{M}(\varphi_\alpha, \varphi_\beta) = \int_0^{L_p} \rho S \varphi_\alpha(x) \varphi_\beta(x) dx \\ &= \delta_{\alpha\beta} \mu_\alpha , \end{aligned} \quad (4.11)$$

$$\begin{aligned} [D]_{\beta\alpha} &= \mathcal{C}(\varphi_\alpha, \varphi_\beta) = \frac{c_p}{\rho S} \mathcal{M}(\varphi_\alpha, \varphi_\beta) \\ &= \frac{c_p}{\rho S} [M]_{\beta\alpha} , \end{aligned} \quad (4.12)$$

$$[K]_{\beta\alpha} = \mathcal{K}(\varphi_\alpha, \varphi_\beta) = \delta_{\alpha\beta} \mu_\alpha \Omega_\alpha^2 , \quad (4.13)$$

in which  $\delta_{\alpha\beta} = 1$  if  $\alpha = \beta$  and  $\delta_{\alpha\beta} = 0$  if  $\alpha \neq \beta$ , and where  $\mu_\alpha$  is the generalized mass for the eigenmode  $\varphi_\alpha$  (constant of normalization).

The generalized external forces applied to the beam is written as

$$\mathcal{F}^{\text{exp}}(\varphi_\beta, t) = F_\beta^{\text{exp}}(t) , \quad (4.14)$$

in which  $F_\beta^{\text{exp}}(t) = \int_0^{L_p} g^{\text{ext}}(x, t) \varphi_\beta(x) dx + F_s(t) \varphi_\beta(L_p)$ . The generalized forces applied to the beam by the oscillators are written as

$$\mathcal{F}_{\text{osc}}(\varphi_\beta, t) = F_\beta^{\text{osc}}(t) = \sum_{j=1}^n F_j(t) \varphi_\beta(x_j) . \quad (4.15)$$

Thus, Eqs. (4.2) and (4.4) can be rewritten as

$$\begin{aligned} m_j \ddot{Z}_j(t) + f_{D,j} \left( Z_j(t) - \{[\varphi] \mathbf{Q}(t)\}_j, \dot{Z}_j(t) - \{[\varphi] \dot{\mathbf{Q}}(t)\}_j \right) \\ + f_{K,j} (Z_j(t) - \{[\varphi] \mathbf{Q}(t)\}_j) = 0 , \\ F_j(t) = f_{D,j} \left( Z_j(t) - \{[\varphi] \mathbf{Q}(t)\}_j, \dot{Z}_j(t) - \{[\varphi] \dot{\mathbf{Q}}(t)\}_j \right) \\ + f_{K,j} (Z_j(t) - \{[\varphi] \mathbf{Q}(t)\}_j) , \end{aligned} \quad (4.16)$$

in which the rectangular  $(n \times N_m)$  matrix  $[\varphi]$  is such that  $[\varphi]_{j\alpha} = \varphi_\alpha(x_j)$ .

Let  $[m]$ ,  $[c_1]$ ,  $[c_2]$ ,  $[k_1]$ , and  $[k_3]$  be respectively the  $(n \times n)$  mass matrix of the oscillators, the  $(n \times n)$  matrix of the first damping parameter of the oscillators, the  $(n \times n)$  matrix of the second damping parameter of the oscillators, the  $(n \times n)$  matrix of the first stiffness parameter of the oscillators, and the  $(n \times n)$

matrix of the second stiffness parameter of the oscillators defined by

$$\begin{aligned}
[m]_{ij} &= m_i \delta_{ij} , \\
[c_1]_{ij} &= c_{1,i} \delta_{ij} , \\
[c_2]_{ij} &= c_{2,i} \delta_{ij} , \\
[k_1]_{ij} &= k_{1,i} \delta_{ij} , \\
[k_3]_{ij} &= k_{3,i} \delta_{ij} .
\end{aligned} \tag{4.17}$$

We introduce the following convention for notation: if  $\mathbf{V} = (V_1, \dots, V_n)$  is a vector, then,  $|\mathbf{V}| = (|V_1|, \dots, |V_n|)$ ,  $\mathbf{V}^3 = (V_1^3, \dots, V_n^3)$ , and  $|\mathbf{V}|\dot{\mathbf{V}} = (|V_1|\dot{V}_1, \dots, |V_n|\dot{V}_n)$ .

Using Eqs. (4.11) to (4.17), Eqs. (4.2) and (4.8) can now be rewritten as

$$\left\{ \begin{array}{l}
[m] \ddot{\mathbf{Z}}(t) + [c_1] \left( \dot{\mathbf{Z}}(t) - [\varphi] \dot{\mathbf{Q}}(t) \right) + [c_2] \left( |\mathbf{Y}(t)| \left( \dot{\mathbf{Z}}(t) - [\varphi] \dot{\mathbf{Q}}(t) \right) \right) \\
\qquad \qquad \qquad + [k_1] \mathbf{Y}(t) + [k_3] (\mathbf{Y}(t))^3 = 0 , \\
[M] \ddot{\mathbf{Q}}(t) + [D] \dot{\mathbf{Q}}(t) + [K] \mathbf{Q}(t) = \mathbf{F}^{\text{exp}}(t) + [\varphi]^T [c_1] \left( \dot{\mathbf{Z}}(t) - [\varphi] \dot{\mathbf{Q}}(t) \right) \\
\qquad \qquad \qquad + [\varphi]^T [c_2] \left( |\mathbf{Y}(t)| \left( \dot{\mathbf{Z}}(t) - [\varphi] \dot{\mathbf{Q}}(t) \right) \right) \\
\qquad \qquad \qquad + [\varphi]^T [k_1] \mathbf{Y}(t) + [\varphi]^T [k_3] (\mathbf{Y}(t))^3 ,
\end{array} \right. \tag{4.18}$$

in which  $\mathbf{Y}(t) = \mathbf{Z}(t) - [\varphi] \mathbf{Q}(t)$ , where  $\mathbf{Z}(t) = (Z_1(t), \dots, Z_n(t))$  is the vector of the displacements in the fixed coordinate system of the nonlinear absorbers, and where  $\mathbf{F}^{\text{exp}}(t) = (F_1^{\text{exp}}(t), \dots, F_{N_m}^{\text{exp}}(t))$  is the vector whose components are defined by Eq. (4.14).

#### 4.4 Expression of powers related to the mechanical system

In order to quantify the efficiency of the nonlinear oscillators, it is necessary to express the different powers of the system. Let  $\Pi_{\text{in}}$ ,  $\Pi_{\text{diss}}([D])$ ,  $\Pi_{\text{trans}}$ , and  $\Pi_{\text{diss}}([f_D])$  be respectively the power introduced into the beam, the power dissipated by the damping of the beam, the power transmitted between the beam and the oscillators, and the power dissipated by the damping of the oscillators. Let  $Z_j^r(t)$  and  $\dot{Z}_j^r(t)$  be respectively the relative displacement and the relative velocity of the oscillator  $j$  such that

$$\begin{aligned}
Z_j^r(t) &= Z_j(t) - W(x_j, t) , \\
\dot{Z}_j^r(t) &= \dot{Z}_j(t) - \frac{\partial W}{\partial t}(x_j, t) .
\end{aligned} \tag{4.19}$$

The following power densities are defined.

- **Input power density introduced into the beam.** The total power introduced in the beam is such that

$$\Pi_{\text{in}} = E \left\{ \int_0^{L_p} g^{\text{ext}}(x, t) \frac{\partial W}{\partial t}(x, t) dx + F_s(t) \frac{\partial W}{\partial t}(L_p, t) \right\} \quad (4.20)$$

$$\begin{aligned} &= E \left\{ \sum_{\alpha=1}^{N_m} \mathcal{F}^{\text{exp}}(\varphi_\alpha, t) \dot{Q}_\alpha(t) \right\} \\ &= \sum_{\alpha=1}^{N_m} E \{ F_\alpha^{\text{exp}}(t) \dot{Q}_\alpha(t) \} . \end{aligned} \quad (4.21)$$

Let  $[R_{\mathbf{F}^{\text{exp}} \dot{\mathbf{Q}}}(\tau)]$  and  $[S_{\mathbf{F}^{\text{exp}} \dot{\mathbf{Q}}}(\omega)]$  be respectively the cross-correlation function and the cross-spectral density function of the stationary processes  $\{\mathbf{F}^{\text{exp}}(t) = (F_1^{\text{exp}}(t), \dots, F_{N_m}^{\text{exp}}(t)), t \in \mathbb{R}\}$  and  $\{\dot{\mathbf{Q}}(t) = (\dot{Q}_1(t), \dots, \dot{Q}_{N_m}(t)), t \in \mathbb{R}\}$ . These two functions are such that

$$[R_{\mathbf{F}^{\text{exp}} \dot{\mathbf{Q}}}(\tau)] = E \{ \mathbf{F}^{\text{exp}}(t + \tau) \dot{\mathbf{Q}}(t)^T \} = \int_{\mathbb{R}} [S_{\mathbf{F}^{\text{exp}} \dot{\mathbf{Q}}}(\omega)] e^{i\omega\tau} d\omega . \quad (4.22)$$

Since  $[R_{\mathbf{F}^{\text{exp}} \dot{\mathbf{Q}}}(\tau)]_{\alpha\beta} = E \{ F_\alpha^{\text{exp}}(t + \tau) \dot{Q}_\beta(t)^T \}$ , the trace of the correlation function at  $\tau = 0$  is such that

$$\text{tr}[R_{\mathbf{F}^{\text{exp}} \dot{\mathbf{Q}}}(0)]_{\alpha\beta} = E \left\{ \sum_{\alpha=1}^{N_m} F_\alpha^{\text{exp}}(t) \dot{Q}_\alpha(t)^T \right\} = \int_{\mathbb{R}} \text{tr}[S_{\mathbf{F}^{\text{exp}} \dot{\mathbf{Q}}}(\omega)] d\omega . \quad (4.23)$$

Thus, the input power density introduced in the beam is such that

$$\pi_{\text{in}}(\omega) = \text{tr}[S_{\mathbf{F}^{\text{exp}} \dot{\mathbf{Q}}}(\omega)] = \sum_{\alpha=1}^{N_m} [S_{\mathbf{F}^{\text{exp}} \dot{\mathbf{Q}}}(\omega)]_{\alpha\alpha} = \sum_{\alpha=1}^{N_m} S_{F_\alpha^{\text{exp}} \dot{Q}_\alpha}(\omega) . \quad (4.24)$$

- **Power density dissipated by the damping of the beam.** The total power dissipated by the damping of the beam is such that

$$\Pi_{\text{diss}}([D]) = E \left\{ \int_0^{L_p} c_p \left( \frac{\partial W}{\partial t}(x, t) \right)^2 dx \right\} \quad (4.25)$$

$$\begin{aligned} &= E \left\{ \mathcal{C} \left( \frac{\partial W}{\partial t}(x, t), \frac{\partial W}{\partial t}(x, t) \right) \right\} \\ &= E \{ \langle [D] \dot{\mathbf{Q}}(t), \dot{\mathbf{Q}}(t) \rangle \} , \end{aligned} \quad (4.26)$$

in which  $\frac{\partial W}{\partial t}(x, t) = \sum_{\alpha=1}^{N_m} \dot{Q}_\alpha(t) \varphi_\alpha(x)$  and where  $\langle \cdot, \cdot \rangle$  is the Euclidean inner product in  $\mathbb{R}^{N_m}$ .

Let  $[R_{[D] \dot{\mathbf{Q}} \dot{\mathbf{Q}}}(\tau)]$  be the cross-correlation function of the stationary stochastic processes  $\{[D] \dot{\mathbf{Q}}(t), t \in \mathbb{R}\}$  and  $\{\dot{\mathbf{Q}}(t), t \in \mathbb{R}\}$ . This function is written

as

$$[R_{[D]\dot{\mathbf{Q}},\dot{\mathbf{Q}}}(\tau)] = E\{([D]\dot{\mathbf{Q}})(t + \tau)\dot{\mathbf{Q}}(t)^T\} \quad (4.27)$$

$$\begin{aligned} &= [D][R_{\dot{\mathbf{Q}}}(\tau)] \\ &= [D] \int_{\mathbb{R}} [S_{\dot{\mathbf{Q}}}(\omega)] e^{i\omega\tau} d\omega, \end{aligned} \quad (4.28)$$

in which  $[R_{\dot{\mathbf{Q}}}(\tau)]$  and  $[S_{\dot{\mathbf{Q}}}(\omega)]$  are respectively the autocorrelation function and the matrix-valued spectral density function of the stationary stochastic process  $\{\dot{\mathbf{Q}}(t), t \in \mathbb{R}\}$ .

The power dissipated by the damping of the beam can then be rewritten

$$\Pi_{\text{diss}}([D]) = \text{tr}[R_{[D]\dot{\mathbf{Q}},\dot{\mathbf{Q}}}(0)] \quad (4.29)$$

$$\begin{aligned} &= \text{tr}\{[D][R_{\dot{\mathbf{Q}}}(0)]\} \\ &= \int_{\mathbb{R}} \sum_{\alpha=1}^{N_m} [D]_{\alpha\alpha} [S_{\dot{\mathbf{Q}}}(\omega)]_{\alpha\alpha} d\omega. \end{aligned} \quad (4.30)$$

The power density dissipated by the damping of the beam  $\pi_{\text{diss}}([D])(\omega)$  is such that

$$\pi_{\text{diss}}([D])(\omega) = \sum_{\alpha=1}^{N_m} [D]_{\alpha\alpha} S_{\dot{\mathbf{Q}}_{\alpha}}(\omega). \quad (4.31)$$

- **Power density transmitted between the beam and the oscillators.** The total power transmitted between the beam and the oscillators is defined by  $\Pi_{\text{trans}} = E\{\sum_{j=1}^n F_j(t)\dot{Z}_j^r(t)\}$ . Let  $[R_{\mathbf{F}\dot{\mathbf{Z}}^r}(\tau)]$  and  $[S_{\mathbf{F}\dot{\mathbf{Z}}^r}(\omega)]$  be respectively the cross-correlation function and the cross-spectral density function of the stationary processes  $\{\mathbf{F}(t) = (F_1(t), \dots, F_n(t)), t \in \mathbb{R}\}$  and  $\{\dot{\mathbf{Z}}^r(t) = (\dot{Z}_1^r(t), \dots, \dot{Z}_n^r(t)), t \in \mathbb{R}\}$ . These two functions are such that

$$[R_{\mathbf{F}\dot{\mathbf{Z}}^r}(\tau)] = E\{\mathbf{F}(t + \tau)\dot{\mathbf{Z}}^r(t)^T\} = \int_{\mathbb{R}} [S_{\mathbf{F}\dot{\mathbf{Z}}^r}(\omega)] e^{i\omega\tau} d\omega. \quad (4.32)$$

Since  $[R_{\mathbf{F}\dot{\mathbf{Z}}^r}(\tau)]_{jk} = E\{F_j(t + \tau)\dot{Z}_k^r(t)\}$ , the trace of the correlation function at  $\tau = 0$  is such that

$$\text{tr}[R_{\mathbf{F}\dot{\mathbf{Z}}^r}(0)] = E\{\sum_{j=1}^n F_j(t)\dot{Z}_j^r(t)\} = \int_{\mathbb{R}} \text{tr}[S_{\mathbf{F}\dot{\mathbf{Z}}^r}(\omega)] d\omega. \quad (4.33)$$

Thus, the transmitted power density is such that

$$\pi_{\text{trans}}(\omega) = \text{tr}[S_{\mathbf{F}\dot{\mathbf{Z}}^r}(\omega)] = \sum_{j=1}^n [S_{\mathbf{F}\dot{\mathbf{Z}}^r}(\omega)]_{jj} = \sum_{j=1}^n S_{F_j\dot{Z}_j^r}(\omega). \quad (4.34)$$

- **Power density dissipated by the damping of the oscillators.** The total power dissipated by the damping of the oscillators is the sum of the power dissipated by the damping of each oscillators,

$$\Pi_{\text{diss}}([f_D]) = \sum_{j=1}^n \Pi_{\text{diss}}([f_{D,j}]) \quad (4.35)$$

$$= \sum_{j=1}^n E\{\dot{Z}_j^r(t), f_{D,j}(Z_j^r(t), \dot{Z}_j^r(t))\} . \quad (4.36)$$

The power density dissipated by the damping of the oscillators is then written as

$$\pi_{\text{diss}}([f_D])(\omega) = \sum_{j=1}^n S_{f_{D,j}\dot{Z}_j^r}(\omega) , \quad (4.37)$$

in which  $S_{f_{D,j}\dot{Z}_j^r}(\omega)$  is the cross-spectral density function of the stationary processes  $\{f_{D,j}(t), t \in \mathbb{R}\}$  and  $\{\dot{Z}_j^r(t), t \in \mathbb{R}\}$ .

## 4.5 Stochastic solver and signal processing

### 4.5.1 Stochastic solver

For constructing the stationary stochastic solution of the nonlinear system of equations defined by Eq. (4.18), the Monte Carlo method is used. We consider  $L$  independent realizations  $\theta_\ell = 1, \dots, L$  in  $\Theta$  constructed with the generator described in a next paragraph of this section. Similarly to Section 2.3.1, for each realization  $\theta_\ell$ , we have to solve the deterministic nonlinear system of equations associated with stochastic Eq. (4.18), such that, for all  $t \in ]0, T]$ ,

$$\left\{ \begin{array}{l} [m] \ddot{\mathbf{Z}}(t; \theta_\ell) + [c_1] \left( \dot{\mathbf{Z}}(t; \theta_\ell) - [\varphi] \dot{\mathbf{Q}}(t; \theta_\ell) \right) + [k_1] \mathbf{Y}(t; \theta_\ell) + [k_3] (\mathbf{Y}(t; \theta_\ell))^3 \\ \quad + [c_2] \left( |\mathbf{Y}(t; \theta_\ell)| \left( \dot{\mathbf{Z}}(t; \theta_\ell) - [\varphi] \dot{\mathbf{Q}}(t; \theta_\ell) \right) \right) = 0 , \\ [M] \ddot{\mathbf{Q}}(t; \theta_\ell) + [D] \dot{\mathbf{Q}}(t; \theta_\ell) + [K] \mathbf{Q}(t; \theta_\ell) = \mathbf{F}^{\text{exp}}(t; \theta_\ell) \\ \quad + [\varphi]^T [c_1] \left( \dot{\mathbf{Z}}(t; \theta_\ell) - [\varphi] \dot{\mathbf{Q}}(t; \theta_\ell) \right) \\ \quad + [\varphi]^T [c_2] \left( |\mathbf{Y}(t; \theta_\ell)| \left( \dot{\mathbf{Z}}(t; \theta_\ell) - [\varphi] \dot{\mathbf{Q}}(t; \theta_\ell) \right) \right) \\ \quad + [\varphi]^T [k_1] \mathbf{Y}(t; \theta_\ell) + [\varphi]^T [k_3] (\mathbf{Y}(t; \theta_\ell))^3 , \end{array} \right. \quad (4.38)$$

in which  $\mathbf{Y}(t; \theta_\ell) = \mathbf{Z}(t; \theta_\ell) - [\varphi] \mathbf{Q}(t; \theta_\ell)$  and with the initial conditions,

$$\mathbf{Z}(0; \theta_\ell) = \mathbf{0} \quad , \quad \dot{\mathbf{Z}}(0; \theta_\ell) = \mathbf{0} \quad , \quad \mathbf{Q}(0; \theta_\ell) = \mathbf{0} \quad , \quad \dot{\mathbf{Q}}(0; \theta_\ell) = \mathbf{0} . \quad (4.39)$$

With such initial conditions, the transient part of the response would be 0 for a linear second-order dynamical system and it is assumed to be 0, or negligible, for the nonlinear second-order dynamical system that is considered (we have effectively checked the validity of this hypothesis for the numerical application presented in the thesis). The part of the trajectory on  $[0, T]$  corresponds to the stationary response,  $X_s(t; \theta_\ell) \simeq X(t; \theta_\ell)$  for  $t$  in  $[0, T]$ . The time  $T$  that is related to the frequency resolution is defined in Section 2.3.2 (the time and frequency sampling are the same that those presented for the absorber and thus are not presented again in this chapter). The deterministic problem defined by Eq. (4.38) for  $t$  in  $]0, T]$  with the initial conditions defined by Eq. (4.39) for  $t = 0$  will be solved by using the Störmer-Verlet scheme presented in Section 4.5.3.

#### 4.5.2 Generation of independent realizations of Gaussian stationary stochastic process $g^{\text{exp}}$

The power spectral density function of the Gaussian stationary second-order centered stochastic process  $g^{\text{exp}}$  is noted  $S_{g^{\text{exp}}}(\omega)$ . The autocorrelation function  $\tau \mapsto R_{g^{\text{exp}}}(\tau)$  of the stationary stochastic process  $g^{\text{exp}}$  is such that  $R_{g^{\text{exp}}}(\tau) = E\{g^{\text{exp}}(t + \tau)g^{\text{exp}}(t)\}$  and  $R_{g^{\text{exp}}}(\tau) = \int_{\mathbb{R}} e^{i\omega\tau} S_{g^{\text{exp}}}(\omega) d\omega$ . The generator of realizations of the Gaussian stationary second-order stochastic process  $g^{\text{exp}}$  is constructed as explained in Section 2.3.3 by substituting  $\ddot{X}_{\text{imp}}(t; \theta_\ell)$  by  $g^{\text{exp}}(t; \theta_\ell)$  and  $S_{\ddot{X}_{\text{imp}}}(\omega)$  by  $S_{g^{\text{exp}}}(\omega)$ .

#### 4.5.3 Störmer-Verlet integration scheme

For the reason given in Section 2.3.4, the Störmer-Verlet integration scheme is well suited for solving the system of equations defined by Eq. (4.38) with the initial conditions defined by Eq. (4.39). In a first step we rewrite the system of second-order differential equations as the following system of first-order differential equations, for  $t$  in  $]0, T]$ ,

$$\left\{ \begin{array}{l} \dot{\mathbf{Z}}(t; \theta_\ell) = \mathbf{U}(t; \theta_\ell) , \\ \dot{\mathbf{Q}}(t; \theta_\ell) = \mathbf{V}(t; \theta_\ell) , \\ \dot{\mathbf{U}}(t; \theta_\ell) + [m]^{-1}[c_1] (\mathbf{U}(t; \theta_\ell) - [\boldsymbol{\varphi}]\mathbf{V}(t; \theta_\ell)) + [m]^{-1}[k_1]\mathbf{Y}(t; \theta_\ell) \\ \quad + [m]^{-1}[c_2] (|\mathbf{Y}(t; \theta_\ell)| (\mathbf{U}(t; \theta_\ell) - [\boldsymbol{\varphi}]\mathbf{V}(t; \theta_\ell))) \\ \quad + [m]^{-1}[k_3] (\mathbf{Y}(t; \theta_\ell))^3 = 0 , \\ \dot{\mathbf{V}}(t; \theta_\ell) + [M]^{-1}[D]\mathbf{V}(t; \theta_\ell) + [M]^{-1}[K]\mathbf{Q}(t; \theta_\ell) = [M]^{-1}\mathbf{F}^{\text{ext}}(t; \theta_\ell) \\ \quad + [M]^{-1}[\boldsymbol{\varphi}]^T [c_1] (\mathbf{U}(t; \theta_\ell) - [\boldsymbol{\varphi}]\mathbf{V}(t; \theta_\ell)) \\ \quad + [M]^{-1}[\boldsymbol{\varphi}]^T [c_2] (|\mathbf{Y}(t; \theta_\ell)| (\mathbf{U}(t; \theta_\ell) - [\boldsymbol{\varphi}]\mathbf{V}(t; \theta_\ell))) \\ \quad + [M]^{-1}[\boldsymbol{\varphi}]^T [k_1]\mathbf{Y}(t; \theta_\ell) \\ \quad + [M]^{-1}[\boldsymbol{\varphi}]^T [k_3] (\mathbf{Y}(t; \theta_\ell))^3 . \end{array} \right. \quad (4.40)$$

with the initial conditions defined by  $\mathbf{Z}(0; \theta_\ell) = \mathbf{Q}(0; \theta_\ell) = \mathbf{U}(0; \theta_\ell) = \mathbf{V}(0; \theta_\ell) = \mathbf{0}$ . We introduce the notations  $\mathbf{z}_\ell^\alpha = \mathbf{Z}(t_\alpha; \theta_\ell)$ ,  $\mathbf{q}_\ell^\alpha = \mathbf{Q}(t_\alpha; \theta_\ell)$ ,  $\mathbf{u}_\ell^\alpha = \mathbf{U}(t_\alpha; \theta_\ell)$ ,  $\mathbf{v}_\ell^\alpha = \mathbf{V}(t_\alpha; \theta_\ell)$ , and  $\mathbf{y}_\ell^\alpha = \mathbf{Y}(t_\alpha; \theta_\ell)$ . The Störmer-Verlet integration scheme applied to Eq. (4.40) is written (more details on the writing of the integration scheme can be found in Section 2.3.4), for  $\alpha = 0, 1, \dots, N_m - 1$ , as

$$\left\{ \begin{array}{l} \mathbf{z}_\ell^{\alpha+1/2} = \mathbf{z}_\ell^\alpha + \frac{\Delta t}{2} \mathbf{u}_\ell^\alpha, \\ \mathbf{q}_\ell^{\alpha+1/2} = \mathbf{q}_\ell^\alpha + \frac{\Delta t}{2} \mathbf{v}_\ell^\alpha, \\ \frac{\mathbf{u}_\ell^{\alpha+1} - \mathbf{u}_\ell^\alpha}{\Delta t} + [m]^{-1}[c_1] \left( \frac{\mathbf{u}_\ell^{\alpha+1} + \mathbf{u}_\ell^\alpha}{2} - [\varphi] \frac{\mathbf{v}_\ell^{\alpha+1} + \mathbf{v}_\ell^\alpha}{2} \right) \\ \quad + [m]^{-1}[c_2] \left( |\mathbf{y}_\ell^{\alpha+1/2}| \left( \frac{\mathbf{u}_\ell^{\alpha+1} + \mathbf{u}_\ell^\alpha}{2} - [\varphi] \frac{\mathbf{v}_\ell^{\alpha+1} + \mathbf{v}_\ell^\alpha}{2} \right) \right) \\ \quad + [m]^{-1}[k_1] \mathbf{y}_\ell^{\alpha+1/2} + [m]^{-1}[k_3] \left( \mathbf{y}_\ell^{\alpha+1/2} \right)^3 = 0, \\ \frac{\mathbf{v}_\ell^{\alpha+1} - \mathbf{v}_\ell^\alpha}{\Delta t} + [M]^{-1}[D] \frac{\mathbf{v}_\ell^{\alpha+1} + \mathbf{v}_\ell^\alpha}{2} + [M]^{-1}[K] \mathbf{q}_\ell^{\alpha+1/2} = [M]^{-1} \mathbf{F}^{\text{ext}}(t_{\alpha+1}; \theta_\ell) \\ \quad + [M]^{-1}[\varphi]^T [c_1] \left( \frac{\mathbf{u}_\ell^{\alpha+1} + \mathbf{u}_\ell^\alpha}{2} - [\varphi] \frac{\mathbf{v}_\ell^{\alpha+1} + \mathbf{v}_\ell^\alpha}{2} \right) \\ \quad + [M]^{-1}[\varphi]^T [c_2] \left( |\mathbf{y}_\ell^{\alpha+1/2}| \left( \frac{\mathbf{u}_\ell^{\alpha+1} + \mathbf{u}_\ell^\alpha}{2} - [\varphi] \frac{\mathbf{v}_\ell^{\alpha+1} + \mathbf{v}_\ell^\alpha}{2} \right) \right) \\ \quad + [M]^{-1}[\varphi]^T [k_1] \mathbf{y}_\ell^{\alpha+1/2} + [M]^{-1}[\varphi]^T [k_3] \left( \mathbf{y}_\ell^{\alpha+1/2} \right)^3, \\ \mathbf{z}_\ell^{\alpha+1} = \mathbf{z}_\ell^{\alpha+1/2} + \frac{\Delta t}{2} \mathbf{u}_\ell^{\alpha+1}, \\ \mathbf{q}_\ell^{\alpha+1} = \mathbf{q}_\ell^{\alpha+1/2} + \frac{\Delta t}{2} \mathbf{v}_\ell^{\alpha+1}, \end{array} \right. \quad (4.41)$$

with  $\mathbf{z}_\ell^0 = \mathbf{q}_\ell^0 = \mathbf{u}_\ell^0 = \mathbf{v}_\ell^0 = \mathbf{0}$ .

It should be noted that the the third and fourth equations of the system are coupled. It is possible to isolate  $\mathbf{u}_\ell^{\alpha+1}$  and  $\mathbf{v}_\ell^{\alpha+1}$  in the left-hand side of the equation in order to calculate them. The system of equations defined by Eq. (4.41) can then be rewritten as the following system, for  $\alpha = 0, 1, \dots, N_m - 1$ ,

$$\left\{ \begin{array}{l} \mathbf{z}_\ell^{\alpha+1/2} = \mathbf{z}_\ell^\alpha + \frac{\Delta t}{2} \mathbf{u}_\ell^\alpha, \\ \mathbf{q}_\ell^{\alpha+1/2} = \mathbf{q}_\ell^\alpha + \frac{\Delta t}{2} \mathbf{v}_\ell^\alpha, \\ \begin{bmatrix} [A_{11}^{\alpha, \ell}] & -[A_{12}^{\alpha, \ell}] \\ -[A_{21}^{\alpha, \ell}] & [A_{22}^{\alpha, \ell}] \end{bmatrix} \begin{bmatrix} \mathbf{u}_\ell^{\alpha+1} \\ \mathbf{v}_\ell^{\alpha+1} \end{bmatrix} = \begin{bmatrix} \mathbf{h}_1^{\alpha, \ell} \\ \mathbf{h}_2^{\alpha, \ell} \end{bmatrix} + \begin{bmatrix} \mathbf{0} \\ \Delta t [M]^{-1} \mathbf{F}^{\text{ext}}(t_{\alpha+1}; \theta_\ell) \end{bmatrix}, \\ \mathbf{z}_\ell^{\alpha+1} = \mathbf{z}_\ell^{\alpha+1/2} + \frac{\Delta t}{2} \mathbf{u}_\ell^{\alpha+1}, \\ \mathbf{q}_\ell^{\alpha+1} = \mathbf{q}_\ell^{\alpha+1/2} + \frac{\Delta t}{2} \mathbf{v}_\ell^{\alpha+1}, \end{array} \right. \quad (4.42)$$

in which

$$\left\{ \begin{array}{l} [A_{11}^{\alpha,\ell}] = [I] + \frac{\Delta t}{2}[m]^{-1} \left( [c_1] + [c_2][\mathbb{Y}_\ell^{\alpha+1/2}] \right), \\ [A_{12}^{\alpha,\ell}] = \frac{\Delta t}{2}[m]^{-1} \left( [c_1] + [c_2][\mathbb{Y}_\ell^{\alpha+1/2}] \right) [\boldsymbol{\varphi}], \\ [A_{21}^{\alpha,\ell}] = \frac{\Delta t}{2}[M]^{-1} [\boldsymbol{\varphi}]^T \left( [c_1] + [c_2][\mathbb{Y}_\ell^{\alpha+1/2}] \right), \\ [A_{22}^{\alpha,\ell}] = [I] + \frac{\Delta t}{2}[M]^{-1} \left( [D] + [\boldsymbol{\varphi}]^T [c_1] [\boldsymbol{\varphi}] + [\boldsymbol{\varphi}]^T [c_2] [\mathbb{Y}_\ell^{\alpha+1/2}] [\boldsymbol{\varphi}] \right), \\ \mathbf{h}_1^{\alpha,\ell} = [B_{11}^{\alpha,\ell}] \mathbf{u}_\ell^\alpha + [B_{12}^{\alpha,\ell}] \mathbf{v}_\ell^\alpha - \Delta t [m]^{-1} \left( [k_1] \mathbf{y}_\ell^{\alpha+1/2} + [k_3] (\mathbf{y}_\ell^{\alpha+1/2})^3 \right), \\ \mathbf{h}_2^{\alpha,\ell} = [B_{21}^{\alpha,\ell}] \mathbf{u}_\ell^\alpha + [B_{22}^{\alpha,\ell}] \mathbf{v}_\ell^\alpha + \Delta t [M]^{-1} \left( [\boldsymbol{\varphi}]^T [k_1] \mathbf{y}_\ell^{\alpha+1/2} \right. \\ \left. + [\boldsymbol{\varphi}]^T [k_3] (\mathbf{y}_\ell^{\alpha+1/2})^3 - [K] \mathbf{q}_\ell^{\alpha+1/2} \right), \end{array} \right. \quad (4.43)$$

with

$$\left\{ \begin{array}{l} [B_{11}^{\alpha,\ell}] = [I] - \frac{\Delta t}{2}[m]^{-1} \left( [c_1] + [c_2][\mathbb{Y}_\ell^{\alpha+1/2}] \right), \\ [B_{12}^{\alpha,\ell}] = \frac{\Delta t}{2}[m]^{-1} \left( [c_1] + [c_2][\mathbb{Y}_\ell^{\alpha+1/2}] \right) [\boldsymbol{\varphi}], \\ [B_{21}^{\alpha,\ell}] = \frac{\Delta t}{2}[M]^{-1} [\boldsymbol{\varphi}]^T \left( [c_1] + [c_2][\mathbb{Y}_\ell^{\alpha+1/2}] \right), \\ [B_{22}^{\alpha,\ell}] = [I] - \frac{\Delta t}{2}[M]^{-1} \left( [D] + [\boldsymbol{\varphi}]^T [c_1] [\boldsymbol{\varphi}] + [\boldsymbol{\varphi}]^T [c_2] [\mathbb{Y}_\ell^{\alpha+1/2}] [\boldsymbol{\varphi}] \right), \end{array} \right. \quad (4.44)$$

and where the notation  $\mathbb{[\cdot]}$  means that, if  $\mathbf{V} = (V_1, \dots, V_N)$  is a vector, then,  $\mathbb{[V]}$  is a diagonal matrix whose entries are  $\mathbb{[V]}_{jk} = \delta_{jk} |V_k|$ .

In case of a strong nonlinearity induced by a high amplitude of excitation, a time oversampling can be required. Time step  $\Delta t$  is splitted in  $n_s$  time steps noted  $\delta_t$  such that

$$\delta_t = \frac{\Delta t}{n_s}. \quad (4.45)$$

The corresponding time sampling is  $t_\gamma = \gamma \delta_t$  with  $\gamma = 0, 1, \dots, n_s(N_m - 1)$ . With the notation introduced before, the system of equations defined by

Eq. (4.42) yields, for  $\gamma = 0, 1, \dots, n_s(N_m - 1)$ , as

$$\left\{ \begin{array}{l}
 \mathbf{z}_\ell^{\gamma+1/2} = \mathbf{z}_\ell^\gamma + \frac{\delta_t}{2} \mathbf{u}_\ell^\gamma, \\
 \mathbf{q}_\ell^{\gamma+1/2} = \mathbf{q}_\ell^\gamma + \frac{\delta_t}{2} \mathbf{v}_\ell^\gamma, \\
 \frac{\mathbf{u}_\ell^{\gamma+1} - \mathbf{u}_\ell^\gamma}{\delta_t} + [m]^{-1}[c_1] \left( \frac{\mathbf{u}_\ell^{\gamma+1} + \mathbf{u}_\ell^\gamma}{2} - [\varphi] \frac{\mathbf{v}_\ell^{\gamma+1} + \mathbf{v}_\ell^\gamma}{2} \right) \\
 \quad + [m]^{-1}[c_2] \left( |\mathbf{y}_\ell^{\gamma+1/2}| \left( \frac{\mathbf{u}_\ell^{\gamma+1} + \mathbf{u}_\ell^\gamma}{2} - [\varphi] \frac{\mathbf{v}_\ell^{\gamma+1} + \mathbf{v}_\ell^\gamma}{2} \right) \right) \\
 \quad + [m]^{-1}[k_1] \mathbf{y}_\ell^{\gamma+1/2} + [m]^{-1}[k_3] \left( \mathbf{y}_\ell^{\gamma+1/2} \right)^3 = 0, \\
 \frac{\mathbf{v}_\ell^{\gamma+1} - \mathbf{v}_\ell^\gamma}{\delta_t} + [M]^{-1}[D] \frac{\mathbf{v}_\ell^{\gamma+1} + \mathbf{v}_\ell^\gamma}{2} + [M]^{-1}[K] \mathbf{q}_\ell^{\gamma+1/2} = [M]^{-1} \mathbf{F}^{\text{ext}}(t_{\alpha+1}; \theta_\ell) \\
 \quad + [M]^{-1}[\varphi]^T [c_1] \left( \frac{\mathbf{u}_\ell^{\gamma+1} + \mathbf{u}_\ell^\gamma}{2} - [\varphi] \frac{\mathbf{v}_\ell^{\gamma+1} + \mathbf{v}_\ell^\gamma}{2} \right) \\
 \quad + [M]^{-1}[\varphi]^T [c_2] \left( |\mathbf{y}_\ell^{\gamma+1/2}| \left( \frac{\mathbf{u}_\ell^{\gamma+1} + \mathbf{u}_\ell^\gamma}{2} - [\varphi] \frac{\mathbf{v}_\ell^{\gamma+1} + \mathbf{v}_\ell^\gamma}{2} \right) \right) \\
 \quad + [M]^{-1}[\varphi]^T [k_1] \mathbf{y}_\ell^{\gamma+1/2} + [M]^{-1}[\varphi]^T [k_3] \left( \mathbf{y}_\ell^{\gamma+1/2} \right)^3, \\
 \mathbf{z}_\ell^{\gamma+1} = \mathbf{z}_\ell^{\gamma+1/2} + \frac{\delta_t}{2} \mathbf{u}_\ell^{\gamma+1}, \\
 \mathbf{q}_\ell^{\gamma+1} = \mathbf{q}_\ell^{\gamma+1/2} + \frac{\delta_t}{2} \mathbf{v}_\ell^{\gamma+1},
 \end{array} \right. \tag{4.46}$$

with  $\mathbf{z}_\ell^0 = \mathbf{q}_\ell^0 = \mathbf{u}_\ell^0 = \mathbf{v}_\ell^0 = 0$ .

It should be noted that the third and the fourth equations in Eq. (4.46) can be rewritten with matrix notations as the one introduced in Eq. (4.42).

#### 4.5.4 Signal processing

For estimating the power spectral density functions and the cross-spectral density functions, the periodogram method is used with the parameters given in Section 2.3.5.

## 4.6 Conclusion

In this chapter, a one-dimensional model of an Euler-Bernoulli beam with nonlinear absorbers has been presented and the related stochastic solver has been developed. The model is constituted of a cantilever Euler-Bernoulli beam on which nonlinear absorbers, constituted of a mass-spring-damper system with

a nonlinear spring and a nonlinear damper, are set up. The beam is subjected to a stochastic excitation at its free end. Some power density functions have been defined in order to represent the results of the model and of the experiments in Chapter 5. The stochastic solver, which allows to calculate the displacement of the beam and the displacement of the different masses of the nonlinear absorbers, is based on the Monte Carlo method. In addition, the time and frequency sampling are performed using the Shannon theorem and the generation of independent realizations of the excitation are achieved by using the usual second-order spectral representation of the stationary stochastic processes. The calculation of the response is then solved by the Störmer-Verlet integration scheme. As well, the power spectral density functions and the cross-spectral density functions are estimated by the periodogram method.

## Chapter 5

# Numerical simulation of absorber effects on the dynamical behavior of an elastic beam

### 5.1 Introduction

In this chapter, we perform a numerical simulation for studying the effects of the absorber on the dynamical behavior of an elastic beam. The absorber is the one that has been designed, experimentally analyzed, modeled, and identified in Chapters 2 and 3. For the elastic beam, we have chosen a fixed-free homogeneous elastic beam with a constant section and with an additional damping model. Two configurations are considered in order to analyze the role played by the absorber when its eigenfrequency coincides either with the fundamental eigenfrequency of the beam or with the third eigenfrequency of the beam. Since the mass of the absorber is given, the coincidence of the eigenfrequencies is obtained by modifying the length of the beam.

The parameterization of the damped elastic beam and the definition of the excitation force are presented in Section 5.2. Section 5.3 deals with the computation of the eigenfrequencies and the associated eigenmodes of the beam. In Section 5.4, the two configurations of the beam are defined. After that, the construction of the reduced model, the choice of the frequency band of analysis, and the parameters used for the signal processing are provided in Sections 5.5 and 5.6. The quantities of interest used for the analysis are defined in Section 5.7. In order to compare the effects of a nonlinear absorber with respect to a linear one, a numerical analysis of the effects of a linear absorber is presented in Section 5.8. In Section 5.9, numerical simulations are presented for analyzing the effects of a nonlinear absorber on the beam vibration.

## 5.2 Parameterization of the damped elastic beam

In this section, we define the parameters of the damped elastic beam whose model has been introduced in Chapter 4. Two configurations are considered. Each one is defined by a given beam length  $L_p$  and a given damping coefficient  $c_p$ . For each one of these two configurations, several values of the amplitude of the stochastic force applied to the beam are introduced. Let  $0xyz$  be the Cartesian frame defined in Figure 4.1. The notations introduced in Section 4.2 are reused. We consider the Euler-Bernoulli beam model in the fixed-free condition with the additional constant viscous damping coefficient  $c_p$  that have been introduced in Eq. (4.3). The transverse displacement along  $z$ -axis at location  $x$  and at time  $t$  is denoted by  $W(x, t)$ . The material is homogeneous with mass density  $\rho = 7,850 \text{ kg/m}^3$ . Let  $L_p$  be the length of the beam,  $S$  be its section that is assumed to be constant with height  $h = 1.6 \times 10^{-3} \text{ m}$  and width  $b = 5 \times 10^{-2} \text{ m}$ . Let  $EI = 3.7547 \text{ N} \times \text{m}^2$  be its stiffness modulus. There is no density of external forces ( $g^{\text{exp}} = 0$ ) applied to the beam but only the external force,  $F_s$ , applied to the end of the beam ( $x = L_p$ ), which is represented by the stochastic process  $\{F_s(t), t \in \mathbb{R}\}$  defined in Chapter 2. This stochastic process is thus completely described by its power spectral density function  $S_{F_s}(\omega)$  that is written as

$$S_{F_s}(\omega) = f_0^2 \mathbb{1}_{[-2\pi f_{\max}, 2\pi f_{\max}]}(\omega), \quad (5.1)$$

in which  $f_0$  is the amplitude of the applied stochastic force in Newton; the considered values of  $f_0$  are 0.0005, 0.001, 0.003, 0.005, and 0.007. For each one of the amplitudes, the power spectral density function of  $F_s$ ,  $\omega \mapsto S_{F_s}(\omega)$ , is represented in Figure 5.1. The boundary conditions are those defined by Eq. (4.3).

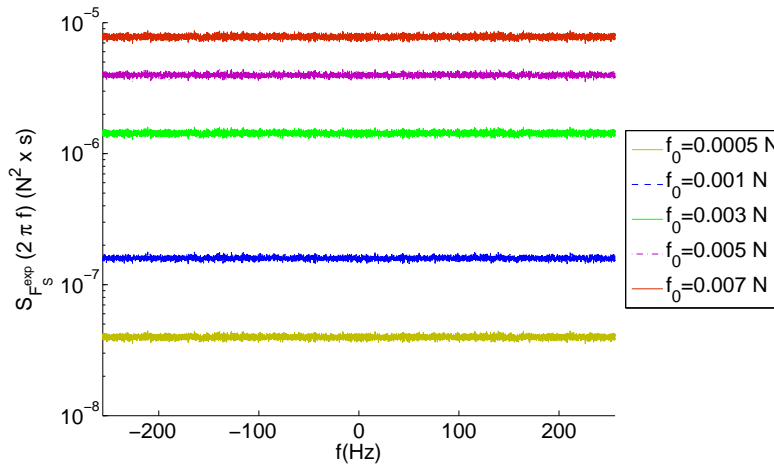


Figure 5.1: Power spectral density function  $f \mapsto S_{F_s}(2\pi f)$  for each one of the considered values of amplitude  $f_0$  on frequency band  $[-f_{\max}, f_{\max}]$ .

### 5.3 Eigenmodes of the beam

The reduced model detailed in Section 4.3 is constructed by using the first  $N_m$  eigenmodes of the undamped beam without any coupling with absorbers. The eigenfrequency  $\Omega_\alpha$  and the corresponding eigenmode  $\varphi_\alpha$  are written as

$$\Omega_\alpha = (\lambda_\alpha L_p)^2 \sqrt{\frac{EI}{\rho S L_p^4}}$$

$$\varphi_\alpha(x) = \cos(\lambda_\alpha x) - \cosh(\lambda_\alpha x) - \frac{\cos(\lambda_\alpha L_p) + \cosh(\lambda_\alpha L_p)}{\sin(\lambda_\alpha L_p) + \sinh(\lambda_\alpha L_p)} (\sin(\lambda_\alpha x) - \sinh(\lambda_\alpha x)) ,$$
(5.2)

in which  $\lambda_1 L_p = 1.875$ ,  $\lambda_2 L_p = 4.694$ ,  $\lambda_3 L_p = 7.855$ , and  $\lambda_\alpha L_p = (2\alpha - 1)\pi/2$  if  $\alpha > 3$ . These eigenmodes are such that (see Eq. (4.11))

$$[M]_{\beta\alpha} = \int_0^{L_p} \rho S \varphi_\alpha(x) \varphi_\beta(x) dx = \delta_{\beta\alpha} \mu_\alpha ,$$
(5.3)

in which the generalized mass  $\mu_\alpha = \rho S$  of eigenmode  $\alpha$  is independent of  $\alpha$ . Consequently, the eigenmodes are orthogonal for the inner product defined by Eq. (4.5), but the norm of each one is equal to  $\rho S$  and not to 1.

### 5.4 Definition of the configurations

As explained in Section 5.2, two configurations are introduced. These configurations are defined by using the following hypothesis concerning the analysis that we want to perform. The first configuration is devoted to the frequency response of the coupled system in the neighborhood of the third eigenfrequency of the beam (without absorber), and the second one in the neighborhood of its first eigenfrequency.

- *Configuration 1.* This configuration is designed in order that the third eigenfrequency of the beam (uncoupled with the absorber) is 24 Hz that coincides with the eigenfrequency of the absorber. For such a configuration,  $L_p = 1 m$ , and the viscous damping coefficient  $c_p$  has been chosen as  $c_p = 2\xi\Omega_3\mu_3$  with  $\xi = 0.01$ . This means that the modal damping rate of the third eigenmode is 0.01. For this configuration, the first four eigenfrequencies of the beam (uncoupled with the absorber) are 1.37, 8.57, 24.01, and 47.05 Hz. The values of the amplitude  $f_0$  that are studied for the excitation are 0.0005, 0.001, 0.003, 0.005, and 0.007 N.
- *Configuration 2.* This configuration is designed in order that the first eigenfrequency of the beam (uncoupled with the absorber) is 24 Hz that coincides with the eigenfrequency of the absorber. For such a configuration,  $L_p = 0.239 m$ , and the viscous damping coefficient  $c_p$  has been chosen as  $c_p = 2\xi\Omega_1\mu_1$  with  $\xi = 0.01$ . Similarly to configuration 1, this

means that the modal damping rate of the first eigenmode is 0.01. For this configuration, the first four eigenfrequencies of the beam (uncoupled with the absorber) are 23.99, 150.36, 421.07, and 825.07 *Hz*. The values of the amplitude  $f_0$  that are studied for the excitation are 0.001, 0.003, and 0.007 *N*.

## 5.5 Construction of the reduced-order model and frequency band of the analysis

As explained in Section 5.4, we are interested in analyzing the dynamical response of the coupled system (beam with an absorber) in a narrow frequency band centered at the eigenfrequency of the absorber, that is to say centered at 24 *Hz*. For the two configurations, the frequency band of analysis has been chosen as [21, 28] *Hz*. We have numerically checked that for each one of the two configurations, the absorber had only an effect on this frequency band and no other effects outside this band as shown in Figures 5.3(a) and 5.5(a). This is due to the fact that the first four eigenmodes of the beam are well separated (the half-power bandwidth of each resonance of the beam coupled with absorber is less than the distance between two consecutive eigenfrequencies). Consequently, the reduced-order model is converged with respect to the dynamic response in frequency band [21, 28] *Hz*, by using only the four eigenmodes of the beam uncoupled with the absorber.

## 5.6 Signal processing

The signal processing parameters that have been used are the same for the two configurations (we recall that the observed frequency band is [21, 28] *Hz*). The maximum  $f_{\max}$  of the frequency band of analysis is 256 *Hz*. The sampling frequency is  $f_e = 2 f_{\max} = 512$  *Hz*. The time step is  $\Delta_t = 1/f_e = 0.002$  *s*. The corresponding time sampling is  $t_\alpha = \alpha \Delta_t$  with  $\alpha = 0, 1, \dots, N-1$  in which  $N = 8,192$ . The corresponding time duration is  $T = N\Delta_t = 16$  *s*. The frequency resolution is  $\Delta_f = 1/T = 0.0625$  *Hz*. The corresponding sampling points in the frequency domain are  $f_\beta = -f_{\max} + (\beta + 1/2)\Delta_f$  for  $\beta = 0, 1, \dots, N-1$ . In order to obtain the convergence of the Störmer-Verlet algorithm detailed in Chapter 4, a time oversampling has been used with a factor  $n_s = 10$ . The number of realizations used for estimating the power spectral density functions and the cross-spectral density functions is  $L = 1,000$  that yields good statistical estimations (relative error of 3%).

## 5.7 Quantities of interest

The quantities of interest that are analyzed are similar to those introduced in Section 2.2 and are defined hereinafter. Let  $\{\dot{W}_s(t), t \in [0, T]\}$  be the real-valued stationary stochastic process such that

$$\dot{W}_s(t) = \frac{\partial W}{\partial t}(L_p, t), \quad (5.4)$$

which represents the random  $z$ -velocity of the beam at its end,  $x = L_p$ . The beam is coupled to the nonlinear absorber identified in Chapter 3. The random field  $\{W(x, t), x \in [0, L_p], t \in \mathbb{R}\}$  is the stationary solution constructed with the reduced-order nonlinear stochastic differential equation defined by Eqs. (4.10) and (4.18).

The quantities of interest are  $\pi_{\text{in, norm}}(\omega)$  and  $\text{FRF}^2(\omega)$  defined as follows.

- The normalized frequency-dependent input power density  $\pi_{\text{in, norm}}(\omega)$  of the coupled system (similar to Eq. (2.8)) is defined by

$$\pi_{\text{in, norm}}(\omega) = \frac{S_{F_s \dot{W}_s}(\omega)}{S_{F_s}(\omega)}, \quad (5.5)$$

in which  $S_{F_s \dot{W}_s}$  is the cross-spectral density function of the stationary stochastic processes  $\{F_s(t), t \in \mathbb{R}\}$  and  $\{\dot{W}_s(t), t \in \mathbb{R}\}$ , and where  $S_{F_s}$  is the power spectral density function of stationary stochastic process  $F_s$ , defined by Eq. (5.1).

- The frequency-dependent function  $\text{FRF}^2(\omega)$  is defined by

$$\text{FRF}^2(\omega) = \frac{|S_{\dot{W}_s F_s}(\omega)|^2}{|S_{F_s}(\omega)|^2} = |\pi_{\text{in, norm}}(\omega)|^2. \quad (5.6)$$

These quantities are of interest for the following reasons. The power density balance of the coupled system at frequency  $\omega$  is written as

$$\pi_{\text{in}}(\omega) = \pi_{\text{diss}}([D])(\omega) + \pi_{\text{diss}}([f_D])(\omega), \quad (5.7)$$

in which  $\pi_{\text{in}}(\omega) = S_{F_s \dot{W}_s}(\omega)$  is the input power density of the coupled system,  $\pi_{\text{diss}}([D])(\omega)$  is the power density dissipated by the damping of the beam, calculated by Eq. (4.31), and where  $\pi_{\text{diss}}([f_D])(\omega)$  is the power density dissipated by the damping of the nonlinear absorber, calculated by Eq. (4.37). The power density,  $\pi_{\text{trans}}(\omega)$ , transmitted from the beam to the nonlinear absorber and calculated by Eq. (4.34), is equal to the power density dissipated by the damping of the nonlinear absorber,

$$\pi_{\text{trans}}(\omega) = \pi_{\text{diss}}([f_D])(\omega). \quad (5.8)$$

Equations (5.7) and (5.8) show that the power density input of the coupled system can be rewritten as

$$\pi_{\text{in}}(\omega) = \pi_{\text{diss}}([D])(\omega) + \pi_{\text{trans}}(\omega). \quad (5.9)$$

Consequently, the normalized input power density  $\pi_{\text{in, norm}}(\omega)$ , defined by Eq.(5.5), allows for quantifying the effects of the absorber on the value of the  $z$ -velocity at the end of the beam and, consequently, of the  $z$ -displacement because  $S_{F_s \dot{W}_s}(\omega) = -i\omega S_{F_s W_s}(\omega)$ .

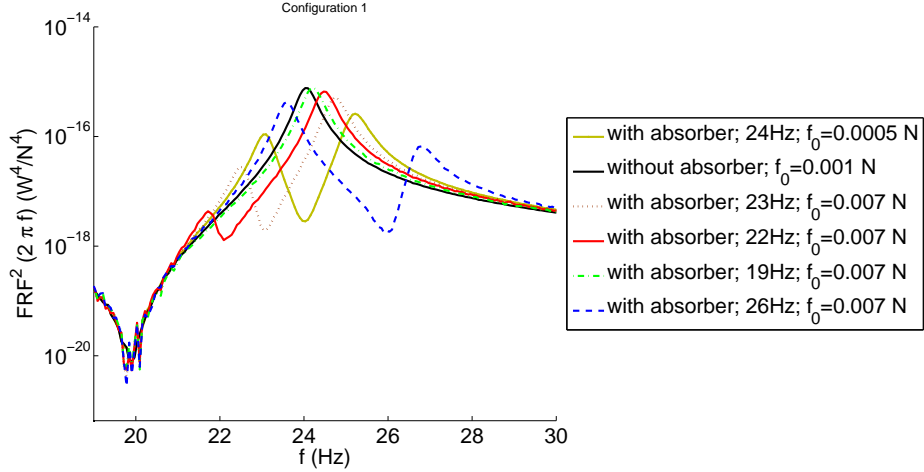


Figure 5.2: First configuration with a linear absorber: graphs of  $f \mapsto \text{FRF}^2(2\pi f)$  on frequency band  $[19, 30]$   $Hz$  centered around the third resonance of the beam. Note that the black thick solid line represents the response of the beam without absorber.

## 5.8 Numerical analysis of the effects of a linear absorber

In this section, we present a numerical analysis of the effects of a linear absorber coupled with a beam in order to evaluate the gain obtained with a nonlinear absorber. This type of linear dynamical analysis and the results obtained are similar for the two configurations. Consequently, this section is limited to an analysis devoted to the first configuration that is to say for a beam with a length  $L_p = 1 m$  and a damping coefficient  $\xi = 0.01$ . For this configuration, the eigenfrequency of the absorber, which is  $24 Hz$ , coincides with the third eigenfrequency of the beam. For such coincidence of the eigenfrequencies, it is known that the resonance of the coupled system localized in the neighborhood of  $24 Hz$  is split into two close resonances. Consequently, we have performed a parametric analysis with respect to the stiffness of the absorber in order that its eigenfrequency belongs to the set  $\{19, 22, 23, 24, 26\} Hz$ . The numerical results obtained for  $\text{FRF}^2$  defined by Eq. (5.6) are displayed in Figure 5.2 on the one hand for the beam without absorber and on the other hand for the beam coupled with a linear absorber. It should be noted that  $\text{FRF}^2$  is independent of the amplitude  $f_0$  because the coupled dynamical system is linear and  $\text{FRF}^2$  is normalized with respect to the excitation. As previously explained, when the eigenfrequency of the absorber is  $24 Hz$ , it can be seen that the unique resonance of the beam without absorber (at  $24 Hz$ ) is, for the beam coupled with the absorber, split into two resonances at  $23.03 Hz$  and  $25.22 Hz$ . When the eigenfrequency of the absorber is  $19, 22, 23,$  and  $24 Hz$ , the corresponding right resonance moves to  $24.22, 24.53, 24.78,$  and  $25.22 Hz$  respectively, that is to say the frequency of the right resonance increases with the eigenfrequency of the absorber. In the same time, the left resonance vanishes for  $19 Hz$  and moves

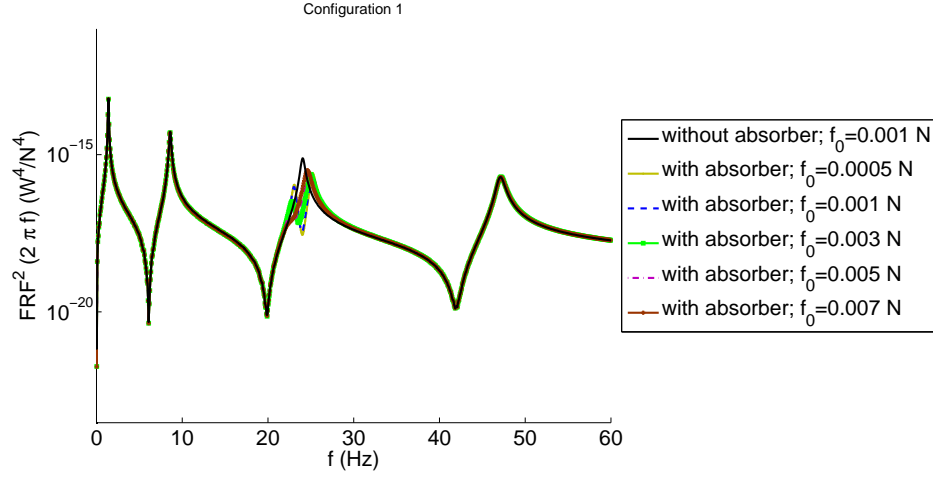
to 21.72, 22.53, and 23.03  $Hz$  respectively. When only one resonance appears for the coupled system (eigenfrequency of the absorber at 19  $Hz$ ), there is no gain concerning the attenuation of the amplitude of the response of the beam coupled with the linear absorber. When two resonances occur, the amplitude of each resonances is smaller than the amplitude of the unique resonance of the beam without absorber (the energy is shared between the two resonances), but, unfortunately, two resonances appear instead of one. This situation does not correspond to the one specified in the objective of this research, as explained in Chapter 1, because we want to increase the bandwidth of the effects of the absorber for killing the resonances and thus we do not want to introduce new resonances in the responses. In Section 5.9, it is shown that the difficulty can be circumvented with a nonlinear absorber, that is to say not splitting the resonance into two resonances and decreasing the amplitude of the resonance obtained in presence of the nonlinear absorber.

## 5.9 Numerical results and analysis for the beam coupled with a nonlinear absorber

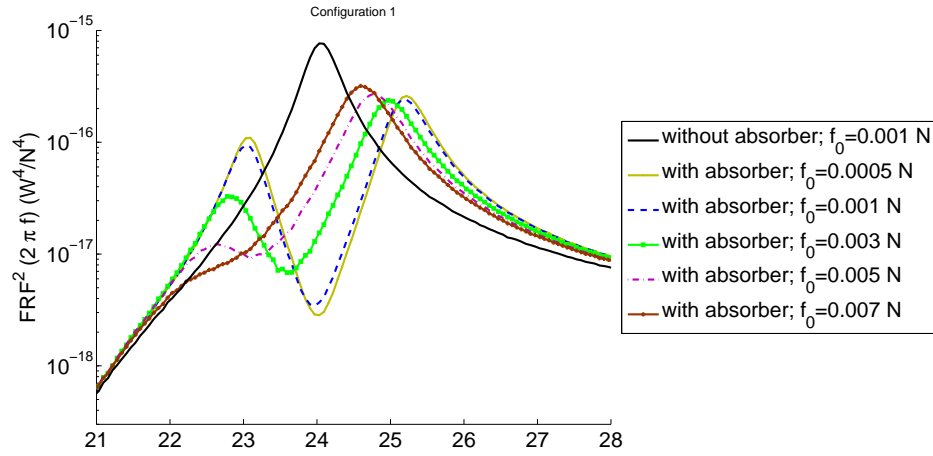
In this section, we present the numerical results that have been obtained for the two studied configurations for which the quantities of interest defined by Eqs. (5.6) and (5.5) are computed and analyzed.

Concerning the first configuration, for each one of considered amplitudes  $f_0$  of the excitation, Figure 5.3 displays the graphs of function  $f \mapsto \text{FRF}^2(2\pi f)$ . In Figure 5.3(a),  $\text{FRF}^2$  is depicted on frequency band  $[0, 60]$   $Hz$  that contains the first four eigenfrequencies of the beam. It can be seen, as expected, that the nonlinear absorber has only an effect on the third eigenfrequency, 24  $Hz$ , and has no effects on the other eigenfrequencies, 1.37, 8.57, and 47.05  $Hz$ . In Figure 5.3(b),  $\text{FRF}^2$  is depicted on frequency band  $[21, 28]$   $Hz$  centered around the third resonance of the beam. It can be seen that the response of the beam is influenced by the presence of the nonlinear absorber. Since the beam without absorber has a linear behavior, the  $\text{FRF}^2$  function is independent of  $f_0$ . Consequently, the graph (without absorber) displayed for  $f_0 = 0.001 N$  does not change for the other values of  $f_0$ . For the beam coupled to the nonlinear absorber, if the value of amplitude  $f_0$  of the excitation is small ( $f_0 = 0.0005 N$  and  $f_0 = 0.001 N$ ), then the absorber has almost the same effect as a linear absorber, and induces a splitting of the resonance as explained in Section 5.8. When amplitude  $f_0$  of the excitation is higher,  $f_0 = 0.005 N$  and  $f_0 = 0.007 N$ , the absorber has a nonlinear behavior and there is only one resonance in the response, as expected. In addition, and above all, it can be seen that the amplitude of the resonance is lower when the nonlinear absorber is present than when the absorber is absent, which was the main expected effect. For  $f_0 = 0.007 N$ , the attenuation factor is 2.4 for the normalized quantity of interest. Certainly, the attenuation could be larger in coupling the beam to several absorbers and it will then be proportional to the number of absorbers.

Figure 5.4 displays the normalized input power density  $f \mapsto \pi_{\text{in, norm}}(2\pi f)$  that is



(a)



(b)

Figure 5.3: First configuration with a nonlinear absorber: for the different values of the considered amplitude, graphs of  $f \mapsto \text{FRF}^2(2\pi f)$  on frequency band  $[0, 60] \text{ Hz}$  (Figure (a)) and on frequency band  $[21, 28] \text{ Hz}$  centered around the third resonance of the beam (Figure (b)). Note that the black thick solid line represents the response of the beam without absorber.

associated with  $\text{FRF}^2$  displayed in Figure 5.3. The conclusions are then the same.

For the second configuration, the analysis, which is performed for the beam coupled with the nonlinear absorber, is similar to the one done for the first configuration. The difference is that, now, the eigenfrequency of the absorber coincides with the fundamental frequency (the first eigenfrequency) of the beam without absorber. For each one of the considered amplitudes  $f_0$  of the excitation, function  $f \mapsto \text{FRF}^2(2\pi f)$ , defined by Eq. (5.6), is displayed in Figure 5.5. As previously, this function is represented on the frequency band of analysis,

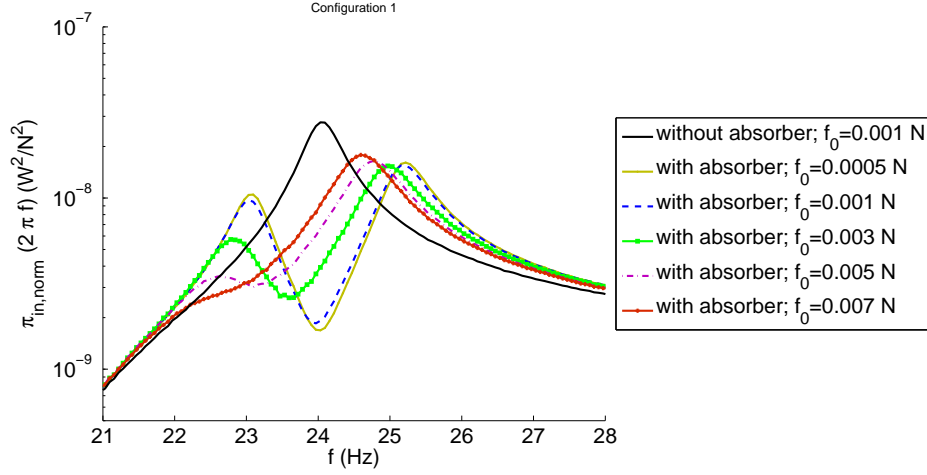


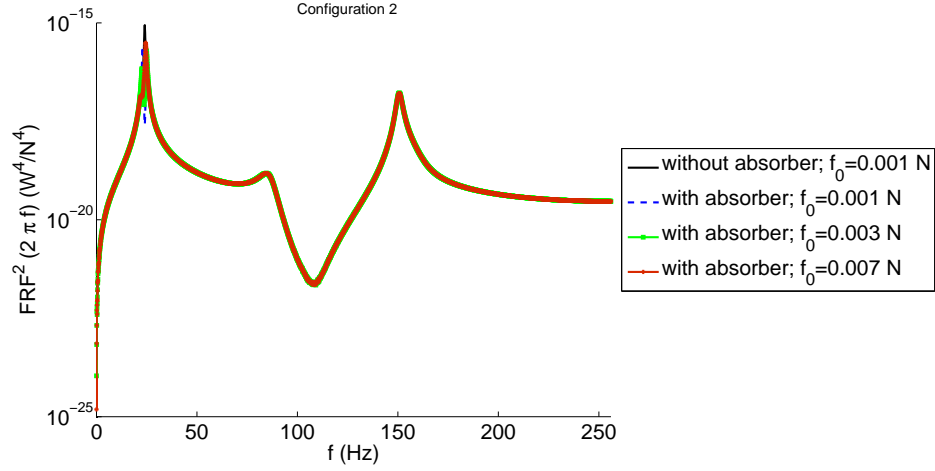
Figure 5.4: First configuration without and with absorber: for the different values of the considered amplitude, graphs of  $f \mapsto \pi_{in, norm}(2\pi f)$  on frequency band  $[21, 28]$  Hz centered around the third resonance of the beam. Note that the black thick solid line represents the response of the beam without absorber.

$[0, 256]$  Hz and on the frequency band  $[21, 28]$  Hz approximately centered around 24 Hz.

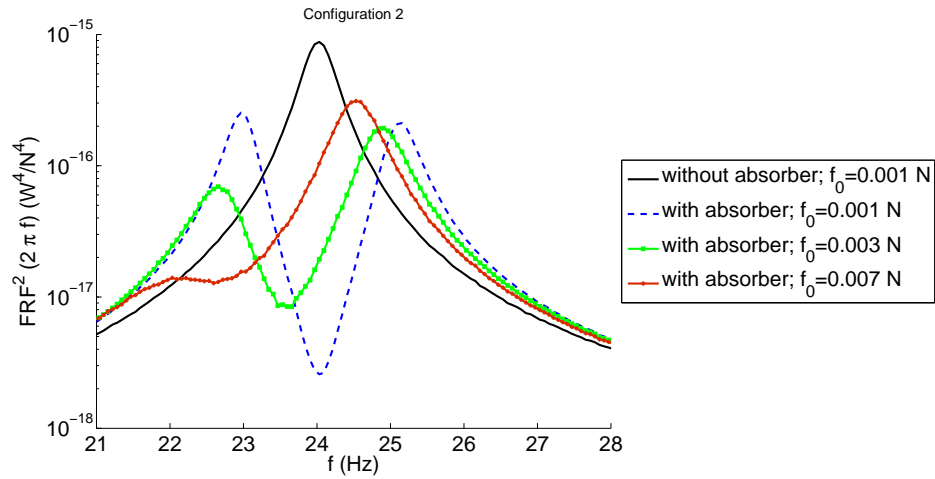
Figure 5.5(a) displays the graphs of function  $FRF^2$  on the frequency band  $[0, 256]$  Hz. The first two eigenfrequencies, 23.99 Hz and 150.36 Hz, of the beam without absorber belong to this frequency band. As it can be seen, the presence of the nonlinear absorber on the beam has only an effect on the first eigenfrequency, 23.99 Hz. Figure 5.5(b) displays function  $FRF^2$  on the frequency band  $[21, 28]$  Hz. The same observations as those carried out for the first configuration can be done.

- The absorber needs a sufficiently large amplitude  $f_0$  of excitation to have a nonlinear behavior, that is to say a nonlinear effect.
- When amplitude  $f_0$  of excitation is not large enough, the absorber has a linear behavior similarly to the first configuration, and the resonance of the beam without absorber is split into two separated resonances when the beam is coupled with the absorber.
- The amplitude at the resonance of the beam is smaller in present of the nonlinear absorber. For instance, for an amplitude of excitation  $f_0 = 0.007 N$ , the gain factor for the attenuation is 2.82. Similarly to the explanations given for the first configuration, this gain factor could be improved in increasing the number of nonlinear absorbers. Note that the gain factor is lightly larger for configuration 2 (attenuation of the fundamental eigenfrequency) than for configuration 1 (attenuation of the third eigenfrequency).

Figure 5.6 displays the normalized input power density  $\pi_{in, norm}$ , defined in Eq. (5.5). The conclusions are the same.



(a)



(b)

Figure 5.5: Second configuration without and with absorber: for the different values of the considered amplitude, graphs of  $f \mapsto \text{FRF}^2(2\pi f)$  on frequency band  $[0, f_{\max}]$  Hz (Figure (a)) and on frequency band  $[21, 28]$  Hz centered around the first resonance of the beam (Figure (b)). Note that the black thick solid line represents the response of the beam without absorber.

## 5.10 Conclusion

In this chapter, a numerical simulation of absorber effects on the dynamical behavior of two configurations of an elastic beam has been presented. The numerical simulation is based on the stochastic model presented in Chapter 4. The nonlinear absorber is the one designed, experimentally analyzed, modeled, and identified in Chapters 2 and 3. This nonlinear absorber, modeled by a one-DOF nonlinear oscillator with nonlinear stiffness and nonlinear damping, has a nonlinear behavior for large displacements. This nonlinear absorber has been

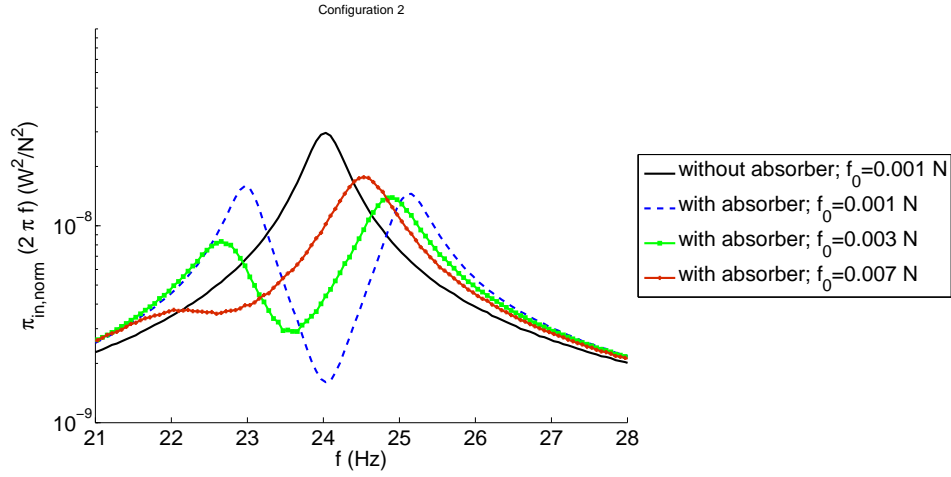


Figure 5.6: Second configuration without and with absorber: for the different values of the considered amplitude, graphs of  $f \mapsto \pi_{in, norm}(2\pi f)$  on frequency band  $[21, 28]$  Hz centered around the first resonance of the beam. Note that the black thick solid line represents the response of the beam without absorber.

fixed at the free end of a cantilever beam for two configurations. These beams have been designed in order that the third eigenfrequency of the first one and the first eigenfrequency of the second one coincide with the eigenfrequency of the nonlinear absorber. For each one of the two configurations, several amplitudes of excitation have been imposed to the beam with and without absorber. It has been shown that the nonlinear absorber has the expected attenuation on the response of the beam while the linear absorber induces difficulties (splitting a unique resonance into two separated resonances or keeping a unique resonance without reducing the amplitude of the response).



## Chapter 6

# Conclusions and Perspectives

### 6.1 Summary

For a very long time, the reduction of noise and vibration is an important concern in the field of research and industry. Although this attenuation is properly managed at middle and high frequencies for which poroelastic dissipative materials are efficient, its remains more difficult at low frequencies. The work performed in this thesis has been developed in the framework of the reduction of vibration at macro-scale at low frequencies for which the first structural modes are excited. The main objective of this thesis, that has been achieved, was to develop a nonlinear absorber, in order to attenuate the vibration at low frequencies, both experimentally, and with modeling and simulations.

As an introduction of this work, a non-exhaustive bibliographical summary on reduction of vibration at low, middle, and high frequencies and with linear and nonlinear devices has been presented. This state of the art has helped position our objectives in relation with the already existing work. We have chosen to study an absorber having a nonlinear dynamical behavior due to nonlinear geometrical effects, in order to pump the energy over a broader frequency band around its resonance frequency than a linear absorber. For that, the first step has been to develop a nonlinear model of the absorber and its related stochastic solver. We have proposed to model the nonlinear dynamical behavior of the absorber by a nonlinear oscillator with one-DOF that is excited by a stochastic force at its base. The oscillator is composed by a mass, a nonlinear spring, and a nonlinear damper. The construction of the nonlinear forces associated with the spring and the damper is based on the linear viscoelasticity theory in finite displacements. The stochastic solver is based on the Monte Carlo method and the Störmer-Verlet integration scheme is used. In order to define the design for the experiments, we have performed some tests for several experimental configurations in order to select the best technology for the nonlinear absorber under some constraints imposed by the manufacturing. Finally, we have chosen a nonlinear absorber constituted of a cantilever beam with a point mass at its free end. This absorber has been printed, in ABS, in a single piece with its support, using a 3D-printing system. Experiments in dynamics of this nonlin-

ear absorber have been performed in order to analyze its nonlinear behavior. Then, an experimental identification of the nonlinear mechanical model has been carried out. Concerning the experimental procedure, the support of the absorber has been fixed to a shaker. The results obtained have made it possible to identify the model and have put forward the fact that this nonlinear absorber induces an attenuation on a broader frequency band around its resonance frequency than a linear absorber. Once the nonlinear absorber has been identified, we have analyzed its attenuation capability on vibrations of a continuous system made up of a damped elastic beam. A complete mechanical model of the nonlinear coupled system has been developed and a reduced-order model has been constructed using the eigenmodes of the beam without absorber. A stochastic solver related to the model has been provided. An analysis of two configurations of the beam with the nonlinear absorber has been performed by numerical simulations. For the first configuration, the beam is designed in order that its third eigenfrequency coincides with the eigenfrequency of the absorber while for the second configuration, it is its first eigenfrequency that coincides with the eigenfrequency of the absorber. The introduction of these two configurations has been done in order to analyze the attenuation gain obtained as a function of the rank of the beam resonances. The analysis of the numerical results has led to several conclusions. The presence of the nonlinear absorber on the beam allows an attenuation of its response to be obtained without splitting the resonance into two separated resonances. It has been shown that the gain is lightly larger for the fundamental frequency of the beam than for its third eigenfrequency. For the nonlinear absorber that has been designed and manufactured, the nonlinear effects are significant if the amplitude of the response is sufficiently large. As expected, the nonlinear absorber is more efficient than a linear absorber under the hypothesis that no additional resonances must occur in the coupled system due to the presence of the absorber.

## 6.2 Perspectives

The first perspective would consist in developing an experiment for testing the attenuation generated by several absorbers on a continuous system such as the beam presented in Chapter 4. In such experiment, the technology of each absorber could be improved in order to decrease its damping rate. Note that when the damping of the absorber decreases, the amplitude of the vibration of the absorber increases and consequently, the mechanical energy transfer to the absorber is larger and thus, the attenuation effect is larger.

The second perspective would consist in developing the design of a set of nonlinear absorbers randomly distributed in a composite panel in order to attenuate the vibration. A model and an experiment should be developed.

## 6.3 Scientific production

The work achieved in this thesis has brought forward publications and communications, which are listed hereinafter.

### Journal publications

- Communication in Nonlinear Science and Numerical Simulations. Paper submitted in September 2017.

### Conferences with proceedings

- D. Lavazec, G. Cumunel, D. Duhamel, C. Soize, A. Batou, Métamatériau microstructuré non linéaire pour l'atténuation du bruit et des vibrations en basses fréquences, in: 13ème Congrès Français d'Acoustique et 20ème colloque Vibrations, SHocks and NOise (CFA-VISHNO), Le Mans, France, 11-15 avril 2016, Actes de la conférence, 2016, pp. 1-7. (ref. [79]).
- D. Lavazec, G. Cumunel, D. Duhamel, C. Soize, A. Batou, Nonlinear microstructured material to reduce noise and vibrations at low frequencies, in: Joint International Conference on Motion and Vibration Control and Recent Advances in Structural Dynamics, Proceedings of MoVIC and RASD 2016, Southampton, United Kingdom, July 6-7 2016, 2016, pp. 1-10. (ref.[80]).
- D. Lavazec, G. Cumunel, D. Duhamel, C. Soize, A. Batou, Attenuation of noise and vibration at low frequencies using a nonlinear microstructured material, in: International Conference on Noise and Vibration Engineering, Proceedings of ISMA 2016, Leuven, Belgium September 19-21 2016, 2016, pp. 1-11. (ref.[81]).
- D. Lavazec, G. Cumunel, D. Duhamel, C. Soize, Attenuation of acoustic waves and mechanical vibrations at low frequencies by a nonlinear dynamical absorber, in: CFM 2017, Lille, August 28, September 1 2017. Proceedings of CFM 2017, 2017, pp. 1-12. (ref.[82]).

### Conferences without proceedings

- D. Lavazec, G. Cumunel, D. Duhamel, C. Soize, Attenuation of acoustic waves and mechanical vibrations at low frequencies by a nonlinear dynamical absorber, in: USNCCM 2017, 14th U. S. National Congress on Computational Mechanics, Montreal, Canada, July 17 - 20 2017, 2017. (ref.[83]).



# Appendix A

## Qualitative effects of stiffness, damping, and shape on the nonlinear behavior of an absorber

### A.1 Qualitative effects of stiffness and damping on the power density of a nonlinear oscillator

In this section, we present a study of effects of the stiffness and the damping on the power transmitted to a nonlinear oscillator with nonlinear stiffness and linear damping.

For that, we have defined nine different elastic forces, noted  $\Phi'_i(x)$ ,  $i = 0, 1, \dots, 8$ , for which the graphs  $x \mapsto \Phi'_i(x)$  are plotted in Figure A.1, such that,

$$\begin{aligned}\Phi'_0(x) &= 100x , \\ \Phi'_i(x) &= a_i \operatorname{sgn}(x)x^2 + b_i x \quad , \quad i = 1, \dots, 4 , \\ \Phi'_i(x) &= a_i \operatorname{sgn}(x) \left( 1 - \frac{1}{(1 + b_i \operatorname{sgn}(x)x)^2} \right) \quad , \quad i = 5, \dots, 8 ,\end{aligned}\tag{A.1}$$

where  $x \mapsto \operatorname{sgn}(x)$  is the sign function such that

$$\operatorname{sgn}(x) = \begin{cases} -1 & \text{if } x < 0 \\ 0 & \text{if } x = 0 \\ 1 & \text{if } x > 0 \end{cases}\tag{A.2}$$

and where the parameters  $a_i$  and  $b_i$  are given in the Table A.1.

With this notation, Eq. (2.1) is rewritten, with a linear damping, as

$$m\ddot{X}_s(t) + c_1\dot{X}_s(t) + \Phi'_i(x) = F_s(t) ,\tag{A.3}$$

in which  $f_K(x) = \Phi'_i(x)$  and where  $m = 0.0329 \text{ kg}$ ,  $c_1 = 2\xi\sqrt{100m}$  (the value of  $\xi$  is given below), and the Gaussian, stationary, centered process  $\{F_s(t), t \in \mathbb{R}\}$

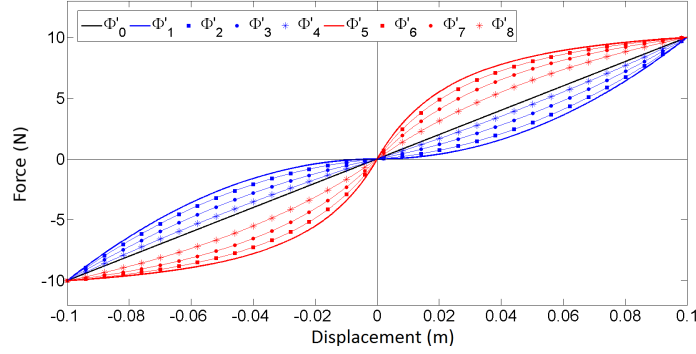


Figure A.1: For  $i = 0, 1, \dots, 8$ , graph of  $x \mapsto \Phi'_i(x)$  giving the elastic force as a function of the displacement  $x$ .

$i$	1	2	3	4	5	6	7	8
$a_i$	1000	800	500	200	45/5	250/21	40/3	45
$b_i$	0	20	50	80	20	15	10	5

Table A.1: Parameters for the models of the elastic forces.

is defined by its power spectral density function  $S_{F_s}(\omega)$  such that

$$S_{F_s}(\omega) = \begin{cases} 1 & \text{for } \omega \in [-100, -10] \cup [10, 100] \text{ rad/s} , \\ 0 & \text{otherwise} . \end{cases} \quad (\text{A.4})$$

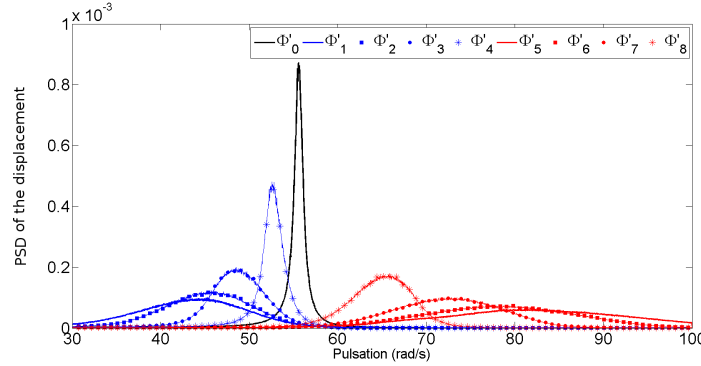


Figure A.2: Power spectral density function  $S_{X_s}(\omega)$  of the displacement for each elastic forces with  $\xi = 0.01$ .

The elastic force  $\Phi'_0$  is linear, the elastic forces  $\Phi'_1, \Phi'_2, \Phi'_3, \Phi'_4$  are nonlinear with stiffening behavior, and the elastic forces  $\Phi'_5, \Phi'_6, \Phi'_7, \Phi'_8$  are nonlinear with softening behavior.

Figure A.2 displays the power spectral density function  $S_{X_s}(\omega)$  of stochastic displacement  $X_s$  for each elastic forces with  $\xi = 0.01$ . It can be seen that there

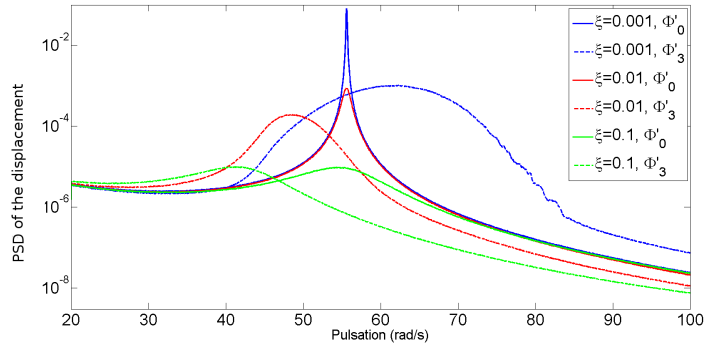


Figure A.3: Power spectral density function  $S_{X_s}(\omega)$  of the stochastic displacement for the elastic forces  $\Phi'_0$  and  $\Phi'_3$  with three different values of damping.

are no consequences on the amplitude of the displacement of the absorber for a softening or a hardening stiffness. Figure A.3 illustrates the power spectral density function of displacement  $X_s$  for two elastic forces ( $\Phi'_0$  and  $\Phi'_3$ ) and for three values of damping ratio ( $\xi = 0.1$ ,  $\xi = 0.01$ , and  $\xi = 0.001$ ). It can be seen that it is better to have the lowest damping possible in order to the resonance response of the absorber occurs on a broad frequency band. The energy of the excitation is thus transferred to the absorber on a broad frequency band.

## A.2 Qualitative effects of the shape of the absorber on its nonlinear behavior

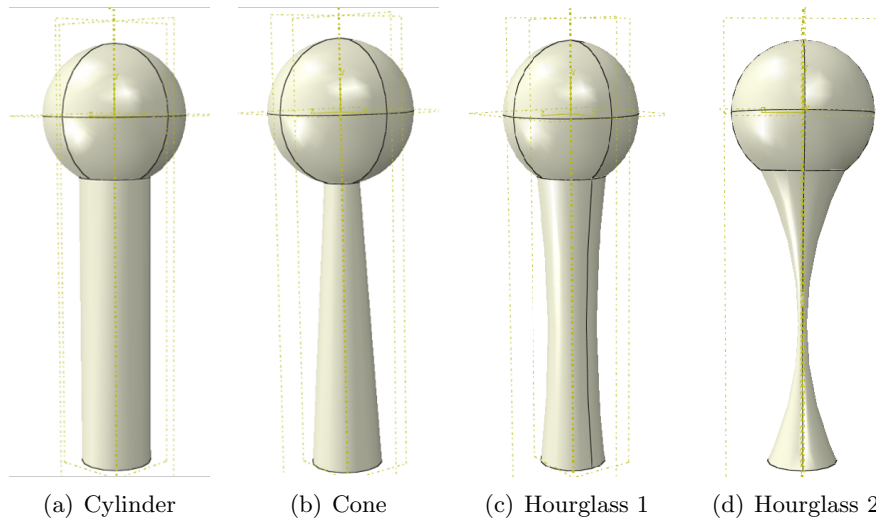


Figure A.4: Shapes of absorbers that have been modeled in 3D using Abaqus software.

In this section, a primary numerical study is presented for analyzing the qualitative effect of the shape of an absorber on its nonlinear behavior. The absorber is composed of a cantilever beam with a mass located at its end. Four shapes of the cantilever beam are modeled in 3D using Abaqus software (see Figure A.4). For each one, the spherical mass is made of lead (Young modulus of  $16,700 \text{ MPa}$ , Poisson coefficient of  $0.44$ , mass density of  $11,350 \text{ kg/m}^3$ ) and have a diameter of  $5 \times 10^{-3} \text{ m}$ , and the cantilever beam is made of Acrylonitrile Butadiene Styrene (ABS) (Young modulus of  $2 \text{ GPa}$ , Poisson coefficient of  $0.35$ , mass density of  $1,100 \text{ kg/m}^3$ ) and have a length of  $10^{-2} \text{ m}$  and a maximal diameter of  $2.5 \times 10^{-3} \text{ m}$ . A force is imposed on the mass and the maximal displacement of the mass is calculated with Abaqus software. In Figure A.5, the equivalent static stiffness computed for each of the four absorbers is displayed. As we can see, the shape of the cantilever beam can have an important influence of the nonlinear stiffness of the absorber.

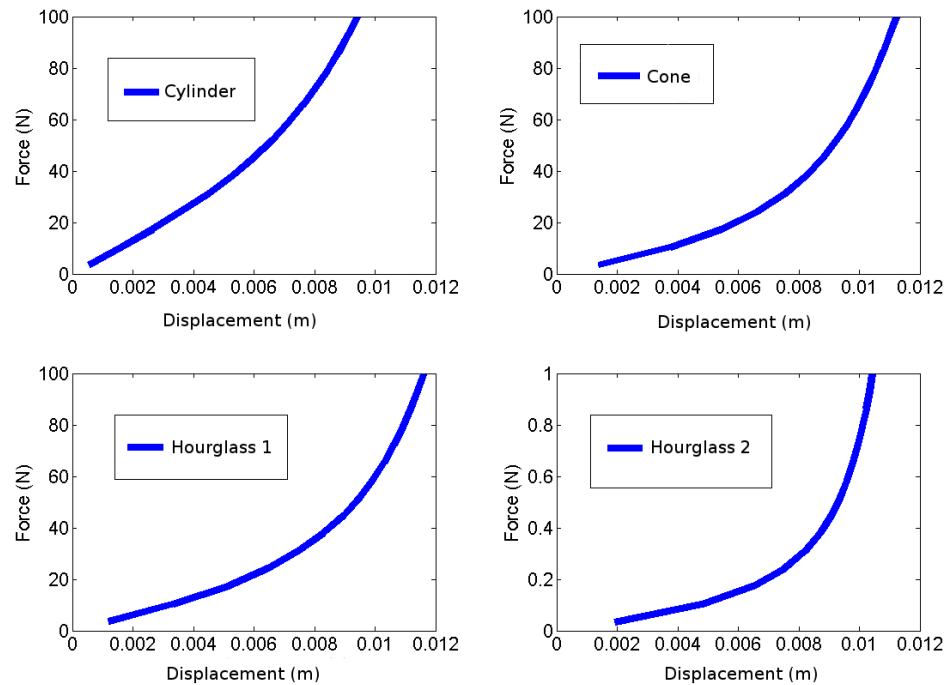


Figure A.5: Force imposed on the mass as a function of the displacement of this mass for each of the four shapes displayed in Figure A.4.

## Appendix B

# Parametric study on the dimension of the beams that compose the absorber

In this appendix, we consider an absorber composed of two beams clamped at one end and fixed to a spherical mass at the other end. For this type of absorber design, we present a parametric study on the dimensions of the two beams, which can be different. In the following, the first beam, named “left beam”, is embedded at its left end and is fixed to a spherical mass at its right end. The diameter of its left end is denoted by D.L.L and the diameter of its right end by D.R.L. In the same way, the second beam, named “right beam”, is fixed to the same spherical mass at its left end and is embedded at its right end. The diameter of its left end is denoted by D.L.R and the diameter of its right end by D.R.R. The notations used are summarized in Figure B.1 for a better understanding. These two beams are cylinders or cones.

For each case, the diameter of the spherical mass is  $6 \times 10^{-3} m$ , the length of the left beam is  $10.5 \times 10^{-3} m$ , and the length of the right beam is  $3.5 \times 10^{-3} m$ . The beams and the spherical mass are made of steel. Nine cases have been studied, their parameters are displayed in Table B.1 and their different designs are illustrated in Figure B.2. The results show that the shape of the two beams have a big impact on the nonlinear behavior of the system composed by the two beams and the spherical mass.

A parametric study is realized on Abaqus for each of the eight designs. A force is applied at the center of the mass in one direction. The maximum displacement of the mass in the direction of excitation is calculated. The results are displayed in Figure B.3. As we can see, the design of the beams can have an important effect on the nonlinear behavior of the absorber.

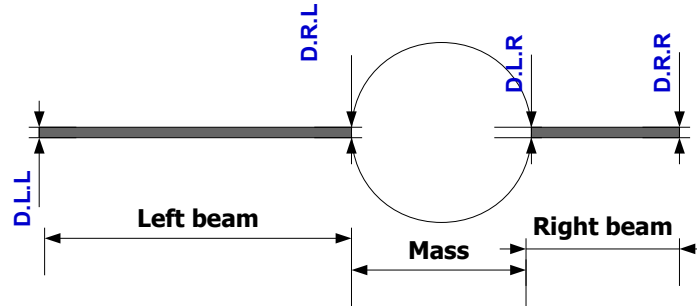


Figure B.1: Scheme of two beams clamped at one end and fixed to a mass at the other one. The diameter of the left end of the left beam is noted D.L.L, the diameter of the right end of the left beam is noted D.R.L., the diameter of the left end of the right beam is noted D.L.R, and the diameter of the right end of the right beam is noted D.R.R.

Design	1	2	3	4	5	6	7	8
Shape of the left beam	Cy	Cy	Co	Co	Co	Co	Co	Co
D.L.L ( $\times 10^{-3} m$ )	0.4	0.2	0.8	0.4	0.4	0.4	0.1	0.1
D.R.L ( $\times 10^{-3} m$ )	0.4	0.2	0.2	0.1	0.1	0.1	0.4	0.4
Shape of the right beam	Cy	Cy	Cy	Cy	Co	Co	Co	Co
D.L.R ( $\times 10^{-3} m$ )	0.8	0.4	0.4	0.4	0.1	0.4	0.1	0.4
D.R.R ( $\times 10^{-3} m$ )	0.8	0.4	0.4	0.4	0.4	0.1	0.4	0.1

Table B.1: Parameters of the two beams studied for each one of the eight designs. “Cy” means cylinder and “Co” means cone.

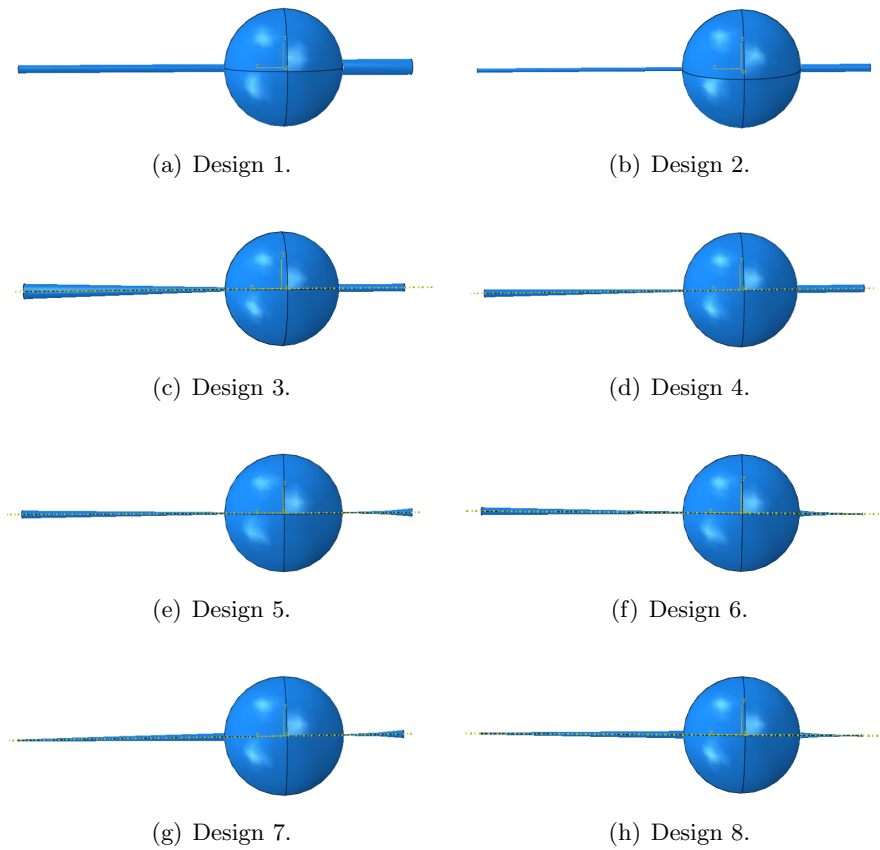


Figure B.2: Different designs of beams bi-clamped with a spherical mass located on them.

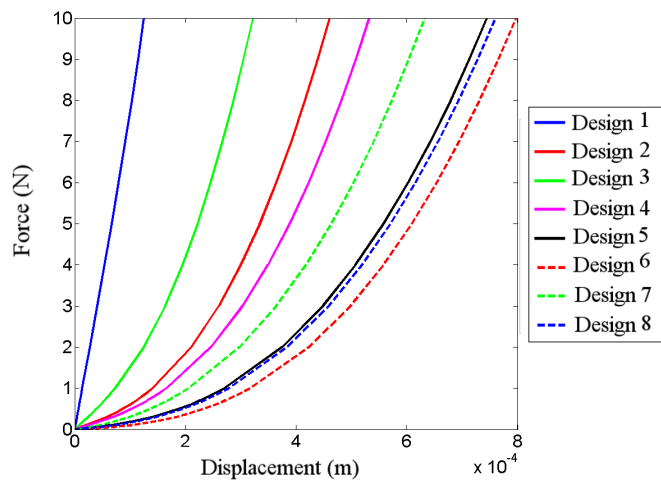


Figure B.3: Force applied at the center of the spherical mass as a function of the maximum displacement of the spherical mass in the same direction that the excitation for each one of the eight designs.



# Bibliography

- [1] G. W. Housner, L. A. Bergman, A. G. Chassiaskos, R. O. Claus, S. F. Marsi, R. E. Skelton, T. T. Soong, B. F. Spencer, J. T. P. Yao, Structural control: past, present and future, *Journal of Engineering Mechanics* 123(9) (1997) 897–971.
- [2] M. J. Crocker, *Handbook of Noise and Vibration Control*, John Wiley & Sons, 2007.
- [3] D. Del Vescovo, I. Giorgio, Dynamic problems for metamaterials: Review of existing models and ideas for further research, *International Journal of Engineering Science* 80 (2014) 153–172.
- [4] R. E. Roberson, Synthesis of a nonlinear dynamic vibration absorber, Portions of a dissertation submitted to the Department of Applied Mechanics, Washington University, in partial fulfillment of the requirements for the degree of Doctor of Philosophy. (1952) 205–220.
- [5] R. Bouc, The power-spectral density of response for a strongly non-linear random oscillator, *Journal of Sound and Vibration* 175 (1999) 317–331.
- [6] C. Soize, Stochastic linearization method with random parameters for SDOF nonlinear dynamical systems: Prediction and identification procedures, *Probabilistic Engineering Mechanics* 10(3) (1995) 143–152.
- [7] S. Bellizzi, R. Bouc, Analysis of multi-degree of freedom strongly non-linear systems with random input, *Probabilistic Engineering Mechanics* 14 (1999) 245–256.
- [8] P. Spanos, I. Kougioumtzoglou, C. Soize, On the determination of the power spectrum of randomly excited oscillators via stochastic averaging: An alternative perspective, *Probabilistic Engineering Mechanics* 26 (2011) 10–15.
- [9] A. Lazarus, O. Thomas, J. F. Deü, Finite element reduced order models for nonlinear vibrations of piezoelectric layered beams with applications to NEMS, *Finite Elements in Analysis and Design* 49 (2012) 35–51.
- [10] W. Larbi, J. F. Deü, R. Ohayon, Finite element reduced order model for noise and vibration reduction of double sandwich panels using shunted piezoelectric patches, *Applied Acoustics* 108 (2016) 40–49.

- [11] O. Thomas, J. Ducarne, J.-F. Deü, Performance of piezoelectric shunts for vibration reduction, *Smart Materials and Structures* 21 (2012) 15008–15021.
- [12] T. Bailey, E. J. Hubbard, Distributed piezoelectric-polymer active vibration control of a cantilever beam, *Journal of Guidance, Control, and Dynamics* 8 (1985) 605–611.
- [13] C. Fuller, S. Elliott, P. Nelson, *Active Control of Vibration*, Academic Press, London, 1996.
- [14] A. Preumont, *Active Control of Vibration*, Third Edition, Springer, Berlin, 2011.
- [15] O. Abdeljaber, O. Avci, D. J. Inman, Active vibration control of flexible cantilever plates using piezoelectric materials and artificial neural networks, *Journal of Sound and Vibration* 363 (2016) 33–53.
- [16] S. Nacivet, C. Pierre, F. Thouverez, L. Jezequel, A dynamic Lagrangian frequency-time method for the vibration of dry-friction-damped systems, *Journal of Sound and Vibration* 265 (2003) 201–219.
- [17] J. F. Allard, N. Atalla, *Propagation of Sound in Porous Media: Modelling Sound Absorbing Materials*, John Wiley & Sons, 2009.
- [18] H. Frahm, Device for damping vibrations of bodies, United states patent office 989.958 (1911) 1–9.
- [19] M. Gutierrez Soto, H. Adeli, Tuned mass dampers, *Archives of Computational Methods in Engineering* 20(4) (2013) 419–431.
- [20] M. Alster, Improved calculation of resonant frequencies of helmholtz resonators, *Journal of Sound and Vibration* 24 (1972) 63–85.
- [21] R. C. Chanaud, Effects of Geometry on the Resonance Frequency of Helmholtz Resonators, *Journal of Sound and Vibration* 178 (3) (1994) 337–348.
- [22] J. M. De Bebout, M. A. Franchek, R. J. Bernhard, L. Mongeau, Adaptive-passive Noise Control with Self-tuning Helmholtz resonators, *Journal of Sound and Vibration* 202 (1997) 109–123.
- [23] S. J. Estève, Control of sound transmission into payload fairings using distributed vibration absorbers and Helmholtz resonators, Ph.D. thesis, Faculty of the Virginia Polytechnic Institute (2004).
- [24] S. J. Esteve, M. E. Johnson, Adaptive Helmholtz resonators and passive vibration absorbers for cylinder interior noise control, *Journal of Sound and Vibration* 288 (2005) 1105–1130.
- [25] H. D. Nam, S. J. Elliott, Adaptive Active Attenuation of Noise Using Multiple Model Approaches, *Mechanical Systems and Signal Processing* 9 (1995) 555–567.

- [26] S. Nagarajaiah, M. Asce, E. Sonmez, Structures with Semiactive Variable Stiffness Single/Multiple Tuned Mass Dampers, *Journal of Structural Engineering* 133(1) (2007) 67–77.
- [27] V. G. Veselago, The electrodynamics of substances with simultaneously negative values of  $\epsilon$  and  $\mu$ , *Soviet Physics* 10 (1968) 509–514.
- [28] D. Smith, N. Kroll, Negative refractive index in left-handed materials, *Physical Review Letters* 85 (2000) 2933–2936.
- [29] K. Xu, T. Igusa, Dynamic characteristics of multiple substructures with closely spaced frequencies, *Earthquake Engineering & Structural Dynamics* 21(12) (1992) 1059–1070.
- [30] N. Fang, D. Xi, J. Xu, M. Ambati, W. Srituravanich, C. Sun, X. Zhang, Ultrasonic metamaterials with negative modulus, *Nature materials* 5(6) (2006) 452–456.
- [31] X. Liu, G. Hu, G. Huang, C. Sun, An elastic metamaterial with simultaneously negative mass density and bulk modulus, *Applied Physics Letters* 98 (2011) 251907.
- [32] R. Zhu, X. Liu, G. Hu, C. Sun, G. Huang, A chiral elastic metamaterial beam for broadband vibration suppression, *Journal of Sound and Vibration* 333 (2014) 2759–2773.
- [33] J. Chen, B. Sharma, C. Sun, Dynamic behaviour of sandwich structure containing spring-mass resonators, *Composite Structures* 93(8) (2011) 2120–2125.
- [34] T. P. Bandivadekar, R. S. Jangid, Mass distribution of multiple tuned mass dampers for vibration control of structures, *International Journal of Civil and Structural Engineering* 3(1) (2012) 70–84.
- [35] Y. Xiao, J. Wen, X. Wen, Sound transmission loss of metamaterial-based thin plates with multiple subwavelength arrays of attached resonators, *Journal of Sound and Vibration* 331 (2012) 5408–5423.
- [36] X. Wang, Dynamic behaviour of a metamaterial system with negative mass and modulus, *International Journal of Solids and Structures* 51 (2014) 1534–1541.
- [37] P. Pai, H. Peng, S. Jiang, Acoustic metamaterial beams based on multi-frequency vibration absorbers, *International Journal of Mechanical Sciences* 79 (2014) 195–205.
- [38] P. Sheng, X. Zhang, Z. Liu, C. Chan, Locally resonant sonic materials, *Physica B: Condensed Matter* 338 (2003) 201–205.
- [39] C. R. Fuller, R. L. Harne, Advanced Passive Treatment of Low Frequency Sound and Vibration, in: Australian Acoustical Society, 2009, pp. 1–7.

- [40] S. Varanasi, J. Bolton, T. Siegmund, R. Cipra, The low frequency performance of metamaterial barriers based on cellular structures, *Applied Acoustics* 74 (2013) 485–495.
- [41] P. Sheng, J. Mei, Z. Liu, W. Wen, Dynamic mass density and acoustic metamaterials, *Physica B* 394 (2007) 256–261.
- [42] Y. Ding, Z. Liu, C. Qiu, J. Shi, Metamaterial with simultaneously negative bulk modulus and mass density, *Physical Review Letters* 99 (2007) 093904.
- [43] Z. Yang, J. Mei, M. Yang, N. Chan, P. Sheng, Membrane-type acoustic metamaterial with negative dynamic mass, *Physical Review Letters* 101(20) (2008) 204301.
- [44] S. Lee, C. Park, Y. Seo, Z. Wang, C. Kim, Acoustic metamaterial with negative density, *Physics Letters A* 373 (2009) 4464–4469.
- [45] X. Zhou, G. Hu, Analytic model of elastic metamaterials with local resonances, *Physical Review B* 79 (2009) 195109.
- [46] Z. Yang, H. Dai, N. Chan, G. Ma, P. Sheng, Acoustic metamaterial panels for sound attenuation in the 50-1000 Hz regime, *Applied Physics Letters* 96 (2010) 041906.
- [47] X. Wang, H. Zhao, X. Luo, Z. Huang, Membrane-constrained acoustic metamaterials for low frequency sound insulation, *Applied Physics Letters* 108(4) (2016) 041905.
- [48] B. Wang, D. Duhamel, On the design and optimization of acoustic network resonators for tire/road noise reduction, *Applied Acoustics* 120 (2017) 75–84.
- [49] Y. S. Lee, A. Vakakis, L. Bergman, D. M. McFarland, G. Kerschen, F. Nucera, S. Tsakirtzis, P. N. Panagopoulos, Passive non-linear targeted energy transfer and its applications to vibration absorption: a review, *Proceedings of the Institution of Mechanical Engineers, Part K: Journal of Multi-body Dynamics* 222(2) (2008) 77–134.
- [50] O. Gendelman, L. Manevitch, A. Vakakis, R. M’Closkey, Energy pumping in nonlinear mechanical oscillators: part I-dynamics of the underlying hamiltonian systems, *Journal of Applied Mechanics* 68 (2001) 34–41.
- [51] A. Vakakis, O. Gendelman, Energy pumping in nonlinear mechanical oscillators: part II-resonance capture, *Journal of Applied Mechanics* 68 (2001) 42–48.
- [52] B. Cochelin, P. Herzog, P.-O. Mattei, Experimental evidence of energy pumping in acoustics, *Comptes Rendus Mécanique* 334(11) (2006) 639–644.

- [53] R. Bellet, B. Cochelin, P. Herzog, P.-O. Mattei, Experimental study of targeted energy transfer from an acoustic system to a nonlinear membrane absorber, *Journal of Sound and Vibration* 329(14) (2010) 2768–2791.
- [54] R. Mariani, S. Bellizzi, B. Cochelin, P. Herzog, P. Mattei, Toward an adjustable nonlinear low frequency acoustic absorber, *Journal of Sound and Vibration* 330(22) (2011) 5245–5258.
- [55] E. Gourdon, N. Alexander, C. Taylor, C. Lamarque, S. Pernot, Nonlinear energy pumping under transient forcing with strongly nonlinear coupling: Theoretical and experimental results, *Journal of Sound and Vibration* 300 (2007) 522–551.
- [56] N. Alexander, F. Schilder, Exploring the performance of a nonlinear tuned mass damper, *Journal of Sound and Vibration* 319 (2009) 445–462.
- [57] Z. Nili Ahmadabadi, S. Khadem, Nonlinear vibration control and energy harvesting of a beam using a nonlinear energy sink and a piezoelectric device, *Journal of Sound and Vibration* 333(19) (2014) 4444–4457.
- [58] P.-O. Mattei, R. Ponçot, M. Pachebat, R. Côte, Nonlinear targeted energy transfer of two coupled cantilever beams coupled to a bistable light attachment, *Journal of Sound and Vibration* 373 (2016) 29–51.
- [59] A. Vakakis, Shock isolation through the use of nonlinear energy sinks, *Journal of Vibration and Control* 9 (2003) 79–93.
- [60] R. Bellet, B. Cochelin, R. Côte, P. O. Mattei, Enhancing the dynamic range of targeted energy transfer in acoustics using several nonlinear membrane absorbers, *Journal of Sound and Vibration* 331(26) (2012) 5657–5668.
- [61] L. Viet, N. Nghi, On a nonlinear single-mass two-frequency pendulum tuned mass damper to reduce horizontal vibration, *Engineering Structures* 81 (2014) 175–180.
- [62] C. Soize, Probabilistic Structural Modeling in Linear Dynamic Analysis of Complex Mechanical Systems, *Recherche Aérospatiale (English Edition)* 4 (1986) 39–51.
- [63] C. Soize, Vibration damping in low-frequency range due to structural complexity. A model based on the theory of fuzzy structures and model parameters estimation, *Computers and Structures* 58 (1995) 901–915.
- [64] F. Georgiadis, A. F. Vakakis, D. M. McFarland, L. Bergman, Shock Isolation Through Passive Energy Pumping Caused By Nonsmooth Nonlinearities, *International Journal of Bifurcation and Chaos* 15(6) (2005) 1989–2001.
- [65] C.-H. Lamarque, F. Thouverez, B. Rozier, Z. Dimitrijevic, Targeted energy transfer in a 2-DOF mechanical system coupled to a non-linear energy sink with varying stiffness, *Journal of Vibration and Control* 23 (2017) 2567–2577.

- [66] R. Rubinstein, D. Kroese, *Simulation and the Monte Carlo Method*, Second Edition, John Wiley & Sons, 2008.
- [67] L. Verlet, Computer “experiments” on classical fluids. I. Thermodynamical properties of Lennard-Jones molecules, *Physical Review* 159(1) (1967) 98–103.
- [68] E. Hairer, C. Lubich, G. Wanner, Geometric numerical integration illustrated by the Störmer/Verlet method, *Acta Numerica* 12 (2003) 399–450.
- [69] B. Coleman, W. Noll, Foundations of Linear Viscoelasticity, *Reviews of Modern Physics* 33 (1961) 239–249.
- [70] C. Desceliers, C. Soize, Non-linear viscoelastodynamic equations of three-dimensional rotating structures in finite displacement and finite element discretization, *International Journal of Non-Linear Mechanics* 39 (2004) 343–368.
- [71] A. Papoulis, *Probability, Random Variables and Stochastic Processes*, McGraw-Hill, New York, 1965.
- [72] L. Guikhman, A. Skorokhod, *The Theory of Stochastic Processes*, Springer Verlag, 1979.
- [73] M. Priestley, *Spectral Analysis and Time Series*, Academic Press, New York, 1981.
- [74] M. Shinozuka, Simulation of multivariate and multidimensional random processes, *Journal of the Acoustical Society America* 49 (1971) 357–367.
- [75] F. Poirion, C. Soize, Numerical methods and mathematical aspects for simulation of homogeneous and non homogeneous Gaussian vector fields, in: P. Krée, W. Wedig (Eds.), *Probabilistic Methods in Applied Physics*, Springer-Verlag, Berlin, 1995, pp. 17–53.
- [76] C. Soize, I. E. Poloskov, Time-domain formulation in computational dynamics for linear viscoelastic media with model uncertainties and stochastic excitation, *Computers and Mathematics with Applications* 64(11) (2012) 3594–3612.
- [77] R. Dautray, J.-L. Lions, *Mathematical Analysis and Numerical Methods for Science and Technology*, Springer-Verlag, Berlin, 1992.
- [78] R. Ohayon, C. Soize, *Structural Acoustics and Vibration*, Academic Press, London, 1998.
- [79] D. Lavazec, G. Cumunel, D. Duhamel, C. Soize, A. Batou, Métamatériau microstructuré non linéaire pour l’atténuation du bruit et des vibrations en basses fréquences, in: 13ème Congrès Français d’Acoustique et 20ème colloque Vibrations, SHocks and NOise, Le Mans, France, 11-15 avril 2016, Actes de la conférence, 2016, pp. 1–7.

- [80] D. Lavazec, G. Cumunel, D. Duhamel, C. Soize, A. Batou, Nonlinear microstructured material to reduce noise and vibrations at low frequencies, in: Joint International Conference on Motion and Vibration Control and Recent Advances in Structural Dynamics, Proceedings of MoVIC and RASD 2016, Southampton, United Kingdom, July 6-7 2016., 2016, pp. 1–10.
- [81] D. Lavazec, G. Cumunel, D. Duhamel, C. Soize, A. Batou, Attenuation of noise and vibration at low frequencies using a nonlinear microstructured material, in: International Conference on Noise and Vibration Engineering, Proceedings of ISMA 2016, Leuven, Belgium September 19-21, 2016., 2016, pp. 1–11.
- [82] D. Lavazec, G. Cumunel, D. Duhamel, C. Soize, Attenuation of acoustic waves and mechanical vibrations at low frequencies by a nonlinear dynamical absorber, in: CFM 2017, Lille, August 28, September 1, 2017. Proceedings of CFM 2017, 2017, pp. 1–12.
- [83] D. Lavazec, G. Cumunel, D. Duhamel, C. Soize, Attenuation of acoustic waves and mechanical vibrations at low frequencies by a nonlinear dynamical absorber, in: USNCCM 2017, 14th U. S. National Congress on Computational Mechanics, Montreal, Canada, July 17 - 20, 2017, 2017.

## **Évaluation expérimentale et modélisation d'un absorbeur non-linéaire pour l'atténuation des vibrations. Conception, identification et analyse.**

**Résumé.** En raison de leurs grandes longueurs d'onde, les vibrations mécaniques en basses fréquences ne peuvent être facilement réduites dans les structures par l'utilisation de matériaux dissipatifs. Malgré ces difficultés, l'atténuation des vibrations en basses fréquences reste un enjeu important. Pour résoudre ce problème, différents axes de recherche ont été étudiés et ont été mis en application pour stocker et dissiper l'énergie vibratoire comme l'utilisation d'oscillateurs linéaires, composés d'une masse, d'un ressort et d'un amortisseur. Leur fréquence de résonance doit coïncider avec la fréquence de résonance de la structure que l'on veut atténuer. L'utilisation d'absorbeurs se comportant comme des oscillateurs ayant un comportement non linéaire est une alternative intéressante. En effet, grâce à un étalement fréquentiel de la réponse de l'oscillateur, celui-ci permet d'atténuer les vibrations de la structure sur une plus large bande de fréquence que ceux ayant un comportement linéaire, sans avoir de dédoublement de la résonance de la réponse en deux pics. Les travaux présentés ici se placent dans le cadre de la réduction vibratoire, à l'échelle macroscopique, en basses fréquences, pour lesquelles les premiers modes structuraux sont excités. Un absorbeur non linéaire a été conçu, réalisé et analysé expérimentalement, modélisé et identifié expérimentalement pour mettre en évidence le phénomène d'élargissement de la bande de fréquence de la réponse. Les effets de cet absorbeur sur le comportement dynamique d'une poutre console ont ensuite été numériquement étudiés, à partir d'un modèle de poutre couplée à des absorbeurs non linéaires. Un modèle réduit et son solveur stochastique ont été développés dans ce cadre. Les résultats ont exposé le fait que l'absorbeur non linéaire permet une atténuation de la réponse de la poutre, sans le dédoublement de la résonance.

**Mots clés :** Absorbeur non linéaire, Atténuation des vibrations, Conception, Expériences, Modélisation, Identification expérimentale, Réduction du bruit

## **Experimental evaluation and modeling of a nonlinear absorber for vibration attenuation. Design, identification, and analysis.**

**Abstract.** Due to their long wavelengths, mechanical vibrations at low frequencies cannot easily be reduced in structures by using dissipative materials. Despite these difficulties, the attenuation of vibration at low frequencies remains an important concern. To solve this problem, several ways of research have been explored and have been applied to vibration energy pumping such as linear oscillators, composed of a mass, a spring, and a damper. Their resonance frequency must coincide with the resonant frequency of the structure that has to be attenuated. The absorbers that are oscillators with a nonlinear behavior constitute an interesting alternative. The response of the nonlinear oscillator allows for obtaining an attenuation of vibration over a broader frequency band than the response of linear oscillator, without splitting the resonance that has to be attenuated into two resonances. The work presented here is in the frame of the vibratory reduction, on a macro-scale, at low frequencies, for which the first structural modes are excited. A nonlinear absorber has been designed, experimentally realized and analyzed, modeled and experimentally identified to highlight the phenomenon of broadening the frequency band of the response. The effects of this absorber on the dynamic behavior of a cantilever beam have been numerically studied, using a model of the beam coupled to nonlinear absorbers. A reduced-model and its stochastic solver have also been developed. The results obtained show that the nonlinear absorber allows for obtaining an attenuation on the beam response, without splitting of the resonance that has to be attenuated.

**Keywords:** Nonlinear absorber, Vibration attenuation, Design, Experiments, Modeling, Experimental identification, Noise reduction